Acta Universitatis Szegediensis

Acta Biologica Szegediensis

Volume 64,
Number 1,
2020

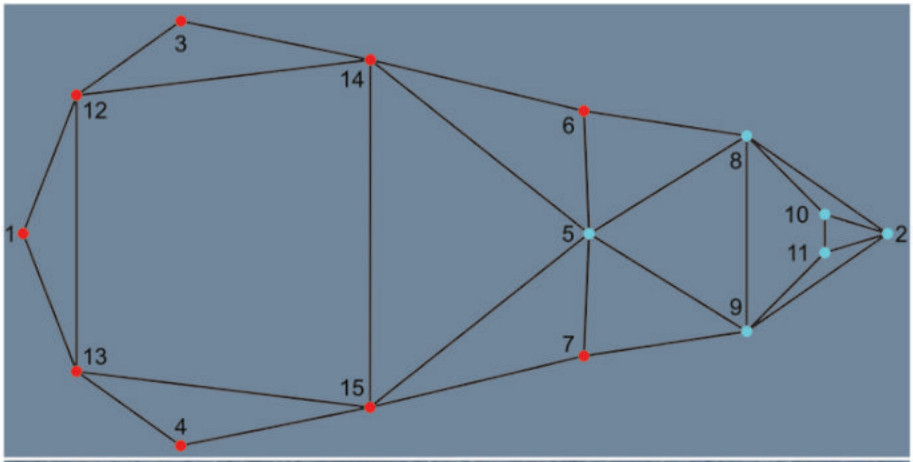

University of Szeged, Szeged, Hungary

http://abs.bibl.u-szeged.hu/index.php/abs

Acta Biologica Szegediensis

Volume 64(1):1-10, 2020
Acta Biologica Szegediensis
http://abs.bibl.u-szeged.hu/index.php/abs

DOI:10.14232/abs.2020.1.1-10

ARTICLE

A permissive approach for optimization of L-glutaminase production using wheat bran as supporting substrate and assessment of its cytotoxic potentialities

Jyoti P. Soren[1], Suman K. Halder[1], Joy Mondal[1], Papan K. Hor[1], Pradeep K. D. Mohapatra[2], Keshab C. Mondal[1]*

[1]Department of Microbiology, Vidyasagar University, Midnapore-721 102, West Bengal, India
[2]Department of Microbiology, Raiganj University, Uttar Dinajpur, West Bengal

ABSTRACT Microbial L-glutaminase has considered as one of the most important therapeutic enzymes considering its anticancer or antitumor activity. In this study, one L-glutaminase producing potent fungus was isolated from the coastal soil and identified as *Fusarium nelsonii* KPJ-2. During parametric optimization, it was noted that wheat bran supported maximum L-glutaminase production than other agro-industrial wastes tested. Solid substrate fermentation was mechanized with optimum pH of 4.0, incubation temperature at 25 °C, inoculums concentration of 2.0% (v/v), substrate concentration of 7.0% (w/v) and moisture of the production media suits at 20.0% (w/v). Statistical optimization using Response Surface Methodology (RSM) was improved the L-glutaminase production by 14.5% (68.93 U/gds) than unoptimized state. The SEM-EDX analysis demonstrated the overgrowth of fungus on wheat bran and utilization of its associated minerals. A comparative cytotoxic effect of the partial purified glutaminase was examined on both cancerous HCT cell and normal Vero cell line. The result clearly demonstrated that L-glutaminase from *F. nelsonii* KPJ-2 is specifically cytotoxic against cancer cell line with IC_{50} of 203.95µg/ml, but, non-responsive against normal cell. The newly isolated fungal strain can produce a considerable amount of L-glutaminase utilizing very low-cost substrate and the enzyme have therapeutic value for real life application owing to its anticancer effectiveness. **Acta Biol Szeged 64(1):1-10 (2020)**

KEY WORDS
anticancer property
Fusarium nelsonii
L-glutaminase
MTT assay
optimization

ARTICLE INFORMATION
Submitted
April 4, 2020.
Accepted
May 21, 2020.
***Corresponding author**
E-mail: mondalkc@gmail.com

Introduction

L-glutaminase (E.C.3.5.1.2) is an amidohydrolase that catalyzes the deamination of L-glutamine and produce L-glutamic acid and ammonia. This enzyme has significant applications in food, therapeutic and analytical industries. In food sector, addition of glutaminase leads to improvement of glutamate content, which enhances pleasant and delicious taste of the foodstuff (Kurihara 2009). The palatable taste of traditional food like soya sauce, miso and sufu is the involvement of L-glutaminase during course of fermentation and leads to accumulation of high content of L-glutamate (Lioe et al. 2010; Binod et al. 2017). In diagnostic and health monitoring, analysis of L-glutamine and glutamate level in the blood is very important (Madeira et al. 2018). Similarly, glutaminase based monitoring of glutamine and glutamate levels in mammalian cell culture media is effective for mass culturing (Cattaneo et al. 1992). Kikkoman Corporation, Japan first developed L-glutaminase based biosensor to determine the L-glutamine levels for diagnostic purpose and now it is worldwide applied. High rate of L-glutamine consumption is a characteristic of cancerous cells for biosynthesis of proteins and nucleic acids. Unlike normal cells, tumor cells have lack of L-glutamine biosynthetic machinery. As a consequence, growth of the tumor cells depends upon uptake of L-glutamine from serum. Administration of exogenous L-glutaminase in serum or at the site of tumor leads to depletion of glutamine level, therefore, tumor cells are starved for glutamine (Soren et al. 2019). Based on this principle, L-glutaminase is being extensively used as therapeutic agent to restrict growth of tumor or cancer cell. Recently for prolonged stability and better distribution of the enzyme, immobilized and *nano* forms of glutaminase are being developed.

Since the discovery of glutaminase, a vast number of microbes belongs to fungi and bacteria have been reported to be L-glutaminase producer (Soren et al. 2019). Among the fungal genera, *Aspergillus* and *Trichoderma* are the major

producer of L-glutaminase. For mass cultivation, both submerged and solid-state fermentation are employed by supplementing glutamine in the culture media. But report on raw or low-cost substrate is scanty in this regard. Due to existence of natural habitat and adequate oxygenation, the rate of productivity in solid state fermentation (SSF) of any metabolite is much higher than submerged fermentation (SmF) (Binod et al. 2017). Sabu et al. (2002) reported that salt stable enzyme from marine origin is effective in the treatment of acute lymphoblastic leukemia (ALL), as the isolated enzyme is more stable in salt-rich human plasma.

Considering these perspectives, the present study deals with the isolation of a potent L-glutaminase producing fungi from the soil of coastal area. The physicochemical environment of the organism has been optimized to recover maximum enzyme and under SSF to minimize the production cost. And finally, the anti-cancerous effectiveness of the isolated enzyme was explored under *in vitro* condition to highlight its therapeutic potentialities.

Materials and Methods

Isolation and identification of L-glutaminase producing fungi

Soil samples were collected from the coastal belt of Bay of Bengal from Bhitarkonika (20°45′N 87°0′E) and Digha (21°38′18″N 87°30′35″E). For exploring L-glutaminase producing fungi, soil samples were serially diluted, and 0.1 ml of each dilution was spread on glutamine supplemented (1.0%, w/v) potato dextrose agar (PDA) that containing 0.75% (w/v) phenol red and 100 mg/l ampicillin. The initial medium pH was maintained at 7.0. The plates were incubated at 28 °C for 7 days. Glutaminase producing fungi were selected by observing the pink zone around the colonies (Meghavarnam and Janakiraman 2017).

In secondary screening, primarily selected fungal isolates were cultured into the liquid medium (pH 7.0) having same composition as like isolation media (without agar) for 96 h. The activity of glutaminase in the culture supernatant was determined. The culture was maintained and sub-cultured on PDA slants frequently. The most potent fungal strain was identified on the basis 28S rDNA sequencing. Phylogenetic tree was constructed by the different nucleotide sequence which have maximum match with the query sequence. The sequences were aligned by ClustalW2 (Larkin et al. 2007) and the phylogenetic tree (dendrogram) was constructed by PHYLIP software (version 3.69) (Felsenstein 1981). Bootstrap value 500 was taken to build the tree by using Neighbour-joining method.

Inoculum preparation

Spore suspension of the potent fungal isolate was prepared by addition of 5 ml sterilized distilled water containing Tween 80 (2 drops/100 ml) onto the 3 days old fungal slants. The final concentration of the spore suspension was adjusted to about 2.0×10^2 spores/ml and preserved at 4 °C for further use.

Optimization of enzyme production through SSF

One variable at a time (OVAT) approach

Raw substrates were first treated with hot 1.0 % NaOH followed by repeated washing with cold and warm water to remove the dirt and other undesirable compounds. The washed substrates were then sun dried and cut into small pieces (2-3 mm). Solid state fermentation was carried out in Roux flasks containing 2.0 g of agro-industrial raw substrates moistened with 1.0 ml of glutamine (1.0%) solution (as inducer). Different raw substrates viz, sugarcane bagasse, wheat bran, rice straw, mustard oil cake and orange peel were used to examine their supporting effect on enzyme production. The effect of medium pH on enzyme production was checked by adjusting the pH (4.0-12.0) of moistening solution. The effect of temperature on enzyme production was studied by incubating the culture flaks at different incubation temperatures (20 - 50 °C). The optimization of important parameters like substrate concentration (1.0-10.0%, w/v), inoculum concentrations (0.5-3.0%, v/v) and moisture content (10-50%, w/v) were also done for enzyme production.

Response surface methodology (RSM) for optimization of L-glutaminase production

Five most influencing parameters (with their respective levels) were selected from OVAT experiments and further optimization was made using RSM. To explore the effects of these variables on the L-glutaminase production, a Box-Behnken factorial design was employed. An experimental design (5 factors with 3 levels) comprising multiple experiments were conducted for statistical optimization. Full experimental design is listed in Table 1. The relation between the coded value and actual values are described as in following.

$$X_i = \frac{x_i - x_o}{\Delta x_i}$$

Where, x_i is the independent variable coded value, x_o is the actual value of independent variable at their center point, and Δx_i is the step change value.

A model was generated by the regression analysis of the responses, and, its efficiency was tested by ANOVA and F-test. Three-dimensional (3D) response surface

Table 1. Experimental design used in RSM studies by using four independent variables each at three levels showing observed and predicted values of L-glutaminase production.

	Factor 1	**Factor 2**	**Factor 3**	**Factor 4**	**Factor 5**	**L-Glutaminase (U/gds)**	
Run	A: pH	B: Temperature	C: Inoculum	D: Substrate	E: Moisture	Observed value	Predicted value
1	4	27.5	2	8	30	64.38	54.77
2	4	30	2	7	10	55.87	55.92
3	3	30	2	7	20	55.8	56.29
4	4	27.5	1	6	20	57.81	65.58
5	5	27.5	3	7	20	64.67	60.86
6	4	25	3	7	20	60.79	62.23
7	/5	27.5	2	6	20	60.85	61.20
8	3	27.5	2	7	10	60.42	68.51
9	4	27.5	2	7	20	68.93	58.61
10	4	25	2	7	10	59.65	68.51
11	4	27.5	2	7	20	68.93	56.63
12	4	30	2	7	30	56.31	57.83
13	3	27.5	2	6	20	57.87	57.12
14	4	30	2	8	20	57.94	64.14
15	4	27.5	2	6	10	63.87	54.99
16	4	25	1	7	20	54.43	58.68
17	4	30	2	6	20	58.22	55.20
18	4	25	2	6	20	53.53	60.41
19	5	27.5	2	7	30	60.34	56.79
20	4	27.5	1	7	10	55.37	54.84
21	3	25	2	7	20	55.95	55.17
22	4	27.5	2	6	30	56.65	62.13
23	3	27.5	1	7	20	63.12	57.12
24	5	25	2	7	20	58.04	67.34
25	4	27.5	1	8	20	67.28	62.43
26	4	27.5	1	7	30	61.19	58.37
27	5	27.5	2	7	10	58.82	68.51
28	4	27.5	2	7	20	67.37	57.86
29	5	27.5	1	7	20	59.23	59.07
30	4	27.5	2	8	10	57.8	55.00
31	3	27.5	2	7	30	53.7	56.23
32	5	30	2	7	20	55.93	58.72
33	3	27.5	3	7	20	57.43	68.51
34	4	27.5	2	7	20	67.98	60.41
35	4	25	2	8	20	60.02	68.51
36	4	27.5	2	7	20	68.93	68.51
37	4	27.5	2	7	20	68.93	60.27
38	4	27.5	3	8	20	59.43	62.77
39	3	27.5	2	8	20	64.11	60.96
40	5	27.5	2	8	20	60.88	56.87
41	4	27.5	3	7	30	58.21	57.24
42	4	30	3	7	20	57.12	67.67
43	4	27.5	3	6	20	68.41	52.60
44	4	25	2	7	30	52.22	66.67
45	4	27.5	3	7	10	67.82	58.80
46	4	30	1	7	20	58.2	57.24

plots were generated to highlight the interactions among variables using Design-Expert 10.0 software (USA) (Das et al. 2013).

Enzyme extraction

After fermentation, sterile distilled water (5.0 ml) was added to each flask and shaked for 30 min at 100 rpm. The mixture was filtered through cheese cloth and centrifuged at 5000 rpm for 10 min. The crude enzyme was subjected to $(NH_4)_2SO_4$ precipitation (80%) and then dialyzed against the phosphate buffer (1M, pH 7.0). Finally, enzyme was collected by membrane filtration using 100 kDa molecular weight cut-off (Amicon, Merck). The partial purified glutaminase was stored for further use.

L-Glutaminase assay

The activity of L-glutaminase was determined by estimating the amount of ammonia liberates from the specific hydrolysis of substrate L-glutamine according to the method described in our previous publication (Soren et al. 2019). In brief, the reaction mixture consisting of 0.2 ml of crude enzyme, 0.5 ml of 0.04 M L-glutamine and 0.5 ml of 0.1 M phosphate buffer (pH 8.0). Then the mixture was incubated at 37 °C for 30 min. After that, 0.5 ml of 1.5 M Tri-chloroacetic acid (TCA) was added to stop the reaction. After dilution with distilled water (200 times), 100 µl of Nessler's reagent was added and absorbance was measured at 450 nm. A blank was prepared in the similar way, where, TCA was added before enzymatic reaction. One unit of L-glutaminase was defined as the amount of enzyme that liberates 1 µmol of ammonia under optimum conditions.

Field emission Scanning Electron Microscopy (FE-SEM) and Energy Dispersive X-ray (EDX) study

The surface morphology of solid substrate before and after fermentation was examined using FE-SEM (MERLIN, Zeiss). For this, dehydrated materials were put onto 1 cm ×1 cm glass slide and kept in an auto-sputter (Quorum-Q150R ES) under vacuum for gold coating. Images of surface morphology of the substrate were taken at various magnifications. Energy dispersive X-ray (EDX) spectrum was also taken for analysis of metal composition of solid substrate (Kar et al. 2013).

In vitro cytotoxicity assay

Vero cell line (kidney of an African *Cercopithecus aethiops*) and cancerous HCT (*Homo sapiens* colon colorectal carcinoma) cell line (IMGENEX, India) were maintained at 37 °C in Dulbecco's modified eagle medium (supplemented with Fetal Bovine Serum and 100 µL each of penicillin and streptomycin) (Himedia, India) in a 5.0% CO_2 incubator. Feasible influence of cell lines by addition of partial purified enzyme was determined through MTT assay. Cells were prepared at a concentration of 1.7 x 10^5 cells per well and incubated with 20 µl of L-glutaminase (30.93 U/ml) for 96 h and 20 µl phosphate buffer saline (PBS, pH 7.0) was used as control. Then 20 µl of MTT stock (Himedia) was added to each well and incubated for 4 h at 37 °C. Thereafter, MTT solubilizing agent was added into each well and color intensity measured at 570 nm. The concentration of enzyme needed for 50% (IC_{50}) inhibition of cell growth was determined from the dose response curves for each cell line. The percentage growth inhibition was calculated using the following formula:

$$Growth\ inhibition\ (\%) = 100 - (AE \times \frac{100}{AC})$$

Where, AE and AC are the mean absorbance measured for cell viability in culture medium containing enzyme and PBS, respectively.

Results

Isolation and primary screening of suitable fungi

After primary and secondary screening, the best extracellular L-glutaminase producing fungus designated as KPJ-2 was selected. The phenotypic identification was confirmed by phylogenetic analysis. The sequence homology of 28S rDNA amplicons revealed that KPJ-2 was most similar with *Fusarium nelsonii* CIB04 (GenBank accession no. MN117676.1) (Fig. 1).

Optimization of solid-state fermentation following OVAT approach

Physicochemical conditions are the key factor that moni-

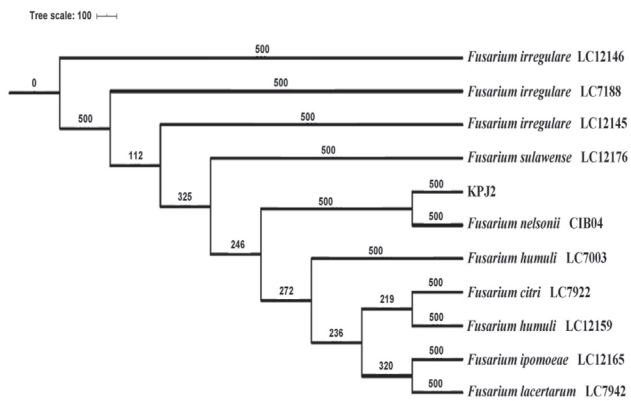

Figure 1. Dendrogram based on 28S rDNA sequence of the isolate KPJ-2 within the genus *Fusarium*. Sequence was aligned with ClustalW2 and tree was constructed by PHYLIP program.

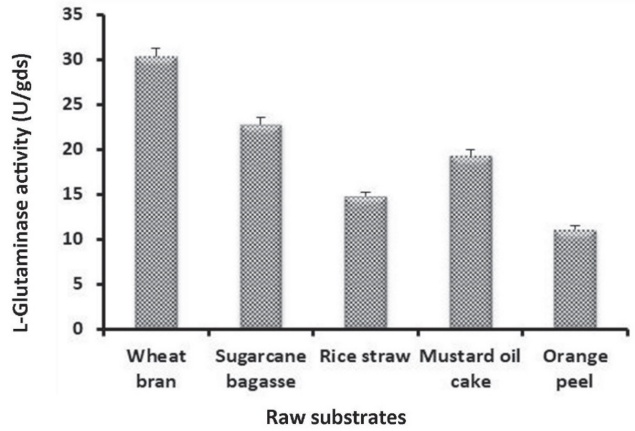

Figure 2. Optimization of different raw substrates for L-glutaminase production.

tored growth of microbes and its productivity (Halder et al. 2012; Elegbede and Lateef 2019). L-glutaminase production by *F. nelsonii* KPJ-2 was carried out under SSF in presence of various agro-industrial residues like sugarcane bagasse, wheat bran, rice straw, mustard oil cake and orange peel. The results revealed that wheat bran supported higher productivity of L-glutaminase (30.38 U/gds) by the isolate (Fig. 2). Among the various concentration of wheat bran, the highest enzyme production of about 47.82 U/gds was found at 7.0% (w/v) (Fig. 3a). Maximum L-glutaminase production by the fungal isolate (47.28 U/gds) was noted in presence of 20.0% (v/w) moistening agent (Fig. 3a).

The pH of the fermentation medium greatly influences the metabolic activities as well as growth of the organism. The highest enzyme activity of 35.53 U/gds was found at pH 4.0 (Fig. 3b). Production of enzyme was also studied in broad range of incubation temperatures (20-50 °C) (Fig. 3b) and optimum enzyme production was noted at 25 °C (41.29 U/gds). Inoculum concentration was found optimum for L-glutaminase production (47.37 U/gds) at 2.0% (v/w, 2×10^2 spore/ml) (Fig. 3b).

Optimization of enzyme production using RSM

Box-Behnken factorial design of RSM was employed for optimization of culture conditions for L-glutaminase production by newly isolated *F. nelsonii* KPJ-2. By taking three levels of five factors, a group of 46 experimental trails were performed. The levels of enzyme production have been represented in Table 1. A quadratic model was generated in response to L-glutaminase production by applying multiple regression analysis of the experimental data. The following second-order polynomial equation was derived:

$$\textit{L-glutaminase activity}\ (Y) = +68.51 + 0.5338 \times A + 0.1756 \times B + 0.9644 \times C + 0.9144 \times D - 1.17 \times E - 0.4900 \times A \times B + 2.33 \times A \times C - 1.55 \times A \times D + 2.06 \times A \times E - 1.86 \times B \times C - 1.69 \times B \times D + 1.46 \times B \times E - 4.61 \times C \times D - 3.86 \times C \times E + 3.45 \times D \times E - 4.85 \times A^2 - 7.62 \times B^2 - 2.90 \times C^2 - 2.87 \times D^2 - 4.91 \times E^2$$

Where, Y represents glutaminase production (U/gds), and A, B, C, D and E are initial pH, temperature (°C),

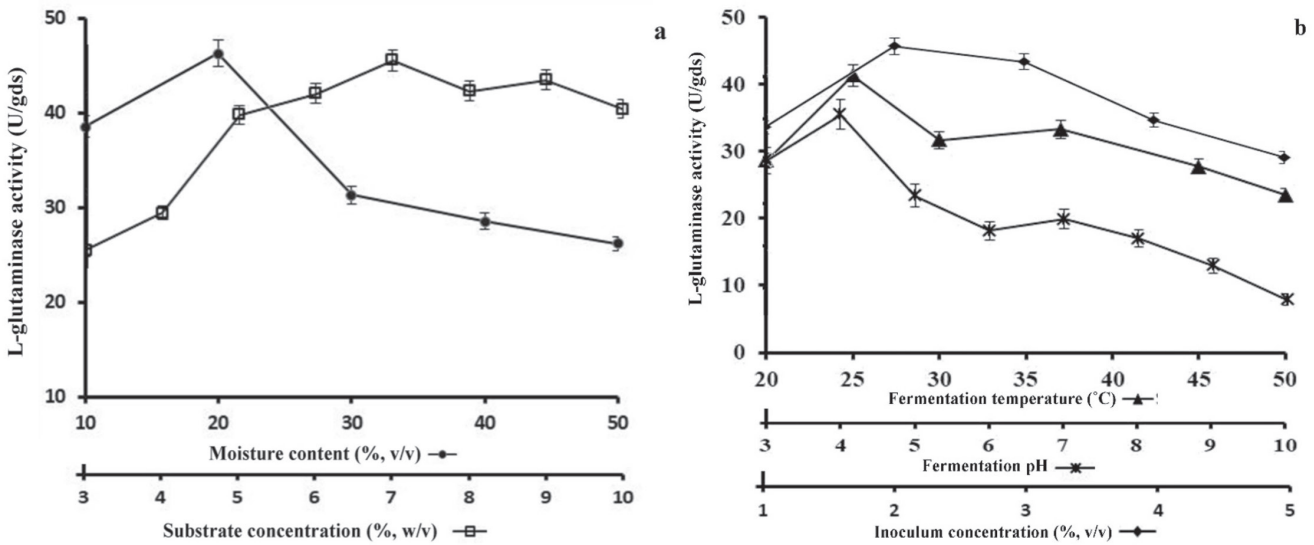

Figure 3. (a) Production of L-glutaminase in different substrate concentration (%, w/v) of wheat bran and moisture content (%, v/v), (b) Production of L-glutaminase in different initial fermentation pH, fermentation temperature (°C) and variable inoculum concentration (%) by strain KPJ-2.

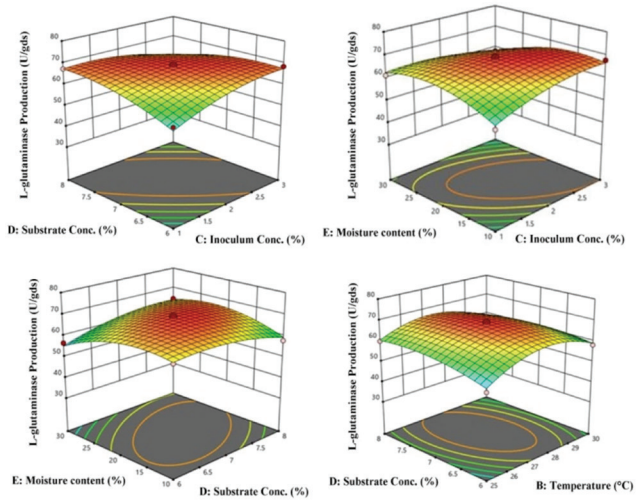

Figure 4. 3D response surface plots showing interactions between l-glutaminase production with substrate and inoculum concentrations, inoculum concentration and pH and temperature concentration and pH respectively using Box-Behnken response surface design.

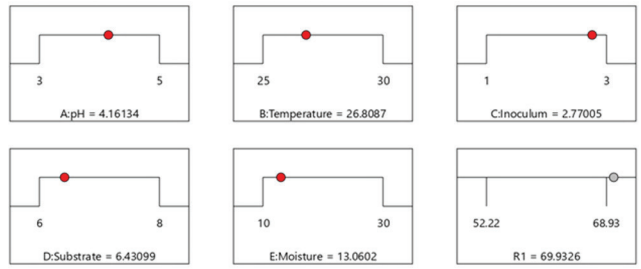

Figure 5. Desirability response surface plots showing the statistically actual concentration of L-glutaminase production using Box-Behnken response surface design.

inoculum concentration (%), substrate concentration (%) and moisture content (%), respectively.

The significant model terms were evaluated by analyzing variance (ANOVA) in the optimization study ($p < 0.01$) and represented in Table 2. The statistical analysis revealed that F-value of 24.61, and Prob > F was less than 0.0001. This result indicated that the model is significant for best utilization of optimized parameters for L-glutaminase production. The lack of fit value 5.08 also implies to be non-significant related to pure error; hence the model seems to be fit (Table 2). There is 3.99% chance of Lack of Fit F-value. The Predicted R^2 of

Table 2 ANOVA for quadratic model representing the F and P value to determine the most significant value.

Source	Sum of Squares	df	Mean Square	F-value	p-value	
Model	997.68	20	49.88	33.26	< 0.0001	Significant
A-pH	6.71	1	6.71	4.47	0.0446	
B-Temperature	0.0361	1	0.0361	0.0241	0.8780	
C-Inoculum	18.60	1	18.60	12.40	0.0017	
D-Substrate	13.38	1	13.38	8.92	0.0062	
E-Moisture	17.26	1	17.26	11.51	0.0023	
AB	0.9604	1	0.9604	0.6404	0.4311	
AC	30.97	1	30.97	20.65	0.0001	
AD	9.64	1	9.64	6.43	0.0179	
AE	16.97	1	16.97	11.32	0.0025	
BC	13.84	1	13.84	9.23	0.0055	
BD	11.46	1	11.46	7.64	0.0106	
BE	15.48	1	15.48	10.32	0.0036	
CD	85.10	1	85.10	56.74	< 0.0001	
CE	59.52	1	59.52	39.69	< 0.0001	
DE	47.61	1	47.61	31.75	< 0.0001	
A^2	192.31	1	192.31	128.23	< 0.0001	
B^2	529.49	1	529.49	353.06	< 0.0001	
C^2	65.92	1	65.92	43.95	< 0.0001	
D^2	71.89	1	71.89	47.93	< 0.0001	
E^2	224.55	1	224.55	149.73	< 0.0001	
Residual	37.49	25	1.50			
Lack of Fit	35.21	20	1.76	3.85	0.0702	not significant
Pure Error	2.29	5	0.4572			
Cor Total	1035.17	45				

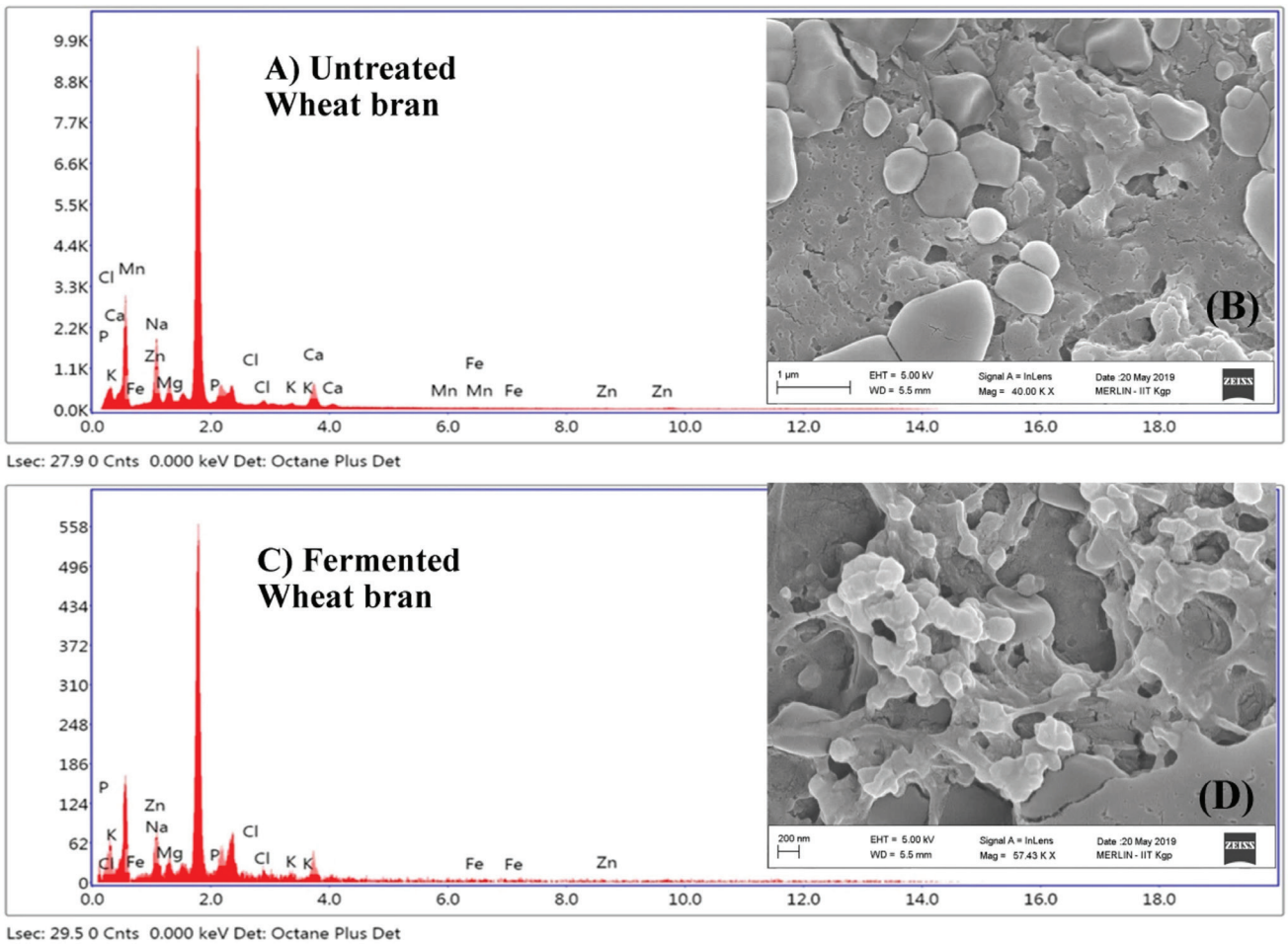

Figure 6. SEM-EDX spectrum of intact wheat bran incubated with strain KPJ-2. Energy dispersion analysis by X-ray (EDX) studies was conducted using the energy dispersive microanalysis of untreated and C) fermented wheat bran. SEM magnification bars show in 200 nm of B) untreated and D) fermented bran.

0.8124 is in reasonable agreement with the Adjusted R^2 of 0.9130 as the difference is less than 0.2. The adequate precision value, which measures the 'signal to noise ratio' was desirable to be > 4.0, and in the present case, the value of the said indices was 16.243. Thus, it can be stated that the model was statistically sound and can be used to navigate the design space (Das et al. 2013). The most significant mutual interaction was noticed among substrate concentration, temperature, moisture content and inoculum concentration for L-glutaminase production by *F. nelsonii* KPJ-2 (Fig. 4).

Confirmation experiment

Using Design Expert 10.0, numerical optimization design space was explored with a fitted quadratic model to arrive at an optimum fermentation condition. The desirability of optimized variables was found using independent function that assigns comparative importance to responses. Solutions with higher desirability for SSF gave an optimum pH of 4.1, fermentation temperature of 26.8 °C, inoculum percentage of 2.3%, moisture content of 13.6% and substrate amount of 6.4% (w/v), which could support L-glutaminase production of 68.93 U/gds (Fig. 5). Under these conditions, confirmation experiments were conducted in three replicates and the activity of 69.75 U/gds was determined, which suggested that experimental and predicted values were in good agreement.

Evaluation of pattern of wheat bran utilization and elemental analysis during glutaminase production

The SEM study revealed the gradual dislodgement of cortical layer and formation of mycelial mat on the surface of wheat bran after 72 h of fermentation. Numerous lateral pores on wheat bran surface were formed due to microbial interaction (Fig. 6). The peak analysis of EDX spectra revealed that the content of sodium, magnesium,

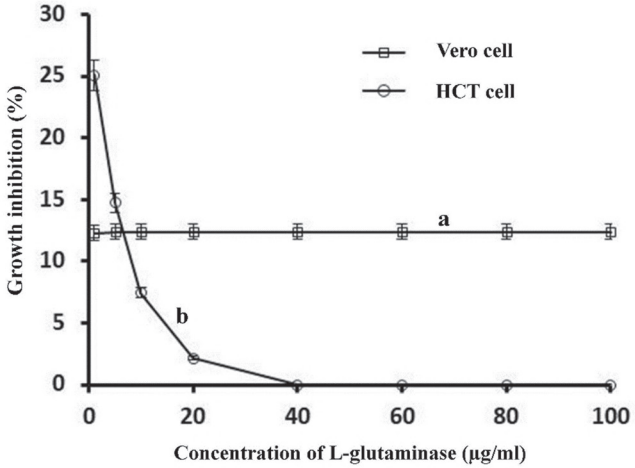

Figure 7. Growth inhibition (%) against different glutaminase concentration (µg/ml) of a) Vero and b) HCT cell line

phosphorous, potassium and calcium ions gradually decreased during course of fermentation and these may utilize for growth of fungus (Fig. 6). These data clearly demonstrated that wheat bran was became decomposed during fungus growth and the ingredients of the bran supported the biosynthesis of L-glutaminase.

In vitro cytotoxicity assay of L-glutaminase

The partial purified L-glutaminase from KPJ-2 has been subjected to cytotoxic study against the HCT and Vero cell line in different doses. The treatment of cancerous cell line (HCT) with increasing concentration of L-glutaminase resulted in appreciable inhibition of cell growth after 48 h in comparison to Vero cells (Fig. 7). This study indicates that this enzyme has potential cytotoxic effect against cancer cells. The concentration of IC_{50} value was found to be 203.95 µg/ml for HCT (Fig. 7). This *in vitro* screening model provides preliminary data on drug selection for clinical trials.

Discussion

In this study, an L-glutaminase producing fungal strain was isolated from the marine resources considering its natural habitat as a salt tolerant organism. Presently marine bioresources have tremendous therapeutic importance for development of anticancer, antibacterial and antiviral drugs (Malve 2016). Based on the morphological and phylogenetic analysis, the isolated organism was identified as *F. nelsonii* KPJ-2. The production of L-glutaminase from marine organism like *Aspergillus* sp. ALAA-2000, and *Beauveria* sp. was also reported by Ahmed et al. (2016) and Sabu et al. (2002), respectively. Selection of suitable substrate for solid state fermentation process is very crucial determinant of fermentation productivity (Nathiya et al. 2011). OVAT method is primarily employed to select the effective physicochemical condition on the growth of organism for production of L-glutaminase. In SSF, among the tested agricultural residues wheat bran supported maximum L-glutaminase production and this suggested the compatibility of this substrate for enzyme production as it may provide optimum carbon, nitrogen and mineral demand for growth of *F. nelsonii* KPJ-2 as well as enzyme synthesis. Nathiya et al. (2011) reported maximum production of L-glutaminase (42.37±0.47 U/g) by *Aspergillus flavus* KUGF009 utilizing tea dust followed by Bengal gram husk, groundnut oilcake, wheat bran and rice bran. Optimum inoculum concentration is essential because low inoculum density may produce insufficient biomass that leads to less product formation, whereas, a higher inoculum size may favor too much biomass formation that deplete the nutrients very fast or accumulates some self-limiting waste products (Kashyap et al. 2002). El-Sayed (2009) and Ye et al. (2013) reported that 2.0% inoculum concentration supports maximum glutaminase production by *Trichoderma koningii* and *Bacillus amyloliquefaciens*, respectively, and our finding is in good agreement with them. Temperature beyond the optimum zone exerted adverse effect on the enzyme production by any microbes as at both low and high temperature the growth of the organism is restricted (Binod et al. 2017). In this study the fungal isolate *F. nelsonii* KPJ-2 produced maximum L-glutaminase at 25 °C, which is in accordance with the report of Kashyap et al. (2002) on *Zygosaccharomyces rouxii.* Moisture level regulates the metabolic activity of the microorganism during SSF process (Pandey et al. 2000). Higher moisture levels may decrease porosity, alter particle structure, enhancement of bacterial growth or low oxygen transfer; whereas, the lower moisture level may lead to improve water tension, lower degree of swelling and reduced solubility of the nutrients of the solid substrate (Raimbault and Alazard 1980; Pandey 1992). For critical analysis of the most vibrant parameters, response surface methodology (RSM) based statistical analysis was carried out. The precise effect of five factors was examined by Box-Behnken factorial design. The relationship between the independent parameter were evaluated by examining the 3D response surfaces curves (Fig. 4) which showed the variation in the yields of L-glutaminase as a function of two variables when the other variables at their central values. Evaluation of response surface curves indicate the range of optimum conditions within the experimental area covered or show the way to confirmative experiments to achieve better results. The observed mean of L-glutaminase activity found to be 68.93 U/gds which is closed to predicted values and hence validates

the model. At optimized condition 14.50% increment in L-glutaminase production was achieved in comparison to un-optimized state.

The SEM-EDX studies show a thin lump of cell aggregates on the surface of wheat bran and distortion of surface layer as well as utilization of its mineral content after 72 h of fermentation. Wheat bran composed of fructans, xylans, cellulose, lignin, galactan in addition to other biomolecules including proteins and minerals (Onipe et al. 2015). The perforation of surface wall of wheat bran indicates KPJ-2 liberated an array hydrolytic enzyme including L-glutaminase which initiates hydrolysis from the surface layer. The enzymatic end products induced the fungus for liberation of reasonable amount of L-glutaminase. The elementary analysis revealed the quantity of iron and zinc ions decrease during fermentation while sodium, magnesium, phosphorous, potassium and calcium ions quantity gradually increase after fermentation. These ions may contribute to maintain the growth of the organism, physiological requirement and conformational stability of the enzyme molecule.

Cytotoxicity study revealed that L-glutaminase arrested cell proliferation of HCT cells with IC_{50} value of 203.95 μg/mL. On the contrary, the enzyme has no impact on Vero cell which implies that it become non-toxic to normal cells and, therefore, well-suited for anticancer or antitumor therapy. The literatures reflected that effectiveness and IC_{50} value of L-glutaminase varied depending upon the target cells. Reda (2015) reported IC_{50} of 64.70 μg/mL as growth inhibition doses for HCT cell line. Singh and Banik (2013) reported that in case of hepatocellular carcinoma (Hep-G2) cell lines IC_{50} dose was 82.27 μg/mL. Also, IC_{50} of 63.30 μg/mL was recorded by Elshafei et al. (2014) against hepatocellular carcinoma (Hep-G2) cell.

Conclusion

This is probably the first report that *F. nelsonii* KPJ-2, which is generally regarded as plant pathogen, is an excellent producer of extracellular L-glutaminase. Utilization of wheat bran as supporting substrate minimizes the production cost, therefore, will be economic and applicable for pharmaceutical and other industries. As the organism isolated from marine environment and the isolated L-glutaminase can restricted the growth of HCT cell line, therefore, this enzyme deserves for human wellness. Future work has been targeted towards the characterization the enzyme property and construction of nano-form structure to enhance its effectiveness.

Acknowledgements

The authors are thankful to the Rajiv Gandhi National Fellowship supported by University Grant Commission, funded by Ministry of Social Justice & Empowerment and Ministry of Tribal Affairs, Government of India for the financial contribution in this study.

References

Ahmed AM, Taha TM, Abo-Dahab NF, Hassan FS (2016) Process optimization of L-glutaminase production; a tumour inhibitor from marine endophytic isolate *Aspergillus* sp. ALAA-2000. J Microb Biochem Technol 8:256-267.

Binod P, Sindhu R, Madhavan A, Abraham A, Mathew AK, Beevi US, Sukumaran RK, Singh SP, Pandey A (2017) Recent developments in L-glutaminase production and applications an overview. Bioresour Technol 245:1766-1774.

Cattaneo MV, Luong JH, Mercille S (1992) Monitoring glutamine in mammalian cell cultures using an amperometric biosensor. Biosens Bioelectron 7:329-334.

Das A, Paul T, Halder SK, Jana A, Maity C, Mohapatra PK, Pati BR, Mondal KC (2013) Production of cellulolytic enzymes by *Aspergillus fumigatus* ABK9 in wheat bran-rice straw mixed substrate and use of cocktail enzymes for deinking of waste office paper pulp. Bioresour Technol 128:290-296.

Elegbede JA, Lateef A (2019) Optimization of the production of xylanases in corncob-based media by *Aspergillus niger* and *Trichoderma longibrachiatum* using Taguchi approach. Acta Biol Szeged 63(1):51-58.

Elshafei AM, Hassan MM, Ali NH, Abouzeid MA, Mahmoud DA, Elghonemy DH (2014) Purification, kinetic properties and antitumor activity of L-glutaminase from *Penicillium brevicompactum* NRC829. British Micro Res J 4:97-115.

El-Sayed AS (2009) L-glutaminase production by *Trichoderma koningii* under solid-state fermentation. Indian J Microbiol 49:243-250.

Felsenstein J (1981) Evolutionary trees from DNA sequences: a maximum likelihood approach. J Mol Evol 17:368-376.

Halder SK, Maity C, Jana A, Pati BR, Mondal KC (2012) Chitinolytic enzymes from the newly isolated *Aeromonas hydrophila* SBK1: study of the mosquitocidal activity. BioControl 57:441-449.

Kar S, Gauri SS, Das A, Jana A, Maity C, Mandal A, Mohapatra PK, Pati BR, Mondal KC (2013) Process optimization of xylanase production using cheap solid substrate by *Trichoderma reesei* SAF3 and study on the alteration of behavioral properties of enzyme obtained from SSF and SmF. Bioproc Biosyst Eng 36:57-68.

Kashyap P, Sabu A, Pandey A, Szakacs G, Soccol CR (2002) Extra-cellular L-glutaminase production by *Zygosaccharomyces rouxii* under solid-state fermentation. Process Biochem 38:307-312.

Kurihara K (2009) Glutamate: from discovery as a food flavor to role as a basic taste (umami). Am J Clin Nutr 90:719S-22S.

Larkin MA, Blackshields G, Brown NP, Chenna R, McGettigan PA, McWilliam H, Valentin F, Wallace IM, Wilm A, Lopez R, Thompson JD (2007) Clustal W and Clustal X version 2.0. Bioinform 23:2947-2948.

Lioe HN, Selamat J, Yasuda M (2010) Soy sauce and its umami taste: a link from the past to current situation. J Food Sci 75:R71-76.

Madeira C, Alheira FV, Calcia MA, Silva T, Tannos FM, Vargas-Lopes C, Fisher M, Goldenstein N, Brasil MA, Vinogradov S, Ferreira ST (2018) Blood levels of glutamate and glutamine in recent onset and chronic schizophrenia. Front Psychiatry 9:713.

Malve H (2016) Exploring the ocean for new drug developments: Marine pharmacology. J Pharm Bioallied Sci 8(2):83-91.

Meghavarnam AK, Janakiraman S (2017) Solid state fermentation: An effective fermentation strategy for the production of L-asparaginase by *Fusarium culmorum* (ASP-87). Biocatal Agric Biotechnol 11:124-130.

Nathiya K, Nath SS, Angayarkanni J, Palaniswamy M (2011) Optimised production of L-glutaminase: A tumour inhibitor from *Aspergillus flavus* cultured on agro-industrial residues. Afr J Biotechnol 10:13887-13894.

Onipe OO, Jideani AI, Beswa D (2015) Composition and functionality of wheat bran and its application in some cereal food products. Int J Food Sci Tech 50:2509-18.

Pandey A (1992) Recent process developments in solid-state fermentation. Process Biochem 27:109-117.

Pandey A, Soccol CR, Nigam P, Soccol VT (2000) Biotechnological potential of agro-industrial residues. I: sugarcane bagasse. Bioresour Technol 74:69-80.

Raimbault M, Alazard D (1980) Culture method to study fungal growth in solid fermentation. Eur J Appl Microbiol Biotechnol 9:199-209.

Reda FM (2015) Kinetic properties of *Streptomyces canarius* L-glutaminase and its anticancer efficiency. Braz J Microbiol 46:957-968.

Sabu A, Kumar SR, Chandrasekaran M (2002) Continuous production of extracellular L-glutaminase by Ca-alginate-immobilized marine *Beauveria bassiana* BTMF S-10 in packed-bed reactor. Appl Biochem Biotechnol 102:71-79.

Singh P, Banik RM (2013) Biochemical characterization and antitumor study of L-glutaminase from *Bacillus cereus* MTCC 1305. Appl Biochem Biotechnol 171:522-531.

Soren JP, Paul T, Banerjee A, Mondal KC, Mohapatra PK (2019) Exploitation of agricultural waste as sole substrate for production of bacterial L-glutaminase under submerged fermentation and the proficient application of fermented hydrolysate as growth promoting agent for probiotic organisms. Waste Biomass Valor 1-13.

Ye M, Liu X, Zhao L (2013) Production of a novel salt-tolerant L-glutaminase from *Bacillus amyloliquefaciens* using agro-industrial residues and its application in Chinese soy sauce fermentation. Biotechnol 12:25-35.

Acta Biologica Szegediensis

Volume 64(1):11-16, 2020
Acta Biologica Szegediensis
http://abs.bibl.u-szeged.hu/index.php/abs
DOI:10.14232/abs.2020.1.11-16

ARTICLE

Bactericidal activity of skin mucus and skin extracts of *Catla catla* and *Channa striatus*

Shanmugavel Ranjini[1], Samuthirapandi Muniasamy[2], Ganesan Rameshkumar[3], Thangavel Rajagopal[4], Thangavel Sivakumar[2], Ponnirul Ponmanickam[5]*

[1]Department of Biotechnology, Arulmigu Kalasalingam Arts and Science College, Krishnan Kovil – 626 126, Tamil Nadu, India.
[2]Department of Microbiology, Ayya Nadar Janaki Ammal College (Autonomous), Sivakasi-626 124, Tamil Nadu, India.
[3]Department of Zoology, V.H.N. Senthikumara Nadar College (Autonomous), Virudhunagar 626 001, Tamil Nadu, India.
[4]Department of Zoology, Thiagarajar College (Autonomous), Madurai- 625 009, Tamil Nadu, India.
[5]Department of Zoology, Ayya Nadar Janaki Ammal College (Autonomous), Sivakasi-626 124, Tamil Nadu, India.

ABSTRACT Fishes counteract certain microbial attacks in water by producing antimicrobial proteins/peptides in their skin surface. The present study focused on screening the bactericidal activity of skin and skin mucus extracts of *Catla catla* and *Channa striatus*. The bactericidal activity was assessed against *Escherichia coli*, *Pseudomonas aeruginosa*, *Klebsiella pneumoniae*, *Proteus vulgaris*, *Aeromonas hydrophila*, *Staphylococcus aureus* and *Bacillus coagulans* by disc diffusion method. The minimal inhibitory concentration was also determined. Protein profiles in skin and skin mucus extracts were analyzed by SDS-PAGE. Samples from both fishes showed antibacterial activity. Detailed analysis of individual protein and peptide would throw light on their medicinal importance to be used against pathogenic microbes. **Acta Biol Szeged 64(1):11-16 (2020)**

KEY WORDS
antimicrobial proteins
Catla catla
Channa striatus
fish skin
skin mucus

ARTICLE INFORMATION
Submitted
31 March 2020
Accepted
6 July 2020
***Corresponding author**
E-mail: ponmanickam_ts228@anjaconline.org

Introduction

Fishes have great economic value due to their taste and rich protein content. In an aquatic environment, a myriad of pathogenic and non-pathogenic organisms is present. Occasionally, fish cultivation results in enormous loss because of infectious diseases caused by the pathogenic microorganisms. Antibiotics are being utilized to manage these diseases; however, pathogens develop resistance against several antibiotics (Lalumera et al. 2004). At the same time, fishes possess excellent defense system against the pathogens by producing biochemically diverse secretions which mainly act on bacterial membranes and induce cell lysis.

The mucus layer on the surface of the fish is constantly replaced, which possibly prevents stable colonization by parasites, bacteria and fungi. Skin secretions have a broad range of polypeptides with antimicrobial properties (Uthayakumar et al. 2012). The bioactive substances like lysozyme, lectins, proteolytic enzymes, flavoenzymes, immunoglobins, C-reactive proteins, apolipoprotein A-1 and antimicrobial peptides are constitutively expressed in the mucus to provide immediate protection to fish against potential pathogens (Kitani et al. 2008).

Further, the mucus layer of the fish skin is presumed to perform several other functions, viz., acts as a lubricant, serves as a barrier for microbial entry, maintains osmoregulation, plays a role in locomotion and pheromone communication (Hellio et al. 2002). By nature, antimicrobial peptides (AMPs) are secreted by the fish skin and function as a first line defense against the microbial attacks. They protect the fish against a wide variety of bacterial, fungal, viral, and other pathogenic infections by disruptive "lytic" or pore-forming "ionophoric" actions (Smith et al. 2010). Fish epidermal mucus AMPs have demonstrated a broad spectrum of activity that is 10-100 times more potent than that of their amphibian counterparts against various fish and human pathogens (Park et al. 1998).

Proteins or peptides present in the fish skin mucus form pores on the bacterial membrane that cause oozing out of cellular contents. This alters the regular ionic gradients of membrane and eventually leads to the death

of bacteria (Fernandes et al. 2004; Silphaduang et al. 2006). Antimicrobial proteins and peptides could also be a source of potential natural antibiotics for pharmaceutical applications (Ying-xia et al. 2008).

In developing countries, most of the ponds in rural as well as urban localities are contaminated by the discharge of sewage water and dumping of solid wastes. Fishes are enduring these adverse conditions by making antimicrobial substances/ peptides in their skin. Interestingly, the secretion and composition of skin mucus are altered in conformity with the changing environment, especially to microbial exposure and hyperosmolarity (Zuchelkowski et al. 1981; Arulvasu et al. 2012). Attempts are being made to identify bioactive principles in the fish skin mucus to obtain potent new antimicrobial agents; several earlier studies described such antimicrobial activity of skin and skin mucus extracts of freshwater fishes (Kumari et al. 2011; Haniffa et al. 2013; Islam et al. 2014; Patil et al. 2015). The present study was aimed to screen the bactericidal activity of skin mucus and skin mucus extracts of *Catla catla* and *Channa striatus*.

Materials and methods

Fish collection and maintenance

Healthy fishes of *Catla catla* (450 g in weight; 20 cm in length) and *Channa striatus* (250 g in weight; 28 cm in length) were collected from the nearby reservoir (Pilavakal dam, Srivilliputtur, India) and brought to the laboratory for the collection of mucus and skin. Only healthy fishes were sampled; dead fish or fish with skin lesions were not chosen for the experiment.

Collection of skin and skin mucus samples

Fish skin mucus was collected carefully from dorsal side of the fish by a sterile scalpel. Then, the skin was removed with sterile scissor and forceps. The samples were stored immediately at -20 °C until further use.

Preparation of mucus and skin extracts

The collected samples were homogenized separately in 100 mM extraction buffer (ammonium bicarbonate, pH 7.8) at 1 mg/mL on ice-cold condition in a glass homogenizer. Insoluble substances were removed by centrifugation at 10 000 rpm for 10 min at 4 °C and the supernatant was collected for further analysis (Anbuchezhian et al. 2011).

Antimicrobial sensitivity

Preliminary screening of skin mucus and skin extracts for their antimicrobial efficacy was carried out against five Gram-negative (*Escherichia coli* ATCC 25922, *Pseudomonas aeruginosa* ATCC 25619, *Aeromonas hydrophila* ATCC 7966, *Proteus vulgaris* ATCC 6380 and *Klebsiella pneumoniae* ATCC 29665) and two Gram-positive (*Bacillus coagulans* ATCC 7050 and *Staphylococcus aureus* ATCC 9144) bacteria. All the microbial strains, except *Aeromonas hydrophila*, were maintained in Luria-Bertani (LB) broth 37 °C. *Aeromonas hydrophila* was grown in nutrient broth at 37 °C.

The antimicrobial activity of skin and skin mucus extracts was determined by agar disc diffusion method (Bauer et al. 1966). Briefly, 100 µl of overnight grown bacterial culture was uniformly seeded on agar plates. Wells of 5 mm diameter were made on the agar using a sterile cork borer. 100 µl each of skin mucus and skin extracts were added to individual wells. Same quantity of extraction buffer, Ammonium bicarbonate, was added to another well which served as control. The agar plates were kept at 37 °C for 24 h and antimicrobial activity was determined by measuring the diameter of zone of inhibition.

Minimum inhibitory concentration (MIC)

MIC was carried out by broth microdilution method as described by Subramanian (2008) with slight modification. 50 µl of skin mucus and skin extracts were added individually to sterile 96 well microtitre plate in different concentrations. To this, 50 µl of overnight grown microbial culture was added. Finally, 50 µl of sterilized Muller-Hinton broth containing 2% NaCl was added to all the wells and incubated at 37 °C for 16-18 hours. After incubation, the wells were observed for microbial growth. The minimal inhibitory concentration was determined by the formation of turbidity and/or button-like structure at the bottom of the well.

SDS-PAGE

The overall protein content of skin mucus and skin extract was calculated by following the method of Bradford (1976). Electrophoresis was performed as described by Laemmli (1970) using 12% separating and 5% stacking gel. 50 µg of protein samples were loaded on to the well. The protein bands were visualized by staining with Coomassie brilliant blue (R250). Molecular mass of bands in the gel was determined by protein standard markers (Protein Molecular Weight Marker-Medium range, Genei, Bangalore).

Results

In the present study, bactericidal activity of skin and skin mucus of *C. catla* and *Ch. striatus* was assessed. The antibacterial activity of mucus and skin extracts of *C. catla* against the tested microorganisms was observed in the following order: *B. coagulans* > *K. pneumoniae* > *A.*

Table 1. Antibacterial activity of skin mucus and skin extracts of *C. catla*. Control: ammonium bicarbonate buffer.

Bacterial pathogens		Diameter of inhibition zone (mm)	
		mucus	skin
Gram negative bacteria			
1.	*E. coli*	10	12
2.	*P. aeruginosa*	0	0
3.	*K. pneumoniae*	13	18
4.	*P. vulgaris*	0	0
5.	*A. hydrophila*	12	15
Gram positive bacteria			
1.	*S. aureus*	0	0
2.	*B. coagulans*	14	20

hydrophila > *E. coli*. Three pathogens such as *P. aeruginosa*, *P. vulgaris* and *S. aureus* exhibited resistance against the mucus and skin extracts (Table 1). For *Ch. striatus,* the outcome was different: *E. coli* > *S. aureus* > *B. coagulans* > *P. aeruginosa* > *A. hydrophila*. *K. pneumoniae* and *P. vulgaris* were not affected by both the samples taken from *Ch. striatus* (Table 2).

The mucus and skin extracts of *C. catla* and *Ch. striatus* were further assayed for minimum inhibitory concentration (Table 3 and Table 4). The extracts showed a broad range of activity against the tested microorganisms. The respective MIC values of mucus and skin extract of *C. catla* against pathogens are as follows: *E. coli* (49.65 μg ml^{-1} and 35.07 μg ml^{-1}), *K. pneumoniae* (66.20 μg ml^{-1} and 17.54 μg ml^{-1}), *A. hydrophila* (49.65 μg ml^{-1} and 35.07 μg ml^{-1}) and *B. coagulans* (16.54 μg ml^{-1} and 17.54 μg ml^{-1}). For *Ch. striatus,* the MIC values are: *E. coli* (6.14 μg ml^{-1} and 4.88 μg ml^{-1}), *P. aeruginosa* (18.42 μg ml^{-1} and 4.88 μg ml^{-1}), *A. hydrophila* (24.56 μg ml^{-1} and 14.65 μg ml^{-1}), *S. aureus* (6.14 μg ml^{-1} and 4.88 μg ml^{-1}) and *B. coagulans* (6.14 μg ml^{-1} and 14.65 μg ml^{-1}).

Table 2. Antibacterial activity of epidermal mucus and skin extracts of *Channa striatus*. Control: ammonium bicarbonate buffer.

Bacterial pathogens		Diameter of inhibition zone (mm)	
		mucus	skin
Gram negative bacteria			
1.	*E. coli*	12	16
2.	*P. aeruginosa*	9	12
3.	*K. pneumoniae*	0	0
4.	*P. vulgaris*	0	0
5.	*A. hydrophila*	8	10
Gram positive bacteria			
1.	*S. aureus*	11	13
2.	*B. coagulans*	10	12

Table 3. MIC of skin mucus and skin samples of *C. catla*.

Bacterial pathogens		MIC of mucus (μg)	MIC of skin (μg)
1	*E. coli*	49.65	35.07
2	*P. aeruginosa*	NI*	NI
3	*K. pneumoniae*	66.20	17.54
4	*P. vulgaris*	NI	NI
5	*A. hydrophila*	49.65	35.07
6	*S. aureus*	NI	NI
7	*B. coagulans*	16.54	17.54

*NI: No inhibition.

The total protein content in the mucus and skin sample was 0.033 ± 0.1 and 0.035 ± 0.0 mg/ml, respectively, for *C. catla*, and 0.031 ± 0.0 mg/ml and 0.090 ± 0.1 mg/ml, respectively, for *Ch. striatus.* The protein profile of *C. catla* revealed the presence of intense protein bands with different molecular masses such as 90.0, 65.0, 40.0, 32.0, 28.0 and 15.0 kDa (Fig. 1). The electrophoretic analysis of *Ch. striatus* samples showed the presence of proteins with molecular masses of 98.0, 49.0 and 38.0 kDa (Fig. 2).

Discussion

Fishes are living in microbe-rich habitat for which they are bestowed with good defense mechanism in their skin mucus. Skin mucus contains antimicrobial peptides as weapons for killing the pathogens. It has been documented that naturally occurring proteins or glycoproteins of non-immunoglobulin nature are present in fish skin and mucus that react with a diverse array of environmental antigens and may confer an undefined extent of natural immunity to fish (Balasubramanian et al. 2012). Pieces of evidences suggest that occurrence of infections in

Table 4. MIC of mucus and skin sample of *Ch. striatus*.

Bacterial pathogens		MIC of mucus (μg)	MIC of skin (μg)
1	*E. coli*	6.14	4.88
2	*P. aeruginosa*	18.42	4.88
3	*K. pneumoniae*	NI*	NI
4	*P. vulgaris*	NI	NI
5	*A. hydrophila*	24.56	14.65
6	*S. aureus*	6.14	4.88
7	*B. coagulans*	6.14	14.65

*NI: No inhibition.

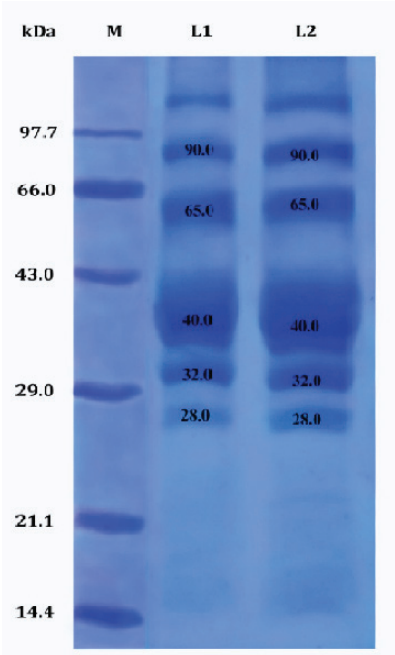

Figure 1. Protein profiles of mucus and skin extracts of *C. catla*. M: marker; L1: mucus; L2: skin

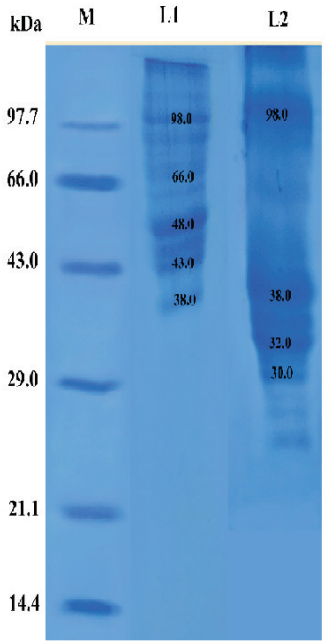

Figure 2. Protein profiles of mucus and skin extracts of *Ch. striatus*. M: marker; L1: mucus; L2: skin

fishes are very rare (Mayer and Hamann 2004; Fuochi et al. 2017). Thus, it makes many scientists to figure out the defense mechanism in fish skin mucus. In the present study, antibacterial effects of proteins from the skin and mucus extracts of *C. catla* and *Ch. striatus* were investigated. The bactericidal assays indicated that the crude mucus and skin extracts of both fishes showed a strong inhibitory effect on both Gram-positive and Gram-negative bacteria. This corroborates the works of Hellio et al. (2002) in which the potential antimicrobial activity of epidermal mucus and epidermal extracts of thirteen fish species were studied. It was reported that both skin and skin mucus play a major role in bactericidal activity. Similar kind of results were obtained by Elavarasi et al. (2013) in the skin mucus and skin extract of freshwater fishes, *Clarias batrachus* and *Tilapia mossambicus*.

The bactericidal activity of fish skin and skin mucus could be accounted for the counteraction of the negatively charged membrane and positively charged antimicrobial peptides. This causes the aggregation of antibacterial proteins to develop pores on the membrane. The mechanism of action of each peptide is distinct even though they belong to same structural class (Merrifield et al. 1994). It is also suggested that the antibacterial activity of fish mucus may be attributed to the antibacterial glycoproteins and their ability to kill bacteria by forming large pores in the target membrane (Ebran et al. 1999; Wei et al. 2010).

In the present study, the effect of skin mucus and skin extracts on bacterial growth was monitored by a liquid growth inhibition assay. The samples of *C. catla* showed a broad range of activity against pathogens. It inhibited the growth of *B. coagulans* at very low concentrations viz.,16.54 µg/ml and 17.54 µg/ml, respectively. The minimal inhibitory concentrations against *A. hydrophila* were found to be 49.65 µg/ml and 35.07 µg/ml, respectively. Among seven pathogens tested, five microorganisms were inhibited by the mucus and skin extracts of *C. catla* and *Ch. striatus*.

As another phase of the present study, electrophoretic analysis of skin and skin mucus of *C. catla* and *Ch. striatus* was carried out. The results showed the presence of proteins with molecular masses of 90.0, 65.0, 40.0 and 32.0 kDa in both skin and skin mucus of *C. catla*. In *Ch. striatus*, 98.0, 49.0 and 38.0 kDa mass proteins were identified. The following antibacterial proteins have so far been found in skin secretions or mucus (although most of them have been poorly characterized): hydrophobic proteins with 27 and 31 kDa from carp (*C. carpio*), 45 kDa protein from eel (*Anguilla anguilla*). 65 kDa protein from rainbow trout (*O. mykiss*) and a 49 kDa protein from doctor fish (*Tinca tinca*). Presumably, these antibacterial proteins form ion channels in the bacterial membrane and kill both Gram-positive and Gram-negative bacteria (Ebran et al. 1999, 2000). Anbuchezian et al. (2011) discovered two peptides, 13.6 kDa and 13.9 kDa, from the catfish mucus. Rao et al. (2015) stated that the low molecular mass proteins in the fish mucus play a major role in bactericidal activity.

Similarly, the mucus secretion of the fresh water spiny eel (*Mastacembelus armatusis*) was proteinaceous and showed potential hemolytic activity (Uthayakumar et al. 2012). Bijalwan et al. (2017) also found an antimicrobial protein (46 kDa) in the skin and muscle homogenate of *Labeo rohita*. These results support the present findings that different AMPs may be responsible for the antibacterial activity of skin mucus and skin extracts of *C. catla* and *Ch. striatus*. Further investigation is needed to purify the specific proteins from mucus and skin extract of these fishes and to characterize them in detail including their exact mode of action.

Acknowledgement

The authors would like to thank the Management and the Principal, Ayya Nadar Janaki Ammal College (Autonomous), Sivakasi for providing facilities to carry out this research work and for their encouragement.

References

Anbuchezhian R, Gobinath C, Ravichandran S (2011) Antimicrobial peptide from the epidermal mucus of some estuarine cat fishes. World Appl Sci J 12(3):256-260.

Arulvasu CS, Babu G, Dhanasekaran G (2012) Effect of crude and partially purified epidermal mucus proteins of marine catfish *Tachysurus dussumieri* on human cancer cell line. J Acad Ind Res 1(4):164-169.

Balasubramanian S, Prakash M, Senthilraja P, Gunasekaran G (2012) Antimicrobial properties of skin mucus from four freshwater cultivable fishes (*Catla catla*, *Hypophthalmichthys molitrix*, *Labeo rohita* and *Ctenopharyngodon idella*). Afr J Microbiol Res 6(24):5110-5120.

Bauer SW, Kirby WM, Sherris JC, Thurck M (1966) Antibiotic susceptibility testing by standardized single disc method. Am J Clin Pathol 45(4):493-496.

Bijalwan K, Verma SK, Mathur A (2017) Isolation and purification of protein from skin and muscles homogenate of *Labeo rohita* (Rohu). Int J Curr Microbiol App Sci 6(8):1493-1500.

Bradford MM (1976) A rapid and sensitive method for the quantitation of microgram quantities of protein utilizing the principle of protein-dye binding. Anal Biochem 72(1-2):248–254.

Ebran N, Julie S, Orange N, Auperin B, Molle G (2000) Isolation and characterization of novel glycoproteins from epidermal mucus: correlation between their pore-forming properties and their antibacterial activities. Biochim Biophys Acta 1467(2):271-280.

Ebran N, Julie S, Orange N, Saglio P, Lemaitre C, Molle G (1999) Pore-forming properties and antibacterial activity of proteins extracted from epidermal mucus of fish. Comp Biochem Physiol A Mol Integr Physiol 122(2):181-189.

Elavarasi K, Ranjini S, Rajagopal T, Rameshkumar G, Ponmanickam P (2013) Bactericidal proteins of skin mucus and skin extracts from fresh water fishes, *Clarias batrachus* and *Tilapia mossambicus*. Thai J Pharm Sci 37:194-200.

Fernandes JM, Molle G, Kemp GD, Smith VJ (2004) Isolation and characterization of oncorhyncin II, a histone H1-derived antimicrobial peptide from skin secretions of rainbow trout, *Oncorhynchus mykiss*. Dev Comp Immunol 28(2):127-138.

Fuochi V, Li Volti G, Camiolo G, Tiralongo F, Giallongo C, Distefano A, Petronio, G, Barbagallo I, Viola M, Furneri PM, Di Rosa M (2017) Antimicrobial and antiproliferative effects of skin mucus derived from *Dasyatis pastinaca* (Linnaeus, 1758). Mar Drugs 15(11):342.

Haniffa MA, Jeyasheela P, Milton MJ (2013) *In vitro* antibacterial activity of tissue extracts from four channids against enteric pathogens. Int J Agric Technol 9(6):1437-1445.

Hellio C, Pons AM, Beaupoil C, Bourgougnon N, Gal YL (2002) Antibacterial, antifungal and cytotoxic activities of extracts from fish epidermis and epidermal mucus. Int J Antimicrob Agents 20(3):214-219.

Islam M, Hossain M, Islam S, Khondoker S, Khatun A (2014) Competitive antibacterial activity of two Indian major carps and two Chinese carps fish mucus against common pathogenic bacteria at aquaculture pond. Int J Fish Aquat Stud 2:158-162.

Kitani Y, Kikuchi N, Zhang G, Shizaki I, Shimakura K, Shiomi K, Nagashima Y (2008) Antibacterial action of L-amino acid oxidase from the skin mucus of rockfish *Sebastes schlegelii*. Comp Biochem Physiol Part B: Biochem Mol Biol 149(2):394-400.

Kumari U, Nigam AK, Mitial S, Mitial AK (2011) Antibacterial properties of the skin mucus of the freshwater fishes, *Rita rita* and *Channa punctatus*. Eur Rev Med Pharmacol Sci 15(7):781-786.

Laemmli UK (1970) Cleavage of structural proteins during the assembly of the head of bacteriophage T4. Nature 227(5259):680-685.

Lalumera GM, Calamari D, Galli P, Castiglioni S, Crosa G, Fanelli R (2004) Preliminary investigation on the environmental occurrence and effects of antibiotics used in aquaculture in Italy. Chemosphere 54(5):661-668.

Mayer AM, Hamann MT (2004) Marine pharmacology in 2000: Marine compounds with antibacterial, anticoagulant, antifungal, anti-inflammatory, antimalarial, antiplatelet, antituberculosis, and antiviral activities; affecting the cardiovascular, immune, and nervous systems and other miscellaneous mechanisms of action.

Mar Biotechnol 6(1):37-52.

Merrifield RB, Merrifield EL, Juvvadi P, Andreu D, Boman HG (1994) Design and synthesis of antimicrobial peptides. In Antimicrobial Peptides. Ciba Foundation Symposium 186. Wiley, Chichester.

Park IY, Par CB, Kim MS, Kim SC (1998) Parasin I, an antimicrobial peptide derived from histone H2A in the catfish, *Parasilurus asotus*. FEBS Letters 437(3):258–262.

Patil RN, Kadam JS, Ingole JR, Sathe TV, Jadhav AD (2015) Antibacterial activity of fish mucus from *Clarias batrachus* (Linn.) against selected microbes. Biolife 3(4):788-791.

Rao V, Marimuthu K, Kupusamy T, Rathinam X, Arasu MV, Al-Dhabi NA, Arockiaraj J (2015) Defense properties in the epidermal mucus of different freshwater fish species. Aquacult Aquarium Conserv Legis 8(2):184-194.

Silphaduang U, Colorni A, Noga EJ (2006) Evidence for widespread distribution of piscidin antimicrobial peptides in teleost fish. Dis Aquat Organ 72(3):241-252.

Smith VJ, Desbois AP, Dyrynda EA (2010) Conventional and unconventional antimicrobials from fish, marine invertebrates and micro-algae. Mar Drugs 8(4):1213-1262.

Subramanian S, Ross NW, MacKinnon SL (2008) Comparison of antimicrobial activity in the epidermal mucus extracts of fish. Comp Biochem Physiol B Biochem Mol Biol 150(1):85-92.

Uthayakumar V, Ramasubramanian V, Senthilkumar D, Priyadarisini VB, Harikrishnan R (2012) Biochemical characterization, antimicrobial and hemolytic studies on skin mucus of fresh water spiny eel *Mastacembelus armatus*. Asian Pac J Trop Biomed 2(2):S863-869.

Wei OY, Xavier R, Marimuthu K (2010) Screening of antibacterial activity of mucus extract of Snakehead fish, *Channa striatus* (Bloch). Eur Rev Med Pharmacol Sci 14(8):675-681.

Ying-xia Z, Aihui Z, Riga M, Yong-can Z, Shifeng W (2008) Purification and antimicrobial activity of antimicrobial protein from brown-spotted grouper, *Epinephelus fario*. Zool Res 29(6):627-632.

Zuchelkowski EM, Lantz RC, Hinton DE (1981) Effects of acid-stress on epidermal mucous cells of the brown bullhead *Ictalurus nebulosus* (LeSeur): A morphometric study. Anat Rec 200(1):33-39.

Acta Biologica Szegediensis

Volume 64(1):17-24, 2020
Acta Biologica Szegediensis
http://abs.bibl.u-szeged.hu/index.php/abs

DOI:10.14232/abs.2020.1.17-24

ARTICLE

Non-antibiotic pharmaceutical agents as antibiotic adjuvants

Márió Gajdács[1,2]

[1]Department of Pharmacodynamics and Biopharmacy, Faculty of Pharmacy, University of Szeged, Szeged, Hungary
[2]Institute of Medical Microbiology, Faculty of Medicine, Semmelweis University, Budapest, Hungary

ABSTRACT The emergence of multidrug-resistant bacteria is a global public health issue, which severely hinders clinicians in providing patients with adequate antimicrobial treatment regimens. The strategy of drug repurposing is an emerging strategy in antimicrobial chemotherapy, during which new pharmacological uses are identified for drugs already approved. The aim of our present study was to assess the adjuvant properties of several existing and widely-used pharmacological agents against bacteria in combination with reference antibiotics. *Staphylococcus aureus* ATCC 25923, *S. epidermidis* ATCC 12228, *Escherichia coli* ATCC 25922 and *Klebsiella pneumoniae* ATCC 700603 were selected for our experiments. The minimum inhibitory concentrations (MICs) of the tested compounds were determined using the broth microdilution method, while a MIC reduction assay was performed to ascertain the effect of the tested compounds on the MICs of standard antibiotics (ciprofloxacin and gentamicin). Eight tested compounds (namely atorvastatin, celecoxib, clotrimazole, diclofenac-epolamine, ivermectin, lidocaine, mebendazole and terbinafine) showed antibacterial activity on the tested bacterial strains and several agents presented with various degrees of adjuvant (MIC-reducing) properties. Further experiments involving the screening of additional pharmaceutical compounds for their secondary antibacterial and adjuvant properties are warranted.
Acta Biol Szeged 64(1):17-24 (2020)

KEY WORDS
ciprofloxacin
combination therapy
gentamicin
non-antibiotic compounds
pharmaceutical compounds

ARTICLE INFORMATION
Submitted
04 June 2020
Accepted
24 July 2020
***Corresponding author**
E-mail: mariopharma92@gmail.com

Introduction

The discovery of antibiotics and their subsequent introduction into clinical medicine has been one of the main prerequisites for our current – modern day – healthcare to develop (Gaynes 2017). Previously lethal infections have become manageable, the life expectancy of people worldwide has changed drastically and novel medical interventions (e.g., cancer chemotherapy, invasive surgery, organ transplantation, and neonatology) were made possible (Laxminarayan et al. 2013). Bacterial pathogens have also reacted to the use of these agents and developed various resistance mechanisms to avoid their lethal effects (Nikaido 2009). The development of resistant isolates was to be expected by the laws of Darwinian evolution; however, the misuse and overuse of these agents have catalyzed this process to become a severe health problem in the span of only a few decades (Chang et al. 2015). Currently, the emergence of multidrug-resistant (MDR) bacteria is a global public health issue, which severely hinders clinicians in providing patients with adequate antimicrobial treatment regimens (Gajdács and Albericio 2019; Munita and Arias 2016). Several national and global public health authorities have published reports and estimates on the global impact of antibiotic resistance (World Health Organization 2014). The grimmest predictions may be found in the O'Neill report (from the National Health Service of the United Kingdom), projecting 10 million deaths per year by 2050 and 100 billion USD worth of economic burden (O'Neill 2014). Rice et al. have defined the „ESKAPE" bacteria (including E: *Enterococcus faecium*, S: *Staphylococcus aureus*, K: *Klebsiella pneumoniae*, A: *Acinetobacter baumannii*, P: *Pseudomonas aeruginosa*, E: *Enterobacter* spp., or recently *Enterobacteriaceae*) as the most concerning from the standpoint of clinical impact, both mortality-wise and economically (Rice 2010).

The issue of antibiotic resistance in the 21st century is a three-sided problem: *i)* on one hand, the emerge of drug-resistant mutants against newly developed antibiotics is an inevitable evolutionary process (which is common against any kind of noxious agents), *ii)* while the non-prudent use of antibiotics (e.g., for viral infections or other inappropriate indications) only exacerbates this process; *iii)* the costs of clinical research and the development of novel antibiotics – coupled with the relatively modest returns on investment from these drugs – lead to a shift in the interest of pharmaceutical companies to instead develop drugs for chronic (i.e. more „profitable") illnesses; this has resulted in a „discovery void", with very limited amount

of novel agents receiving marketing authorization since the 2000s (Gajdács 2019; Gajdács et al. 2020). In fact, no new broad-spectrum antibiotics were developed since the introduction of the fluoroquinolones in the 1980s (Darrow and Kesselheim 2014). Without new agents, researchers have investigated alternative strategies to combat bacterial pathogens more effectively (Rios et al. 2016). One of the proposed strategies is combination therapy: while the use of two or more existing antibiotics simultaneously in clinical situations is a controversial topic (with very few verified indications), however, the inclusion of non-antibiotic adjuvants seems to be a promising strategy (Ahmed et al. 2014; Tangdén 2014; Szerencsés et al. 2019). These adjuvants include enzyme inhibitors (e.g., clavulanic acid, a β-lactamase inhibitor), efflux pump inhibitors, modulators of bacterial membrane potential, membrane permeabilizers, inhibitors of bacterial cell-cell communication (quorum sensing) and monoclonal antibodies (Wright 2016; Kealey et al. 2017; Drawz and Bonomo 2010). However, it must be noted that most of these molecules did not receive clinical approval due to their toxicity *in vivo* (Tegos et al. 2011). Recently, the adjuvant properties of existing pharmaceutical compounds have received substantial attention. This strategy is termed „drug repurposing" (or drug re-profiling), during which new pharmacological uses are identified for drugs already approved, outside of their original indications (Pushpakom et al. 2019). As the physicochemical, pharmacokinetic and toxicological profile of these compounds have already been established, the initial stages of the drug authorization process (Phase I–II clinical trials) may be avoided, leading to substantial monetary benefits for the pharmaceutical companies; if this new indication of the tested compound is appropriate, pharmaceutical companies may once again expect financial returns for their investments (Miró-Canturri et al. 2019; Paul et al. 2010; Pushpakom et al. 2019; Soo et al. 2017). Drug re-profiling is also an emerging strategy in antimicrobial chemotherapy: some of these compounds have antibacterial properties themselves, while others have secondary mechanisms of action (some of which are unknown as of now). These mechanisms may include: bacteriostatic properties, inhibition of bacterial cell-cell communication, modulation of virulence factor-expression, biofilm-inhibition and so on (Miró-Canturri et al. 2019; Paul et al. 2010; Pushpakom et al. 2019; Soo et al. 2017; Yang et al. 2009) However, there are still significant gaps in the knowledge in the field of drug repurposing for antimicrobial purposes.

The aim of our present study was to assess the adjuvant properties of several existing and widely-used pharmacological agents against bacteria in combination with reference antibiotics, in an *in vitro* study.

Materials and methods

Culture media

The following culture media were used during our experiments: cation-adjusted Mueller-Hinton broth (Bio-Rad, Hercules, CA, USA), Luria–Bertani broth (Bio-Rad, Hercules, CA, USA), 5% sheep blood agar (bioMérieux, Marcy-l'Étoile, France) and eosine-methylene blue agar (bioMérieux, Marcy-l'Étoile, France).

Bacterial strains

Staphylococcus aureus ATCC 25923 and *S. epidermidis* ATCC 12228 were used as representative Gram-positive strains, while *E. coli* ATCC 25922 and *K. pneumoniae* ATCC 700603 were selected as representative Gram-negative strains for our experiments. For shorter time periods (<1 month), the bacterial strains were maintained on blood agar and eosine-methylene blue agar plates (for Gram-negatives) with continuous passage. For longer periods, the strains were kept in a -80 °C freezer, in a 1:4 mixture of 85% glycerol and liquid Luria-Bertani medium.

Antibiotics and non-antibiotic compounds

Ciprofloxacin and gentamicin (Sigma-Aldrich, St. Louis, MI, USA; will be listed as SA in the subsequent text) were selected as antibiotic controls for our studies. Twenty (n = 20) pharmacological agents, encompassing drug with different chemical structures and mechanisms of action were tested during our experiments: acetaminophen (SA), amantadine (SA), acyclovir (Teva Pharmaceuticals, Petah Tikva, Israel; will be listed as TPh in the subsequent text), atorvastatin (SA), azelastine (SA), celecoxib (Pfizer Hungary, Budapest, Hungary), cetirizine (SA), clotrimazole (TPh), diclofenac-epolamine (SA), enalapril-maleate (SA), ivermectin (SA), lidocaine (SA), mebendazole (SA), metformin (SA), metoprolol-succinate (SA), prazozine (SA), sitagliptine (SA), terbinafine (GlaxoSmithKline, Brentford, UK), valsartan (SA) and xylomethazoline (SA). The compounds were chosen on the basis of being available as over-the-counter (OTC) medication or being frequently prescribed for common chronic conditions as hypertension or diabetes mellitus. Pharmaceutical compounds were dissolved in phosphate-buffered saline (PBS), except for atorvastatin, which was dissolved in dimethyl sulfoxide (DMSO). All solutions were prepared on the day of the assay. The concentration of DMSO was below 1 V/V% in all experiments.

Antibacterial activity of non-antibiotic compounds, MIC determination

The minimum inhibitory concentrations (MICs) of the tested compounds were determined using the standard broth microdilution method, based on the recommenda-

Table 1 Minimum inhibitory concentrations (MICs) of the tested pharmaceutical compounds on reference bacterial strains.

	Minimal inhibitory concentrations (μg/mL)			
Compounds	*S. aureus* ATCC 25923	*S. epidermidis* ATCC 12228	*E. coli* ATCC 25922	*K. pneumoniae* ATCC 700603
Acetaminophen	>250	>250	>250	>250
Amantadine	>250	>250	>250	>250
Acyclovir	>250	>250	>250	>250
Atorvastatin	125	125	250	>250
Azelastine	>250	>250	>250	>250
Celecoxib	15.6	31.2	>250	>250
Cetirizine	>250	>250	>250	>250
Clotrimazole	125	62.5	>250	>250
Diclofenac-epolamine	250	250	>250	>250
Enalapril-maleate	>250	>250	>250	>250
Ivermectin	31.2	125	>250	>250
Lidocaine	250	250	250	250
Mebendazole	62.5	125	62.5	250
Metformin	>250	>250	>250	>250
Metoprolol-succinate	>250	>250	>250	>250
Prazozine	>250	>250	>250	>250
Sitagliptine	>250	>250	>250	>250
Terbinafine	250	125	>250	>250
Valsartan	>250	>250	>250	>250
Xylomethazoline	>250	>250	>250	>250

tions of the Clinical and Laboratory Standards Institute (CLSI; M07-A10). The experiments were performed in 96-well polystyrene microtiter plates, using cation-adjusted Mueller–Hinton broth. The tested concentrations of the compounds were ranging between 1.95-250 μg/mL, the two-fold serial dilutions of the tested compounds were made starting in the third row of the microtiter plates. During the experiments with *S. aureus* ATCC 25922 and *S. epidermidis* ATCC 12228, the Mueller-Hinton broth was supplemented by 2% NaCl, as based on CLSI protocols. The plates were incubated at 37 °C in an air thermostat. The MIC values of the tested compounds were recorded after 16-18 h of incubation; the interpretation of the results was performed visually. All experiments were performed in triplicate.

MIC reduction assay

To ascertain the effect of the tested compounds on the MICs of standard antibiotics (i.e. ciprofloxacin and gentamicin), a MIC reduction assay was performed (Sarker et al. 2007). The assay was performed in a 96-well microtiter plate, using cation-adjusted Mueller-Hinton broth. The setup of the plates was the following: in rows A-D of the plate, serial dilutions were made for the reference antibiotic, in rows E-H the same serial dilutions were performed for the reference antibiotic with the addition of the non-antibiotic compounds in a constant concentration as adjuvants (MIC/4 in cases where MIC was ≤ 250 μg/mL and 125 μg/mL where MICs were higher than 250 μg/mL) in all the wells, except for medium control and cell control wells (Sarker et al. 2007). The inoculation of the plates and the incubation was performed according to a standard broth microdilution method, described previously. The modified MICs (compared to the MICs of the antibiotics alone) were determined visually, as the concentration, where no visible growth of bacteria could be observed. All experiments were carried out in triplicate.

Results

Antibacterial activity of pharmaceutical compounds

The MICs observed for the non-antibiotic pharmaceutical compounds is presented in Table 1. Eight tested compounds (namely atorvastatin, celecoxib, clotrimazole, diclofenac-epolamine, ivermectin, lidocaine, mebendazole and terbinafine) showed antibacterial activities in the tested concentration range, while compounds with MICs >250 μg/mL were not considered to be active.

MIC reduction assays

The results of the MIC reduction assays for Gram-positive

Table 2 Results of the MIC reduction assays on Gram-positive bacterial strains using ciprofloxacin and gentamicin as reference antibiotics.

	Minimal inhibitory concentrations (μg/mL)			
Compounds	*S. aureus* ATCC 25923		*S. epidermidis* ATCC 12228	
MICs of reference antibiotics:	Ciprofloxacin: 0.12 μg/mL	Gentamicin: 0.12 μg/mL	Ciprofloxacin: 0.12 μg/mL	Gentamicin: 0.06 μg/mL
Acetaminophen	0.12	0.12	0.12	0.06
Amantadine	0.12	0.12	0.12	0.06
Acyclovir	0.12	0.12	0.12	0.06
Atorvastatin	**0.015**	**0.06**	**0.0075**	**0.03**
Azelastine	**0.06**	0.12	0.12	0.06
Celecoxib	**0.015**	0.12	**0.03**	0.06
Cetirizine	0.12	0.12	0.12	0.06
Clotrimazole	**0.06**	**0.06**	**0.06**	**0.03**
Diclofenac-epolamine	**0.06**	0.12	**0.03**	0.06
Enalapril-maleate	0.12	0.12	0.12	0.06
Ivermectin	**0.03**	0.12	**0.03**	0.06
Lidocaine	**0.06**	**0.06**	**0.06**	0.06
Mebendazole	**0.03**	0.12	0.12	0.06
Metformin	0.12	0.12	0.12	0.06
Metoprolol-succinate	0.12	0.12	0.12	0.06
Prazozine	0.12	0.12	0.12	0.06
Sitagliptine	0.12	0.12	0.12	0.06
Terbinafine	**0.015**	0.12	**0.03**	0.06
Valsartan	**0.06**	**0.06**	**0.03**	**0.03**
Xylomethazoline	0.12	0.12	0.12	0.06

Results in boldface represent cases when the MICs have decreased due to the effect of the adjuvants.

bacteria are presented in Table 2., while results for Gram-negative bacteria are shown in Table 3. Overall, the tested non-antibiotics were the most potent adjuvants against Gram-positive bacteria and they enhanced the antibacterial activity (i.e. they reduced the MICs) or ciprofloxacin to the highest extent (reducing the MICs 50-93.25% or 2-5-fold), while having modest effects on Gram-negative bacteria (*E. coli* and *K. pneumoniae*) and on the MICs of gentamicin. Interestingly, azelastine and valsartan on Gram-positive bacteria, while cetirizine, enalapril, valsartan and xylomethazoline on Gram-negative bacteria had MIC-reducing effects, without having any intrinsic antibacterial properties themselves (see Table 1.).

Discussion

Infections caused by MDR bacteria are associated with an increased mortality rate and decreased quality of life in the affected patients worldwide (Falagas et al. 2008). Since the 2000s, the development of novel antibiotics has been shown to keep up with the development in the levels of bacterial resistance (Falagas et al. 2008). Combination therapy with non-antibiotic compounds may provide a straightforward, attractive and financially reasonable drug development avenue (Medina and Pieper 2016; Lyddiard et al. 2016; Spellberg 2014). Several reports have been published in the literature on the antibacterial properties of non-antibiotic drugs; however, the systematic screening of drugs for such purposes have not yet been performed (Kruszewska et al. 2002; Lagadinou et al. 2020). Doxorubicin and bleomycin are antitumor agents (frequently termed as "anticancer antibiotics") show antibacterial properties on a variety of bacterial strains: the proposed mechanism of action is related to their intercalation into bacterial DNA (similar to the mechanism of the fluoroquinolones) and the generation of oxidative free radicals in the presence of Fe^{2+}-ions (which are indispensable for the biochemical pathways of bacteria) (Kruszewska et al. 2002; Lagadinou et al. 2020; Soo et al. 2017). Several antipsychotic drugs (e.g., phenothiazine, thioridazine) have also been described as DNA-intercalators; in addition, their efflux pump-inhibitory properties were also experimentally verified on many bacterial strains (Amaral et al., 2004). The adjuvant properties of non-steroidal anti-inflammatory drugs (NSAIDs) in bacterial infections have been supported in the clinical practice by empirical evidence, while laboratory studies have also

Table 3 Results of the MIC reduction assays on Gram-negative bacterial strains using ciprofloxacin and gentamicin as reference antibiotics.

	Minimal inhibitory concentrations (μg/mL)			
Compounds	*E. coli* ATCC 25922		*K. pneumoniae* ATCC 700603	
MICs of reference antibiotics:	Ciprofloxacin: 0.004 μg/mL	Gentamicin: 0.5 μg/mL	Ciprofloxacin: 0.12 μg/mL	Gentamicin: 0.05 μg/mL
Acetaminophen	0.004	0.5	0.12	0.5
Amantadine	0.004	0.5	0.12	0.5
Acyclovir	0.004	0.5	0.12	0.5
Atorvastatin	0.004	0.5	0.12	0.5
Azelastine	0.004	0.5	0.12	0.5
Celecoxib	**0.001**	0.5	**0.03**	0.5
Cetirizine	**0.001**	**0.25**	**0.6**	0.5
Clotrimazole	0.004	0.5	0.12	0.5
Diclofenac-epolamine	**0.002**	0.5	**0.6**	0.5
Enalapril-maleate	**0.002**	0.5	0.12	0.5
Ivermectin	0.004	0.5	0.12	0.5
Lidocaine	**0.001**	0.5	**0.03**	0.5
Mebendazole	0.004	0.5	0.12	0.5
Metformin	0.004	0.5	0.12	0.5
Metoprolol-succinate	0.004	0.5	0.12	0.5
Prazozine	0.004	0.5	0.12	0.5
Sitagliptine	0.004	0.5	0.12	0.5
Terbinafine	0.004	0.5	0.12	0.5
Valsartan	**0.001**	**0.125**	**0.6**	0.5
Xylomethazoline	**0.002**	0.5	0.12	0.5

Results in boldface represent cases when the MICs have decreased due to the effect of the adjuvants.

provided results that some NSAIDs (e.g., acetaminophen, acetyl-salicylic acid, ibuprofen, indomethacin, metamizol-sodium, etoricoxib) and local anesthetics (e.g., lidocaine) may have mechanisms enhancing the effects of antibiotics *in vivo* (Al-Bakri et al. 2009; Chan et al. 2017; D'Angelo et al. 2018; Johnson et al. 2008; Ogundeji et al. 2016; Thangamani et al. 2015). These mechanisms may include inhibition of biofilm-formation, adherence, reduction of motility and the modulating the release of antibiotics by leukocytes (Al-Bakri et al. 2009; Chan et al. 2017; D'Angelo et al. 2018; Johnson et al. 2008; Ogundeji et al. 2016; Thangamani et al. 2015). Allopurinol (a gout medication) increased the potency of anti-tuberculosis medications against *Mycobacterium tuberculosis* (Naftalin et al. 2017). The antibacterial activity of azole antifungals and ivermectin against Gram-positive bacteria only was previously described (Ghannoum and Rice 1999; Ashraf et al. 2018). The exact mechanism of action is not well-defined, but it is probably associated with affecting the binding to the terminal D-alanyl-D-alanine of the pentapeptide peptidoglycan precursors in the cell wall (Ghannoum and Rice 1999; Ashraf et al. 2018). The mechanism of statins (including simvastatin and atorvastatin among others) regarding their antibacterial potency also needs further studies, however, it has been suggested that they interfere with the mevalonate pathway, limiting the synthesis of the major lipid constituents of cell membrane microdomains (Ko et al. 2017). Apart from drugs, some publications also reported on the adjuvant properties of vitamins, enhancing the bactericidal activity of antibiotics; these publications highlight the role of high-dose of lipid soluble vitamins (ADEK) and Vitamin C (Andrade et al. 2014; Kwiencinska-Piróg et al. 2019).

Conclusions

The aim of our present study was to assess a selection of non-antibiotic pharmaceutical compounds – sourced from diverse clinical indications and molecular characteristics – as antibiotic adjuvants. Currently, there are around 6000-9000 drug compounds marketed for human therapeutic purposes; these agents may be considered as potential combination agents with reference antibiotics, to potentiate their antibacterial properties in clinical situations. The pharmacokinetic parameters and *in vivo* tolerability of these compounds have already been described; thus, these compounds are already one

step closer into their clinical utilization. The highlights of the study include the study of twenty pharmaceutical compounds that are frequently used by patients. Eight tested compounds showed antibacterial activity on the tested bacterial strains and several agents presented with various degrees of adjuvant (MIC-reducing) properties. Further experiments involving the screening of additional pharmaceutical compounds for their secondary antibacterial and adjuvant properties is definitely warranted.

Acknowledgements

M.G. was supported by the János Bolyai Research Scholarship of the Hungarian Academy of Sciences (BO/00144/20/5). M.G. would also like to acknowledge the support of the ESCMID's "30 under 30" Award.

References

Ahmed A, Azim A, Gurjar M, Baronia AK (2014) Current concepts in combination antibiotic therapy for critically ill patients. Indian J Crit Care Med 18:310-314.

Al-Bakri AG, Othman G, Bustanji Y (2009) The assessment of the antibacterial and antifungal activities of aspirin, EDTA and aspirin–EDTA combination and their effectiveness as antibiofilm agents. J Appl Microbiol 107:280-286.

Amaral L, Viveiros M, Molnár J (2004) Antimicrobial activity of phenothiazines. In vivo 18:725-731.

Andrade JC, Morais-Braga, MFB, Guedes GMM, Freitas TMA, Menezes IRA, Coutinho DMH (2014) Enhancement of the antibiotic activity of aminoglycosides by alpha-tocopherol and other cholesterol derivates. Biomed Pharmacother 68:1065-1069.

Ashraf S, Chaudhry U, Raza A, Ghosh D, Zhao X (2018) In vitro activity of ivermectin against *Staphylococcus aureus* clinical isolates. Antimicrob Res Infect Control 7:e27.

Chan EWL, Yee ZY, Raja I, Yap JKY (2017) Synergistic effect of non-steroidal anti-inflammatory drugs (NSAIDs) on antibacterial activity of cefuroxime and chloramphenicol against methicillin-resistant *Staphylococcus aureus*. J Glob Antimicrob Resist 10:70-74.

Chang HH, Cohen T, Grad YH, Hanage WP, O'Brien TF, Lipsitch M (2015) Origin and proliferation of multiple-drug resistance in bacterial pathogens. Microbiol Mol Biol Rev 79:101-116.

D'Angelo F, Baldelli V, Halliday N, Pantalone P, Polticelli F, Fiscarelli E, Williams P, Visca P, Leoni L, Rampioni (2018) Identification of FDA-approved drugs as antivirulence agents targeting the pqs quorum-sensing system of *Pseudomonas aeruginosa*. Antimicrob Agents Chemother 24:e01296-18.

Darrow JJ, Kesselheim AS (2014) Drug development and FDA approval, 1938-2013. N Engl J Med 370:e39.

Drawz SM, Bonomo RA (2010) Three decades of β-lactamase inhibitors. Clin Microbiol Rev 23:160-201.

Falagas ME, Rafailidis PI, Matthaiou DK, Virtzili S, Nikita D, Michalopoulos A (2008) Pandrug-resistant *Klebsiella pneumoniae*, *Pseudomonas aeruginosa* and *Acinetobacter baumannii* infections: Characteristics and outcome in a series of 28 patients. Int J Antimicrob Agents 32:450-454.

Gajdács M, Albericio F (2019) Antibiotic resistance: From the bench to patients. Antibiotics 8:e129.

Gajdács M (2019) The concept of an ideal antibiotic: Implications for drug design. Molecules 24:e892.

Gajdács M, Paulik E, Szabó A (2020) Knowledge, attitude and practice of community pharmacists regarding antibiotic use and infectious diseases: A cross-sectional survey in Hungary (KAPPhA-HU). Antibiotics 9:e41.

Gaynes R (2017) The discovery of penicillin—New insights after more than 75 Years of clinical use. Emerg Infect Dis 23:849-853.

Ghannoum MA, Rice LB (1999) Antifungal agents: Mode of action, mechanisms of resistance, and correlation of these mechanisms with bacterial resistance. Clin Microbiol Rev 12:501-517.

Johnson SM, Saint John BE, Dine AP (2008) Local anesthetics as antimicrobial agents: A review. Surg Infect 9:205-213.

Kealey C, Creaven CA, Murphy CD, Brady CB (2017) New approaches to antibiotic discovery. Biotechnol Lett 39:805-817.

Ko HTH, Lareu RR, Dix BR, Hughes JD (2017) Statins: antimicrobial resistance breakers or makers? PeerJ http://dx.doi.org/10.7717/peerj.3952

Kwietcinska-Piróg J, Skowron K, Bogiel T, Bialucha A, Przekwas J, Gospodarek-Komkowksa E (2019) Vitamin C in the presence of sub-inhibitory concentration of aminoglycosides and fluoroquinolones alters *Proteus mirabilis* biofilm inhibitory rate. Antibiotics 8:e116.

Kruszewska H, Zareba T, Tyski S (2002) Search of antimicrobial activity of selected non-antibiotic drugs. Acta Pol Pharm 59:436-439.

Lagadinou M, Onisor MO, Rigas A, Musetescu DV, Gkentzi D, Assimakopoulos SF, Panos G, Marangos M (2020) Antimicrobial properties on non-antibiotic drugs in the era of increased bacterial resistance. Antibiotics 9:e107.

Laxminarayan R, Duse A, Wattal C, Zaidi AKM, Wertheim HFL, Sumpradit N, Vlieghe E, Hara GL, Gould IM, Goossens H, Greko C, So AD, Bigdeli M, Tomson G, Woodhouse W, Ombaka E, Peralta AQ, Qamar FN, Mir F, Kariuki S, Bhutta ZA, Coates A, Bergstrom R, Wright GD, Brown ED, Cars O (2013) Antibiotic resistance-the need for global solutions. Lancet Infect Dis 13:1057-1098.

Lyddiard D, Jones GL, Greatrex BW (2016) Keeping it simple:

Lessons from the golden era of antibiotic discovery. FEMS Microbiol Lett 363:fnw084.

Medina E, Pieper DH (2016) Tackling threats and future problems of multidrug-resistant bacteria. Curr Top Microbiol Immunol 398:3-33.

Miró-Canturri A, Ayerbe-Algaba R, Smani Y (2019) Drug repurposing for the treatment of bacterial and fungal infections. Front Microbiol 10:e41.

Munita JM, Arias CA (2016) Mechanisms of antibiotic resistance. Microbiol Spectr doi:10.1128/microbiolspec.VMBF-0016-2015.

Naftalin CM, Verma R, Gurumurthy M, Lu Q, Zimmerman M, Yeo BCM, Tan KH, Lin W, Yu B, Dartois Y, Paton NI (2017) Coadministration of allopurinol to increase antimycobacterial efficacy of pyrazinamide as evaluated in a whole-blood bactericidal activity model. Antimicrob Agents Chemother 61:e00482-17.

Nikaido H (2009) Multidrug resistance in bacteria. Annu Rev Biochem 78:119-146.

Ogundeji AO, Pohl CH, Sebolal OM (2016) Repurposing of aspirin and ibuprofen as candidate anti-cryptococcus drugs. Antimicrob Agents Chemother 60:4799-4808.

O'Neill J (2014) Antimicrobial resistance: Tackling a crisis for the health and wealth of nations. Available online: https://amr-review.org/sites/default/files/AMRReviewPaper-Tacklingacrisisforthehealthandwealthofnations_1.pdf (accessed on 4th of July, 2020).

Paul SM, Mytelka DS, Dunwiddie CT, Persinger CC, Munos BH, Lindborg SR, Schacht AL (2010) How to improve R&D productivity: The pharmaceutical industry's grand challenge. Nat Rev Drug Discov 9:203-214.

Pushpakom S, Iorio F, Eyers PA, Escott KJ, Hopper S, Wells A, Doig A, Guilliams T, Latimer J, McNamee C, Norris A, Sanseau P, Cavalla D, Pirmohamed M (2019) Drug repurposing: Progress, challenges and recommendations. Nat Rev Drug Discov 18:41-58.

Rice LB (2010) Progress and challenges in implementing the research on ESKAPE pathogens. Infect Control Hosp Epidemiol 31:S7-S10.

Rios AC, Moutinho CG, Pinto FC, Del Fiol FS, Jozala A, Chaud MC, Vila MCDM, Teixeria JA, Balcao VM (2016) Alternatives to overcoming bacterial resistances: State-of-the-art. Microbiol Res 191:51-80.

Sarker SD, Nahar L, Kumarasamy Y (2007) Microtitre plate-based antibacterial assay incorporating resazurin as an indicator of cell growth, and its application in the in vitro antibacterial screening of phytochemicals. Methods 42:321-324.

Shallcross LJ, Howard SJ, Fowler T, Davies SC (2015) Tackling the threat of antimicrobial resistance: From policy to sustainable action. Philos Trans R Soc Lond B Biol Sci 370:20140082.

Soo VWC, Kwan BW, Quezada H, Castillo-Juárez I, Pérez-Eretza B, García-Contreras SJ, Martínez-Vázquez M, Wood TK, García-Contreras R (2017) Repurposing of anticancer drugs for the treatment of bacterial infections. Curr Top Med Chem 17:1157-1176.

Spellberg B (2014) The future of antibiotics. Crit Care 18:e228.

Szerecsés B, Mülbacher A, Vágvölgyi C, Pfeiffer I (2019) In vitro interactions of amphotericin B and non-antifungal compounds against opportunistic human pathogen *Cryptococcus neoformans*. Acta Biol Szeged 63:181-184.

Tandgén T (2014) Combination antibiotic therapy for multidrug-resistant Gram-negative bacteria. Ups J Med Sci 119:149-153.

Thangamani S, Younis W, Seleem MN (2015) Repurposing celecoxib as a topical antimicrobial agent. Front Microbiol 28:e750.

Tegos GP, Haynes M, Strouse JJ, Khan MM, Bologa CG, Oprea TI, Sklar LA (2011) Microbial efflux pump inhibition: Tactics and strategies. Curr Pharm Des 17:1291-1302.

World Health Organisation (2014) Antimicrobial resistance: Global report on surveillance. 2014, pp. 1–256. Available online: http://apps.who.int/iris/bitstream/10665/112642/1/9789241564748_eng.pdf?ua=1 (accessed on 4th of July, 2020).

Wright GD (2016) Antibiotic adjuvants: Rescuing antibiotics from resistance. Trends Microbiol 24:862-871.

Yang L, Rybtke MT, Jakobsen TH, Hentzer M, Bjarnsholt T, Givskov M, Tolker-Nielsen T (2009) Computer-aided identification of recognized drugs as *Pseudomonas aeruginosa* quorum-sensing inhibitors. Antimicrob Agents Chemother 53:2432-2443.

Acta Biologica Szegediensis

Volume 64(1):25-35, 2020
Acta Biologica Szegediensis
http://abs.bibl.u-szeged.hu/index.php/abs

DOI:10.14232/abs.2020.1.25-35

ARTICLE

Long-lasting effects of red and blue light exposure on the growth of soil fungi

Olga I. Vinnikova

Department of Physiology and Biochemistry of Plant and Microorganisms, School of Biology, V. N. Karazin Kharkiv National University, Kharkiv, 61001, Ukraine

ABSTRACT The experimental assessment of inter-species difference in long lasting effects produced in fungi by a brief exposure to the monochromatic light was performed. 24-h cultures grown from 1 mm mycelium fragments of *Alternaria alternata*, *Aspergillus clavatus*, *Fusarium fujikuroi*, *Penicillium citrinum* and *Trichoderma viride* were exposed for 30 min to blue light (BL, 450 nm) or red light (RL, 660 nm) and cultured for the next 10 days. Radial growth rate, conidial yield and germination, contents of proteins and phenolsand fungal antibacterial activity were estimated. BL- or RL-exposure did not essentially affect the final size of colonies of *A. clavatus* but delayed the growth of *P. citrinum* and stimulated it in *A. alternata* and *F. fujikuroi*; these changes were more profound after BL, than after RL. In *T. viride* the BL exposure led to a remarkable delay of growth, whereas the RL significantly increased the growth rate. Photo-induced changes in the conidial yield, conidial germination, contents of proteins and phenols also were dependent on the light wavelength and showed strong inter-species heterogeneity. Fungal antibacterial activity in exposed cultures was similar to the unexposed control. The observed effects are indicative targets for future research of possible molecular regulatory mechanisms underlying the photobiology in different fungal taxons.

Acta Biol Szeged 64(1):25-35 (2020)

KEY WORDS

conidiation
fungal photobiology
phenol content
radial growth rate
soil fungi

ARTICLE INFORMATION

Submitted
09 June 2020.
Accepted
22 July 2020.
***Corresponding author**
E-mail: o.i.vinnikova@karazin.ua

Introduction

Illumination is an important environmental factor for soil microscopic fungi and has an essential impact on their survival. By contrast to phototrophs, fungi use the light not as a source of energy, but as a trigger or regulatory signal which influences their growth and behavior. In ecological context, the light helps the mycelium to discriminate between different habitats, thus increasing their competitiveness against other soil microbiota (Fuller et al. 2015). Mechanisms of sensing and further transmission of the light signals in fungi includes complex molecular network, which ends up in differential gene expression and metabolic changes (Idnurm and Heitman 2005; Purschwitz et al. 2006; Corrochano 2007, 2011, 2019; Yu and Fischer 2019). A lot of data has been accumulated regarding the effects produced by the ultraviolet (UV), blue, green or red light in fungal species belonging to different systematic groups and their respective molecular machinery of the light reception has been extensively explored (Laringuet and Dunand 2005; Purschwitz et al. 2006, 2009; Herrera-Estrella and Horwitz 2007; Kritsky et al. 2010; Tisch and Schmoll 2010; Corrochano 2011).

Reports and reviews cited above shows that physiological responses of fungi to the light exposure comprise changes in their growth, conidiation, sexual development, spore release, phototropism and shifts in their circadian clock. A number of photo-induced effects were detected at subcellular and biochemical levels, e.g. hyperpolarization of the cell membrane, alterations in intracellular levels of energy carriers, changes in the oxygen consumption rate, carbon and sulphur metabolism, modulations of enzyme activity and biosynthesis of various products, and response to oxidative stress. At the genomic level hundreds of light-regulated genes were identified in fungi, and many of these genes are related to stress responses (Herrera-Estrella and Horwitz 2007; Schmoll et al. 2010; Lokhadwala et al. 2015; Brancini et al. 2019).

Mechanisms of photoreception and responses to the light exposure were extensively explored in different taxons of Kingdom Fungi. There are plenty of publications presenting data on light-induced effects and light sensors in one particular fungal genera, e.g. *Aspergillus* (Hill 1976; Kato et al. 2003; Sprote and Brakhage 2007; Purschwitz et al. 2009; Bayram et al 2010), *Alternaria* (Soderhall et al. 1978; Igbalajobi et al. 2019), *Botrytis* (Canessa et al. 2013; Schumaher 2017), *Fusarium* (Myung et al. 2009; Avalos and Estrada 2010), *Metarhizium* (Rangel et al. 2011, 2015; Brancini et al. 2016, 2018a; Oliveira et al. 2018; Dias et al.

2020), *Trichoderma* (Betina and Zajacova 1978; Strigácová et al. 2001; Pokorný et al. 2005; Schmoll et al. 2010), or broader systematic groups, like *Zygomycota* (Corrochano and Garre 2010). The photoresponsive proteins appeared to be highly conserved across the entire fungal kingdom, but different taxons may potentially show very divergent growth or biochemical responses to the same light signal. However, there is a lack of reports in modern literature containing a direct comparison of photoreactions assessed in two or more fungal species within one experiment.

Also, in a number of studies, photoinduced responses were measured after constant or protracted exposure of fungi to the light of various wavelengths. By contrast, much less data are available on the long lasting or delayed responses occurring after brief exposure, while such 'memory'-based effects in fungi has been known from classic studies (Zalokar 1955; Betina and Zajacova 1978; Schrott 1980) and confirmed in more recent experiments (Schmoll et al. 2010; Brancini et al. 2016, 2018a, 2019). And again, there is a gap in current knowledge regarding the species-related peculiarities of gross photoinduced reactions in such experimental conditions.

Therefore, the aim of the present research was to assess long lasting responses, including changes in the growth rate and basic biochemical and physiological characteristics, in soil microscopic fungi from different taxonomic groups after a relatively brief exposure to the light of different wavelengths.

Materials and methods

Light exposure and culturing of fungi

The strains of microorganisms for this experiment were obtained from the microbiological collection hold at the Department of Physiology and Biochemistry of Plants and Microorganisms of the School of Biology of V. N. Karazin Kharkiv National University (Kharkiv, Ukraine). Five fungal species – *Aspergillus clavatus* Desm., *Alternaria alternata* (Fr.) Keissl., *Fusarium fujikuroi* Nirenberg, *Penicillium citrinum* Thom and *Trichoderma viride* Pers., and two bacterial species – *Escherichia coli* and *Bacillus subtilis* were used in the study.

Microscopic fungi were grown on Petri dishes on the solid medium comprising non-boiled wort with 1.5% agar. Cultures were initiated by placing 1 mm fragment of mycelium into the center of Petri dish with 20 mL of solid medium and incubated in darkness at 22 ± 1 °C for 24 h. After that cultures were exposed for 30 min to the monochromatic light generated by the light diode matrix array (Korobov and Korobov 2012). The matrix array had dimensions 190 × 98 mm and contains 24 light diodes of total power 120 MW, providing the output light flux density of 6444 MW×m^{-2}. The distance from the light matrix to culture surface was 15 cm. Two arrays of diodes emitting different wavelengths were used: Red light (RL) of 660 nm, or blue light (BL) of 450 nm. Control cultures were sham exposed; for that cultures were kept wrapped in a foil and light source was not turned on. The day of exposure was set as day 0 in the experimental time scale. After the light exposure or sham exposure, cultures were returned to the incubator and kept in darkness at 22 ± 1 °C for the next 10 days.

Cultures on liquid medium were set up from exposed or sham exposed fungi grown on solid medium, when their colony diameter reached 20 mm (3 to 5 days of culturing). A round shape fragment of 10 mm diameter was cut out from the center of the fungal lawn, placed into a glass flask with 200 mL non-boiled wort supplemented with 4% sugars and cultured in darkness at 22 ± 1 °C.

Measurements of physiological and biochemical parameters

The diameter of growing fungal colonies was measured periodically, with 24 h intervals for 10 days, starting from day 1 after the light exposure. The number and size of conidia were estimated at the stage of active sporogenesis, at 5 to 7 day of culturing depending on the strain (Bilay 1982). A round shape fragment of 10 mm diameter was cut from the solid lawn of the fungal culture, placed into a flask with 100 ml distilled water and shaken intensively for 15 min. A drop of the resultant suspension was analyzed in a cell-counting chamber (hemocytometer) using a light microscope. The number of conidia per 1 ml was estimated. Simultaneously, the linear size (diameter or length) was measured using eyepiece micrometer in 50 conidia randomly chosen in different fields of view. In *F. fujikuroi* the number (contents) and the length of macrconidia were assessed.

For conidium germination assay, 100 µl of conidiospore suspension (1×10^7 conidia × ml^{-1}) was inoculated evenly onto Petri dishes with solid medium and incubated in darkness at 22 ± 1 °C as described above. The number of colonies was counted on 2 to 4 days of culturing.

Samples from liquid cultures were taken at the stage of active sporogenesis and used for measurements of protein and polyphenol contents in the mycelium. For this, Lowry method (Waterborg and Matthews 1994) and Löwenthal method (Protsenko and Kostina 2015; Ma et al. 2019) were applied, respectively.

The antagonistic properties of microscopic fungi against bacteria were assessed using the technique of counter co-culture on agar plates (Bilay 1982). Fungal cultures were exposed to RL or BL in 24 h after their mycelium fragment inoculation, as described above. The inoculation of test bacteria *E. coli* or *B. subtilis* into counter

co-cultures was carried out by a needle-dash technique, taking samples from their cultures grown for 24 h on Nutrient Agar (Himedia Laboratories, India). Fungal antagonistic action towards bacteria was estimated by periodic visual examination of the cultures. The effects were assessed as:

- Total oppression (TO), if the growth of test bacteria was completely stopped;
- Active antagonism (AA), if test bacterial colonies displayed a remarkable shrinkage compared to control, and a fungal lawn proliferated over the bacterial side of Petri dish;
- Passive antagonism (PA), if a visible delay in bacterial growth occurred, but without hyperexpansion of fungi;
- Neutralism, if no remarkable impact on the test bacteria was observed.

Statistical analysis of the data

The experiment was performed thrice. In each independent repeat three identical replicates of fungal cultures on solid or liquid media were set up. All endpoints were measured in each of these replicates. The values of the measured parameters in three replicates within each experiment were pooled together and their mean was calculated. Means from three independent experiments were averaged, and the respective standard error (SE) for the overall mean was estimated.

For each fungal species the patterns occurred in the experimental series of RL- or BL-exposure were compared to that observed in sham exposed, control series. Means with associated SE were compared using Student's *t*-test, considering the difference significant at $p \leq 0.05$ for 4 degrees of freedom (d.f. = $n_1 + n_2 - 2 = 3 + 3 - 2 = 4$).

Also, for demonstration purposes, conidial yield, size of conidia and conidial germination data in RL- or BL-exposed fungal cultures were normalized as a percent of the respective control values in sham-exposed cultures. In this case, SE for the mean were calculated from the dispersion of the 'exposed to control' ratios in three repeats of the experiment (n = 3).

Regression analysis of the time-effect relationship for radial growth of fungal cultures from day 1 to day 10 after exposure was performed using the respective option of the Microsoft Excel ™ package. Fitting of the data to sigmoid curve included the intermediate step of double logarithming of the colony size values.

Results

The radial growth of different fungal species after the exposure to RL or BL is presented on Fig. 1 (A-E). The sizes of fungal colonies at the moment of their exposure to the light (day 0) were too small for any accurate measurement. Starting from day 1 after exposure the changes of the colony diameter followed, as expected, a sigmoid curve with an elongated left part. The data on the colony growth between day 1 and day 10 were fitted to the equation:

$$S(t) = A \times e^{(1-e^{b-c\times t})}$$

where S is the size of the colony (diameter in mm), t is time in days, A is the asymptote of the colony growth, e is the natural logarithm base, b and c are regression coefficients. In this formula the coefficient c corresponds to the growth rate and the coefficient b determines the virtual "starting constant" for the size of the colony, i.e. the overall vertical shift of the curve from the baseline zero value, which is intuitively understood and easy to compare between experimental series. The estimated growth parameters are given in Table 1.

The response to the light exposure appeared to be rather heterogeneous between species. *A. clavatus* after either RL or BL exposure started growth from smaller colonies in compare with control (Fig. 1A). The difference in colony diameter became statistically significant between BL-cultures and control on days 3 (t = 3,51; p<0,05) and 4 (t = 3,79; p<0,05). However, in the interval between days 4 and 6 the growth rate of the exposed colonies increased, and their diameter became similar to control values till the end of the culturing period.

The growth of *P. citrinum* initially was delayed in BL-cultures: on day 1 the difference with control was significant (t = 3,27; p<0,05) (Fig. 1B). Due to the similar growth rate the smaller colony size in BL-cultures persisted till the end of the experiment; the difference with control was significant on day 9 and day 10 (t = 2,81 and 2,91, respectively; p<0,05 in both cases). In RL-cultures the starting size was similar to that in control; however, the growth rate was lower, therefore colonies had smaller diameter on day 5 and later on; on day 10 the difference between RL-cultures and control became meaningful (t = 2,91; p<0,05).

The remarkable delay at the start of growth was found in BL-cultures of *T. viride*: for the colony size on day 1 *versus* control t = 4,62 (p<0,01) (Fig. 1C). The growth rate was not affected by BL exposure, therefore the diameter of colonies in BL-cultures remained significantly smaller than in control during all the experiment, e.g., t =4,59 (p<0,05) on day 2, t = 5,68 (p<0,01) on day 4, t = 3,24 (p<0,05) on day 10. By contrast to that, RL produced no effect on the starting size but enhanced a growth rate of *T. viride*, so that RL-cultures had continually larger colonies than control cultures, especially in the second half of the

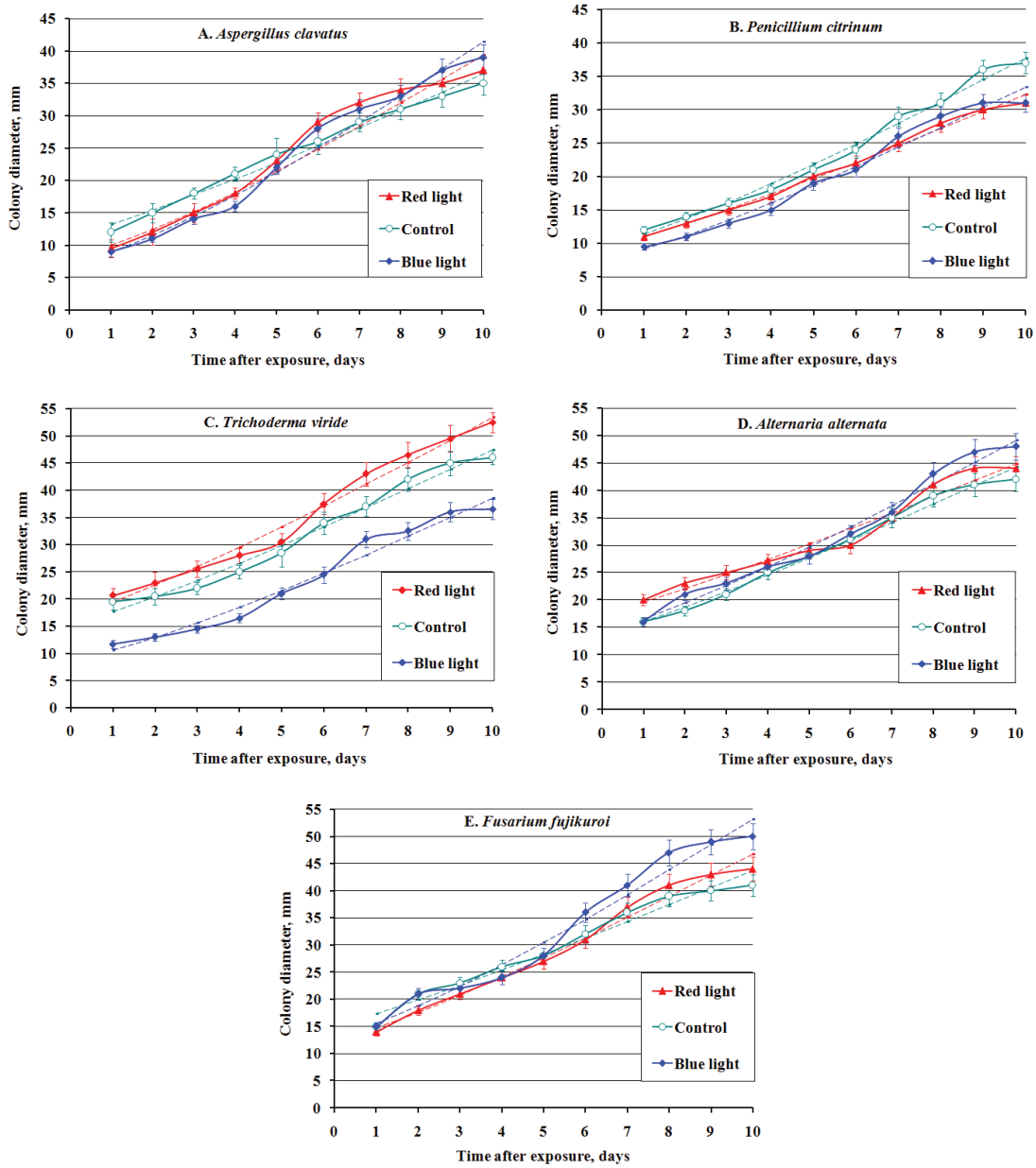

Figure 1. Time course of radial growth of different fungi species in cultures grown after brief exposure to red or blue monochromatic light. A: *Aspergillus clavatus*; B: *Penicillium citrinum*; C: *Trichoderma viride*; D: *Alternaria alternata*; E: *Fusarium fujikuroi*. Filled triangles: cultures exposed to red light. Filled diamonds: cultures exposed to blue light. Open circles: sham-exposed, control cultures. Dashed lines: growth predicted by the model (Equation 1 and estimated coefficients are given in Table 1).

experiment; on day 10 this difference became significant ($t = 2,90$; $p<0,05$). The size of colonies in RL-cultures remarkably exceeded that of in BL-cultures either on day 1 ($t = 5,76$; $p<0,01$) or day 10 ($t = 5,00$; $p<0,01$).

In *A. alternata* the size of colonies in BL-cultures was statistically indistinguishable from that in control, including the last day ($t = 1,88$; $p>0,05$) (Fig. 1d). RL-cultures had a noticeable increase of the starting size in compare to control ($t = 3,12$ $p<0,05$) on day 1. However, the growth rate of RL-cultures was slightly lower, therefore at the end of the observation period the colony size difference with the control diminished.

The dynamics of culture growth in RL-cultures of *F. fujikuroi* overlapped with that in control cultures (Fig. 1e). The growth of BL-cultures had a starting index similar to the control value, but the higher rate, that lead

Table 1. Growth parameters of fungi cultured after exposure to the light of different wavelength.

Exposure conditions	*A. clavatus*	*P. citrinum*	*T. viride*	*A. alternata*	*F. fujikuroi*
	Regression free coefficient (b*)				
Control	0.759	0.868	0.749	0.754	0.697
Red light	0.929	0.790	0.769	0.662	0.826
Blue light	1.012	0.896	0.903	0.811	0.868
	Growth rate coefficient (c*)				
Control	0.080	0.089	0.078	0.081	0.076
Red light	0.103	0.083	0.079	0.068	0.089
Blue light	0.107	0.097	0.096	0.083	0.,093
	Asymptote (A*)				
Control	35	37	46	42	41
Red light	37	31	52	44	44
Blue light	39	31	37	48	50
	Modeled, virtual "starting constant" of the colony size (mm)**				
Control	11.24	9.28	15.09	13.63	12.11
Red light	8.04	9.31	16.51	17.22	12.57
Blue light	6.78	7.28	8.53	13.77	12.18

* = coefficients are estimated for the fungal colony growth formula $S(t) = A \times e^{(1-e^{b-ct})}$, where S is the size of the colony (diameter in mm), t is time in days, A is the asymptote of the colony growth, e is the natural logarithm base, b and c are regression coefficients.
** = virtual "starting constant" of the colony size is calculated for $t = 0$.

to the meaningful increase in colony size at the end of the experiment (t = 3,08 on day 9 and t = 2,88 on day 10, p<0,05 in both cases).

Mean conidial yield, size and germination rate in RL and BL experimental series were normalized against the respective control values (Fig. 2). Conidial yield appeared to be lower in *A. clavatus* RL-cultures and BL-cultures than in control; t = 3,55 (p<0,05), and t = 6,17 (p<0,01), respectively (Fig. 2A). The decrease of conidial yield in RL-cultures of *P. citrinum* was insignificant (t = 1,77; p>0,05). *T. viride* showed a nearly two-fold decline of conidial counts in RL-cultures (t = 4,58; p<0,05) and three-fold – in BL-cultures (t = 7,45; p<0,01); the difference between RL- and BL-exposed cultures was also significant (t = 4,08; p<0,05). In *A. alternata* conidial yields increased in RL- and BL-cultures *versus* control cultures (t = 3,65 and t = 3,02, respectively; p<0,05 in both cases). In *F. fujikuroi* no light-induced changes were observed for this parameter.

No effect of RL or BL exposure on the size of conidia in studied fungal species was observed (Fig. 2B). The germination of conidia collected in RL-cultures was indistinguishable from that in control cultures of *A. alternata* and *F. fujikuroi* and slightly suppressed in other three microscopic fungi (Fig. 2C). Some decline of conidial germination was found in BL-exposed cultures of all five fungi species, and for *F. fujikuroi* a difference with control was significant (t = 3,14; p<0,05).

Biochemical parameters measured in RL- or BL-exposed fungal cultures are given in Table 2. RL exposure led to some elevation of protein contents in *A. clavatus*, *T. viride* and *A. alternata* (p>0,05 for all three species) and to significant decrease in *P. citrinum* (t = 4,67; p<0,01) and *F. fujikuroi* (t = 6,83; p<0,01). Also, protein contents were lower in BL-cultures of *P. citrinum* (t = 3,18; p<0,05) and *F. fujikuroi* (t = 7,7; p<0,01), than in their controls. Due to the opposite directions of the changes of protein contents in RL- and BL-cultures of *T. viride* the meaningful difference occurred between these experimental series (t = 3,13; p<0,05).

A tendency of increased phenolic content occurred in the exposed cultures of all studied species, but the difference in comparison to the control didn't reach a statistical significance even for the 20% increase in RL-cultures of *A. alternata* (t = 1,54; p>0,05).

The assessment of fungal antagonistic properties gave results as follows. *A. clavatus* caused TO of both test bacteria species. *P. citrinum* showed TO of *E. coli* and AA against *B. subtilis*. *F. fujikuroi* provided AA against *E. coli* and PA towards *B. subtilis*. *T. viride* and *A. alternata* appeared to be neutral towards both the tested bacterial species. These patterns occurred in all experimental series of a particular fungal species; i.e. RL- or BL-exposure didn't influence the antagonistic properties of the studied microscopic fungi.

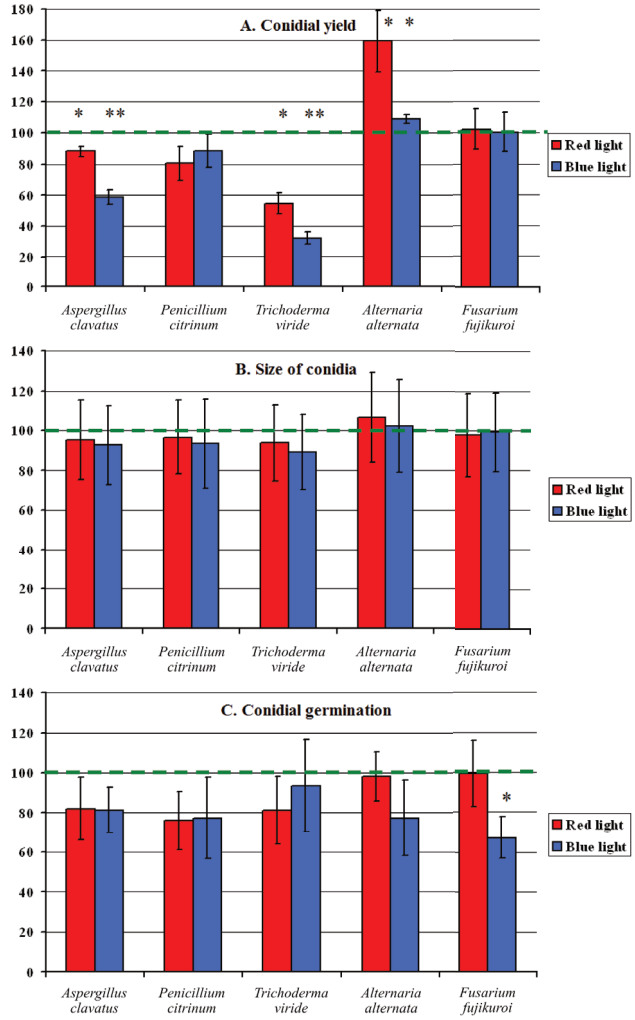

Figure 2. Conidial production in cultures of different species of soil microscopic fungi grown after brief exposure to red or blue monochromatic light. A: Conidial yield; B: Size of conidia; C: Conidial germination rate. Data are presented as a percent of the respective control values (the latter is indicated by the dashed line). Statistically significant changes of measured parameters in light exposed cultures in comparison to the control are indicated by the asterisk: * = p<0,05; ** = p<0,01.

Discussion

The responses to the light signal are very diverse between fungal species and can be either up- or down-regulative, depending on duration, intensity and spectral characteristics of the light fluence (Tisch and Schmoll 2010; Fuller et al. 2015; Corrochano 2019). It is still impossible to predict a total range of photoinduced effects for a certain fungal genus, or family, or even class. The results of our study confirm this opinion. Each of five soil fungal species used in present experiment displayed its own, unique pattern of growth reactions and biochemical changes caused by brief exposure of the 24-h culture, initiated from a small piece of mycelium, to monochromatic blue or red light.

Comparison of the end-sizes of colonies (day 10) in the exposed and unexposed series revealed that RL illumination resulted in growth reduction in *P. citrinum* (16%) and increase of growth in other species (5-13%), while BL exposure reduced the growth of *P. citrinum* and *T. viride* (16 and 20%, respectively) but increased the growth of the other three species (6-22%). However, such variations actually resulted from a combination of an early growth response and more prolonged growth rate reaction. BL caused a growth delay at the starting phase in *A. clavatus*, *P. citrinum* and *T. viride* and speeded up of the subsequent growth in *A. clavatus*, *P. citrinum*, *T. viride* and *F. fujikuroi*, as estimated from changes of *c* coefficient of the growth equation (Table 1). RL effects included a delay of initial growth phase in *A. clavatus* and its remarkable stimulation in *A. alternata*, while growth rate was increased in *A. clavatus* and *F. fujikuroi* but reduced in *A. alternata*. The overall changes of the fungal growth rate, either stimulation or reduction, appeared to be somewhat more prominent after BL exposure, than in RL-treated cultures. That agrees with findings of other researchers, who concluded stronger effect of BL, than of other wavelengths, on fungal morphogenesis, metabolic activity, development and behavior (Corrochano 2007, 2011; Herrera-Estrella and Horwitz 2007; Tisch and Schmoll 2010).

The radial growth is widely accepted as the integral parameter of physiological status of microscopic fungi, but growth reactions, probably, are the most complex phenomena in fungal photobiology (Moore 1998; Kotov and Reshetnikov 1990; Kotov et al. 2005; Karpenko 2010). In our study, the exposure of *T. viride* to RL led to a remarkable intensification of the radial growth, meanwhile there are reported data that RL provoked reduction in mycelial growth in *Trichoderma* (Schmoll et al. 2010). This is a good example of the intra-species and inter-experiment heterogeneity in fungal photobiology.

A photoinduced decline in mycelial growth was observed for numerous fungal species, and the mechanism appeared to be based on the activation of oxidative stress (Fuller et al. 2015). That was proved by the experiment, in which a white light-dependent reduction in growth rate of *Botritis cinerea* was abolished simply by an addition of the antioxidant to the medium (Canessa et al. 2013). The phenomenon of the regulation of fungal growth response to the light by the contents of culture medium had been known for decades (Tisch and Schmoll 2010). This underlines the importance of keeping the culture conditions identical for all species used in such comparative experiments.

Conidial yield and conidial germination are very important characteristics in fungal photobiology, and

Table 2. Changes of biochemical parameters measured in fungal cultures grown after their exposure to the light of different wavelength (mean ± SE).

Exposure conditions	*A. clavatus*	*P. citrinum*	*T. viride*	*A. alternata*	*F. fujikuroi*
	Protein contents (mg/g of raw mass)				
Control	311 ± 27	746 ± 65	280 ± 24	498 ± 43	639 ± 55
Red light	361 ± 31	40 1± 35**	356 ± 31	632 ± 55	237 ± 21**
Blue light	371 ± 32	498 ± 43*	239 ± 21#	558 ± 48	194 ± 17**
	Phenol contents (% of mycelium mass)				
Control	1,05 ± 0,15	1,03 ± 0,19	1,13 ± 0,17	4,50 ± 0,39	0,91 ± 0,14
Red light	1,22 ± 0,18	1,35 ± 0,20	1,40 ± 0,21	5,44 ± 0,47	1,12 ± 0,19
Blue light	1,13 ± 0,17	1,24 ± 0,16	1,21 ± 0,22	4,93 ± 0,43	1,23 ± 0,18

Difference is statistically significant: * = versus control at p<0,05; ** = versus control at p<0,01; # = between RL- and BL-cultures at p<0,05.

high heterogeneity of the photo-induced changes of these parameters arises in classic or recent reports (Calpouzous and Chang 1971; Hill 1976; Betina and Zajacova 1978; Pokorný et al. 2005; Schmoll et al. 2010; Corrochano and Garre 2010; Rangel et al. 2011; Oliveira et al. 2018). In our study the size of conidia was not affected by either BL or RL (Fig. 2). However, the exposure of the starting culture to RL led to the decrease of conidia numbers and their reduced germination in *A. clavatus, P. citrinum* and *T. viride*. By contrast, RL-treated cultures of *A. alternata* showed an elevated conidial yield. The exposure to BL produced a negative effect on the conidial yield again in *A. clavatus, P. citrinum* and *T. viride*, while a decrease in the germination rate did not occur in the latter species but was noticeable in four other species.

Such a diversity of the positive or negative effects of the monochromatic light on conidiation is not surprising (Schumaher 2017). It was regularly shown that blue and/or red light can repress or stimulate the asexual development in fungal species of the same genera. At one hand, in many fungi the conidiogenesis requires a light pulse to be initiated (Tisch and Schmoll 2010). A near-UV light, alone or combined with cool-white light, enhances conidiation in *Fusarium* and many other fungi (Avalos and Estrada 2010). On another hand, a negative influence of light signal on the conidiation is also well known. In *Fusarium graminearum* a significant decrease of the viability of conidia under BL exposure was shown (De Lucca et al. 2012), and in *Alternaria* a photo-induced downregulation of the conidial production can be effectively blocked by riboflavin (Soderhall et al. 1978; Kritsky et al. 2010). Experiments on *Aspergillus nidulans* showed that light-regulated morphogenetic pathways integrate blue and red-light action, and full stimulation of conidial production was only achieved with a combination of red and blue light (Bayram et al. 2010).

The results of our study support the opinion that fungi perceive a brief light exposure, especially to BL, primarily as a stress signal and due to this conidiation and/or germination become repressed in favor of the induction of stress resistance pathways (Fuller et al. 2015). This hypothesis is partially confirmed by 'no negative effect' on the conidiation in RL-exposed cultures of both pigmented species – *A. alternata* and *F. fujikuroi*, for which RL probably is not that effective stress messenger, because these fungi are evolutionary better prepared to protect themselves against light-induced damage, e.g. by the increase of carotenoid content (Stahl and Sies 2005; Avalos and Estrada 2010).

The assessment of potential changes in protein content and antimicrobial activity seems to be a reasonable part of our study in view of the biotechnological usage of many fungal species. The effects of light exposure on growth, metabolism and productivity were investigated in microscopic fungi, which can produce biologically active secondary metabolites, including carotenoids and antibiotics (Kato et al. 2003; Sprote and Brakhage 2007; Myung et al. 2009; Tisch and Schmoll 2010; Avalos and Estrada 2010; Corrochano and Garre 2010). The idea of the intentional stimulation of protein production or enhancement of bacteriostatic properties by a simple procedure of brief light exposure is very attractive. However, in our experiment neither BL, nor RL exposure of microscopic fungi changed their species-specific antagonistic activity towards bacteria. The fluctuations in protein content corresponded to the respective growth reactions in all studied species except *F. fujikuroi*, in which the decrease in protein contents in exposed cultures contrasted to the elevation of colony size; a divergence between growth and biochemical parameters was especially apparent in BL series (Table 2). A possible reason for this finding needs to be further explored.

Inter-taxons differences in the changes of the fungal protein metabolism in response to light exposure were already described in the literature (Hill 1976; Strigácová et al. 2001; Pokorný et al. 2005; Tisch and Schmoll 2010).

Several reports with transcriptomic data showed that fungal photoreactions require new proteins in sufficient quantities. However, the underlying molecular mechanisms are also rather diverse. The well studied fungal blue light photoreceptor class, the White Collar complex (WCC), works as a general transcriptional activator in *Neurospora*, but it is thought to play repressive roles in other species, including *Aspergillus*, *Alternaria*, *Trichoderma*, *Fusarium* and *Cercospora* (Fuller et al. 2015).

The moderate elevation of phenol content in BL- or RL-exposed cultures appeared to be a common trait for all five fungal species in present work (Table 2). That can be an adaptive reaction, aimed at the development of tolerance to possible further damaging impact of light via the regulation of pigment synthesis (Corrochano and Garre 2010; Karpenko 2010; Schumacher 2017). The modulation of the UV stress response by a preliminary light exposure is a well known phenomenon, e.g. observed in *Metarhizium acridum*, and the respective molecular machinery of the signaling cascade leading to the up-regulation of certain genes involved in the UV protection has been already described (Rangel et al. 2015; Brancini et al. 2016, 2018a, 2019; Dias et al. 2020). Experiments with testing different fungal species to UV stress may clarify this hypothesis. Also, it seems reasonable to check whether a brief exposure to the monochromatic light may affect the differential susceptibility of microscopic fungi to antifungal agents, similarly to what has been done using *Metarhizium* species (Brancini et al. 2018b), as this characteristic can be an important species-specific trait in different ecological niches.

It should be underlined that the design of present experiment included a relatively brief exposure of the starting fungal culture. Such a methodology had been applied earlier in classic studies; e.g. there were reports that just 1-min illumination exposure of *Neurospora crassa* mycelia resulted in a minor but significant induction of colored carotenoid biosynthesis (Zalokar 1955; Schrott 1980). The exposure to the light lasted for 2 seconds appeared to be enough to induce detectable induction of sporulation in *T. viride* (Betina and Zajacova 1978). Moreover, the photoinduction of conidiation in *Trichoderma* can be 'remembered' while the culture is maintained in conditions that do not allow cellular growth (e.g., low temperature or hypoxia); as soon as growth is resumed, under optimal conditions, the colony conidiates (Schmoll et al. 2010).

Obviously, our results can be hardly compared to published datasets and conclusions, which were obtained using protracted exposure of fungal mycelium or conidia. The experiments involving a longer term, continuous or fractionated light exposure suit better for revealing complex adaptive reactions, which are based on the feedback regulation, e.g. phototropism, circadian rhythm or changes in sporulation or sexual development. Under the prolonged illumination the photoinduced gene expression is increased or decreased according to positive or negative feedbacks, respectively (Schumaher 2017). In contrast to that, a single brief action of the monochromatic light induces longer term or delayed responses via one-way triggering mechanism, which probably involves a quick alteration of several key global metabolic regulators, like photo-induced fungal protein velvet A (Kato et al. 2003; Sprote and Brakhage 2007; Purschwitz et al. 2009; Tisch and Schmoll 2010).

The starting stage of the photosensing in fungi is already quite well understood; it is mediated by highly sophisticated signaling machinery, which may contain at least eleven potential photoreceptors (Schumaher 2017). The set of photoresponsive proteins in microscopic fungi is evolutionary conserved and include orthologs of White Collar proteins (in *Trichoderma* it is "Blue Light-Receptors" BLR1 and BLR2), cryptochromes, photolyases, phytochromes and photoactive opsins (Avalos and Estrada 2010; Bayram et al. 2010; Igbalajobi et al. 2019; Schmoll et al. 2010; Schumaher 2017). Such a complex fungal 'eye' allows it to react to a broad spectrum of wavelengths, integrating (near)-UV, blue, green, red and far-red light signals. Photoreceptors typically consist of an apoprotein and a chromophore that reacts by isomerization or reduction to light of a certain wavelength through absorption of a photon with a defined amount of energy. The associated structural changes in the chromophore induce conformational changes in the apoprotein leading to signal transduction via the output domains – if present – or via protein-protein interactions (Bayram et al. 2010).

The early phase of the photoinduced gene expression in fungi is very eventful; in *N. crassa* new transcripts were detectable as early as 2 min after the BL signal and within 30 min from 60 to 80 genes were regulated (Sommer et al. 1989). It seems possible, that the subsequent downstream chain of events includes the occurrence of a self-sustaining cascade or cycle of signals. However, the exact ontogenetic links between the elements of such a regulatory network that finally ends up in protracted metabolic changes and physiological reactions still need to be elucidated.

In general, our study showed that photo-induced effects in soil microscopic fungi depend on the light wavelength and had a remarkable inter-species heterogeneity. Gross, long lasting physiological and biochemical responses occurring in microscopic fungi after brief light exposure point at the directions of future studies that might be aimed at the discovering of the underlying regulatory mechanisms, signaling cascades and transcriptional changes in fungal species from different taxons. It is

particularly desirable to revise the photo-induced fungal reactions in the experiments involving various stress impacts and non-optimal growth conditions, which might occur in natural habitats. That might contribute to better understanding of fungal biology with regard to their role in various ecological niches.

Conclusions

A relatively brief (30 min) exposure of 24-h cultures of soil microscopic fungi to monochromatic blue or red light is sufficient to induce long-lasting effects observed during their long-term culture. The responses to the light signal appeared to be species-specific and dependent on the wavelength.

Overall radial growth was not remarkably affected by any of the two light wavelengths in *A. clavatus* but delayed in *P. citrinum* and stimulated in *A. alternata* and *F. fujikuroi*, and these changes were more pronounced after BL, than after RL exposure. The BL illumination of *T. viride* culture led to its growth delay, whereas the RL caused the enhancement of the growth rate. Protein content followed the patterns of radial growth changes in all species except *Fusarium,* in which it was decreased after both BL and RL exposure. The moderate elevation of phenol content in BL- or RL-exposed cultures was noted in all five fungal species and probably was an adoptive reaction aimed to help their resistance against possible further light exposure. Conidial yield and conidial germination were reduced in RL-exposed cultures of *Aspergillus, Penicillium* and *Trichoderma*. By contrast, RL-treated *Alternaria* cultures showed a significantly elevated conidial yield and normal conidial germination. The exposure to BL negatively affected both conidial yield and germination in *A. clavatus* and *P. citrinum*, while *T. viride* showed a reduced conidial yield only, and BL-exposed *A. alternata* and *F. fujikuroi* had a decreased conidial germination rate. The size of conidia and fungal antagonism towards test bacteria showed no changes in response to the light signal.

Future research, particularly using transcriptomic and proteomic methods, must reveal the molecular machinery and signaling pathways underlying long-lasting effects induced in fungi by a brief light exposure.

Acknowledgement

The study was performed as a part of the general Research Program of V.N. Karazin Kharkiv National University (Kharkiv, Ukraine).

References

Avalos J, Estrada AF (2010) Regulation by light in *Fusarium*. Fungal Genet Biol 47(11):930-938.

Bayram O, Braus GH, Fischer R, Rodriguez-Romero J (2010) Spotlight on *Aspergillus nidulans* photosensory systems. Fungal Genet Biol 47(11):900-908.

Betina V, Zajacova J (1978) Regulation of periodicity and intensity of photo-induced conidiation of *Trichoderma viride*. Folia Microbiol (Praha) 23:453-459.

Bilay VI (Ed.) (1982) Methods of Experimental Mycology. Reference Handbook. Naukova Dumka, Kyiv [in Russian].

Brancini GT, Rangel DE, Braga GÚ (2016) Exposure of *Metarhizium acridum* mycelium to light induces tolerance to UV-B radiation. FEMS Microbiol Lett 363(6). pii: fnw036.

Brancini GTP, Bachmann L, Ferreira MEdS, Rangel DEN, Braga GÚL (2018a) Exposing *Metarhizium acridum* mycelium to visible light up-regulates a photolyase gene and increases photoreactivating ability. J Invertebr Pathol 152:35-37.

Brancini GTP, Tonani L, Rangel DEN, Roberts DW, Braga GUL (2018b) Species of the *Metarhizium anisopliae* complex with diverse ecological niches display different susceptibilities to antifungal agents. Fungal Biol 122(6):563-569.

Brancini GTP, Ferreira MES, Rangel DEN, Braga GÚL (2019) Combining transcriptomics and proteomics reveals potential post-transcriptional control of gene expression after light exposure in *Metarhizium acridum*. G3: Genes Genom Genet 9:2951-2961.

Calpouzous L, Ho-Shii Chang (1971) Fungus spore germination inhibited by blue and far red radiation. Plant Physiol 47(5):729-730.

Canessa P, Schumacher J, Hevia M, Tudzynski P, Larrondo L (2013) Assessing the effects of light on differentiation and virulence of the plant pathogen *Botrytis cinerea*: characterization of the *White Collar* complex. PLoS One 8:84223.

Corrochano LM (2007) Fungal photoreceptors sensory molecules for fungal development and behaviour. Photochem Photobiol Sci 6(7):725-736.

Corrochano LM (2011) Fungal photobiology: a synopsis. IMA Fungus. 2(1):25-28.

Corrochano LM (2019) Light in the fungal world: From photoreception to gene transcription and beyond. Annu Rev Genet 53:149-170.

Corrochano LM, Garre V (2010) Photobiology in the *Zygomycota*: multiple photoreceptor genes for complex responses to light. Fungal Genet Biol 47(11):893-899.

De Lucca AJ, Carter-Wientjes C, Williams KA, Bhatnagar D (2012) Blue light (470 nm) effectively inhibits bacterial

and fungal growth. Lett Appl Microbiol 55(6):460-466.
Dias LP, Pedrini N, Braga GUL, Ferreira PC, Pupin B, Araújo CAS, Corrochano LM, Rangel DEN (2020) Outcome of blue, green, red, and white light on *Metarhizium robertsii* during mycelial growth on conidial stress tolerance and gene expression. Fungal Biol 2020 124(5):263-272.
Fuller KK, Loros JJ, Dunlap, JC (2015) Fungal photobiology: visible light as a signal for stress, space and time. Curr Genet 61(3):275-288.
Herrera-Estrella A, Horwitz BA (2007) Looking through the eyes of fungi: molecular genetics of photoreception. Mol Microbiol 6(1):5-15.
Hill EP (1976) Effect of light on growth and sporulation of *Aspergillus ornatus*. J Gen Microbiol 95(1):39-44.
Idnurm A, Heitman J (2005) Photosensing fungi: phytochrome in the spotlight. Curr Biol 15:R829-R832.
Igbalajobi O, Yu Z, Fischer R (2019) Red- and blue-light sensing in the plant pathogen *Alternaria alternata* depends on phytochrome and the white-collar protein LreA. mBio 10:e00371-19.
Kato N, Brooks W, Calvo AM (2003) The expression of sterigmatocystin and penicillin genes in *Aspergillus nidulans* is controlled by veA, a gene required for sexual development. Eukaryot Cell 2(6):1178-1186.
Karpenko IuV (2010) Influence of light of different spectral composition on growth characteristics of microscopic fungi. Mikrobiol Zh 72(6):36-42. [in Ukrainian; English abstract].
Korobov AM, Korobov VA (2012) Photon-magnetic matrices "Barva-Flex/PM24". Photobiol Photomed 9(1,2):132-142. [in Russian; English abstract].
Kotov VN, Reshetnikov SV (1990) A stochastic model for early mycelial growth. Mycol Res 94(5):577-586.
Kotov V, Anishchenko I, Sirenko I, Reshetnikov S (2005) Statistical analysis of structural and kinetic characteristics of fungal colony growth with *Trichoderma viride* Pers.: S.F. Gray. Microbiol Res 160:273-278.
Kritsky MS, Telegina TA, Vechtomova YL, Kolesnikov MP, Lyudnikova TA, Golub OA (2010) Excited molecules of flavin and pterin coenzyme in evolution. Biochemistry 75(10):1348-1366 [in Russian; English abstract].
Laringuet P, Dunand C (2005) Plant photoreceptors: Phylogenetic overview. J Mol Evol 61(4):559-569.
Lokhandwala J, Hopkins HC, Rodriguez-Iglesias A, Dattenböck C, Schmoll M, Zoltowski BD (2015) Structural biochemistry of a fungal LOV domain photoreceptor reveals an evolutionarily conserved pathway integrating light and oxidative stress. Structure 23(1):116-125.
Ma S, Kim C, Neilson AP, Griffin LE, Peck GM, O'Keefe SF, Stewart AC (2019) Comparison of common analytical methods for the quantification of total polyphenols and flavanols in fruit juices and ciders. J Food Sci 84(8):2147-2158.
Moore D (1998) Hyphal growth. Metabolism and biochemistry of hyphal systems. In Moore D, Ed., Fungal Morphogenesis. University Press, Cambridge, pp. 26-134.
Myung K, Li S, Butchko RA, Busman M, Proctor RH, Abbas HK, Calvo AM (2009) FvVE1 regulates biosynthesis of the mycotoxins fumonisins and fusarins in *Fusarium verticillioides*. J Agric Food Chem 57(11):5089-5094.
Oliveira AS, Braga GUL, Rangel DEN (2018) *Metarhizium robertsii* illuminated during mycelial growth produces conidia with increased germination speed and virulence. Fungal Biol 122(6):555-562.
Pokorný R, Vargovic P, Hölker U, Janssen M, Bend J, Hudecová D, Varečka L (2005) Developmental changes in *Trichoderma viride* enzymes abundant in conidia and the light-induced conidiation signalling pathway. J Basic Microbiol 45(3):219-229.
Protsenko MA, Kostina NE (2015) Elaboration and validation of methods of quantitative analysis of phenolic compounds and flavonoids in the extracts of higher fungi. Chemistry of plant materials 3:117-126. [in Russian].
Purschwitz J, Muller S, Kastner C, Fischer R (2006) Seeing the rainbow: light sensing in fungi. Curr Opin Microbiol 9(6):566-571.
Purschwitz J, Muller S, Fischer R (2009) Mapping the interaction sites of *Aspergillus nidulans* phytochrome FphA with the global regulator VeA and the White Collar protein LreB. Mol Genet Genom 281(1):35-42.
Rangel DEN, Braga GUL, Fernandes ÉKK, Keyser CA, Hallsworth JE, Roberts DW (2015) Stress tolerance and virulence of insect-pathogenic fungi are determined by environmental conditions during conidial formation. Curr Gen 61:383-404.
Rangel DEN, Fernandes EKK, Braga GUL, Roberts DW (2011) Visible light during mycelial growth and conidiation of *Metarhizium robertsii* produces conidia with increased stress tolerance. FEMS Microbiol Lett 315:81-86.
Schmoll M, Esquivel-Naranjo EU, Herrera-Estrella A (2010) *Trichoderma* in the light of day – physiology and development. Fungal Genet Biol 47(11):909-916.
Schrott EL (1980) Fluence response relationship of carotenogenesis in *Neurospora crassa*. Planta 150:174-179.
Schumacher J (2017) How light affects the life of *Botrytis*. Fungal Genet Biol 106:26-41.
Soderhall K, Svensson E, Unestam T (1978) Light inhibits the production of alternariol and alternariol monomethyl ether in *Alternaria alternata*. Appl Environ Microbiol 36(5):655-657.
Sommer T, Chambers JA, Eberle J, Lauter FR, Russo VE (1989) Fast light-regulated genes of *Neurospora crassa*. Nucleic Acids Res 17:5713-5723.
Sprote P, Brakhage AA (2007) The light-dependent regulator velvet A of *Aspergillus nidulans* acts as a repressor of the penicillin biosynthesis. Arch Microbiol 188:69-79.

Stahl W, Sies H (2005) Bioactivity and protective effects of natural carotenoids. Biochim Biophys Acta 1740:101-107.

Strigácová J, Chovanec P, Liptaj T et al (2001) Glutamate decarboxylase activity in *Trichoderma viride* conidia and developing mycelia. Arch Microbiol 175(1-2):32-40.

Tisch D, Schmoll M (2010) Light regulation of metabolic pathways in fungi. Appl Microbiol Biotechnol 85(5):1259-1277.

Waterborg JH, Matthews HR (1994) The Lowry method for protein quantitation. In Walker JM, Ed. Methods in Molecular Biology. Vol. 32. Basic Protein and Peptide Protocols. The Humana Press, Totowa, NJ, USA, pp. 1-4.

Yu Zh, Fischer R (2019) Light sensing and responses in fungi. Nat Rev Microbiol 17(1):25-36.

Zalokar M (1955) Biosynthesis of carotenoids in *Neurospora*. Action spectrum of photoactivation. Arch Biochem Biophys 56:318-325.

Acta Biologica Szegediensis

Volume 64(1):37-42, 2020
Acta Biologica Szegediensis
http://abs.bibl.u-szeged.hu/index.php/abs
DOI:10.14232/abs.2020.1.37-42

ARTICLE

Functional skull asymmetries in *Carollia perspicillata* (Phyllostomidae Gray, 1825: Carollinae)

Pere M. Parés-Casanova*, Gerard Otin

Department of Animal Science, School of Agrifood and Forestry Science and Engineering (ETSEA), University of Lleida, 25198 Lleida, Catalonia, Spain

ABSTRACT Analysing asymmetry in wild or domestic species enables the evaluation of the morphological responses to functional requirements and/or stress. This report is a study of the cranial asymmetry of Seba's short-tailed bat *Carollia perspicillata* by means of geometric morphometric techniques. We studied three types of bilateral asymmetries -fluctuating asymmetry, directional asymmetry and antisymmetry- using 15 skull landmarks on dorsal aspect of 45 skulls of *Carollia perspicillata* (21 males and 24 females) from different localities in Colombia. Directional asymmetry appeared to be significant and clearly higher than fluctuating asymmetry, with the braincase presenting the larger variance. There were no differences between sexes. Echolocation has a great anatomical effect on the bat cranium, and this would explain detected asymmetry.
Acta Biol Szeged 64(1):37-42 (2020)

KEY WORDS
Chiroptera
echolocation
neurocranium
shape sexual dimorphism
Seba's short tailed bat

ARTICLE INFORMATION
Submitted
01 June 2020.
Accepted
24 July 2020.
***Corresponding author**
E-mail: peremiquelp@ca.udl.cat

Introduction

Bilateral asymmetry refers to the non-correspondence in size and/or shape, and location of landmarks on opposite sides of the median sagittal plane. There are three main types of bilateral asymmetry: directional asymmetry (DA), fluctuating asymmetry (FA) and antisymmetry (AS) (Mendes 2008). DA is present when left and right sides consistently differ from each other (Klingenberg et al. 2002). FA is a pattern of subtle non-directional differences between sides (Klingenberg et al. 2002). AS, finally, represents a directional deviation from symmetry towards either the right or left side (Graham et al. 1993).

The use of FA variance has been considered a measure of developmental stability, constituting an indicator for the influence of environmental factors on a population (Tuyttens et al. 2005; Nuffel et al. 2007) and large values of FA are interpreted to reflect worse environmental conditions and hence decreased welfare (Tuyttens et al. 2005). DA and AS are considered inappropriate for the estimation of the underlying developmental instability because of their presumed heritable component (Graham et al. 1993; Tuyttens et al. 2005).

Carollia Gray, 1838 is a genus in the Phyllostomidae family, which is located on South and Central America, being among the most common mammal group in the Neotropics (Gardner 2007; Bolzan et al. 2015). They are bats of robust and medium size, with prominent nose leaves, consisting of a lower part immediately surrounding the nostrils and a pronounced lancet extending dorsally, thought to be associated with sound emission for echolocation but trade-off with other sensory modalities such as olfaction and vision (Arbour et al. 2019). Some researchers have suggested that variation in nostrils size is the main source of the morphological plasticity of phyllostomes, although there is a lack of studies on the patterns of variation (López-Aguirre et al. 2015). Eight species are currently recognized (Gardner 2007): *Carollia sowelli, C. subrufa, C. manu, C. monohernandezi, C. benkeithi, C. brevicauda, C. castanea* and *C. perspicillata* (López-Aguirre et al. 2015). Colombia holds the highest variety of philostomide species, where until now four species have been described: *C. brevicauda, C. castanea, C. monohernandezi* and *C. perspicillata* (López-Aguirre et al. 2015). Seba's short-tailed bat (*Carollia perspicillata*) inhabits wet perennials and dry deciduous forests, usually below 1,000 meters of altitude, usually perched on groups of till 100 animals in caves, hollow trees, tunnels and sewers of roads. It feeds on fruits as well as pollen and insects (Brinkløv et al. 2011).

The skull is a complex morphological structure with high adaptative significance and often used in studies of asymmetries (Urošević et al. 2015). Variation in skull and

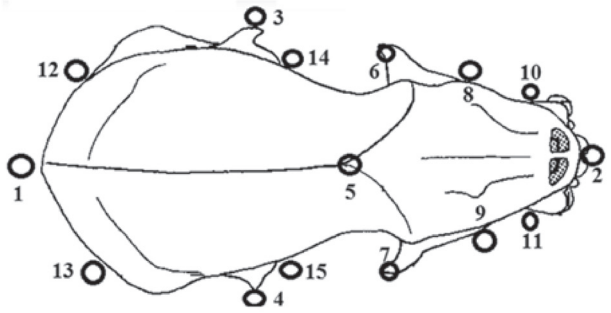

Figure 1. *Carollia* sp. Location of the 15 landmarks on the dorsal view.

body morphology has been used extensively to reconstruct ontogenetic processes in bats (McLellan 1984; Willig et al. 1986; Ruelas 2017; Ruelas and López 2018), but much less work has been done on asymmetries (López-Aguirre and Pérez-Torres 2015). Against this background, the main aims of our study were to (i) examine a sample of *C. perspicillata* for the presence of AS, FA and DA, (ii) test whether sexes differ in the extent of DA. We hypothesize that symmetry of skull in that species can be modified as an adaptation for echolocation.

Materials and methods

Sample collection

A total of 45 specimens of *Carollia perspicillata* (21 males and 24 females) originated from Colombia and initially collected for use in other studies was studied. This material is currently deposited in the Universidad del Cauca, in Popayán (Colombia). Damaged skulls had been previously excluded. Images were captured on the dorsal aspect using a digital camera (Nikon D1500) equipped with a lens (Nikon DX de 18-105 mm), with skull levelled on the horizontal plane. Each image included a 10 mm ruler. The images were later stored in JPEG format.

Geometric morphometrics

We employed landmark-based geometric morphometric techniques for the study. Fifteen landmarks -5 on the neurocranium –braincase, which surrounds and protects the brain-, 7 on the viscerocranium -which supports the functions of feeding and breathing, and forms the face in mammals- and 3 on the midline- (Fig. 1) were positioned on dorsal aspect of each skull using the TpsDig v. 2.26 software (Rohlf 2010). These landmarks, expressed as *x, y* coordinates in Cartesian space, were considered to be homologous and topographically equivalent and sufficiently summarise the skull morphology of the dorsal structures. They were digitized by second author. Differences in size, position, translation, and rotation were deleted using Generalised Procrustes Analysis (Bookstein 1991). To quantify and minimize measurement error, skulls were digitized two times.

Statistical analysis

Prior to calculation of measurement error and asymmetry, the data were checked for AS. For this we used the Kolmogorov-Smirnov *D* test to test for overall equal distribution of signed right–left hemiskull size, expressed as centroid size (CS, the square root of the sum of squared distance between each landmark and the skull centroid) (Bookstein 1991). A Procrustes ANOVA on Procrustes coordinates were used to assess the contribution of individual variation, DA ("Sides" as the fixed factor), FA ("Individuals*Sides" interaction), and measurement error to the overall shape variation (Klingenberg et al. 2002). Shape variation was separated into a symmetric component (among-individual variation) and an asymmetric component (within-individual variation), but only the asymmetric component was considered in this study. The asymmetric component was quantified through the landmark deviation of the original configuration from the symmetric consensus of the original and mirror images.

Shape symmetric differences between sexes were assessed by a Canonical Variates Analysis (CVA), with sex as the grouping variable using Mahalanobis distance and a 10 000 permutations test. The pattern of asymmetric shape variation among the sexes was studied by means of a Principal Component Analysis (PCA). Furthermore, Partial Least Squares (PLS) analysis of covariation within the configuration of neurocranial and viscerocranial landmarks and a modularity check were performed to test if shape changes were independent between those two parts of the skull. Finally, we analysed allometry to determine whether size had an effect on shape asymmetry. Shape asymmetry (asymmetric component) was regressed onto CS (values log-transformed). The statistical significance of this regression was estimated using the permutation test with 10,000 iterations.

Morphometric and statistical analyses were conducted using the MorphoJ v. 1.07a (Klingenberg 2011) and PAST v. 2.17c (Hammer et al. 2001) packages.

RESULTS

Measurement error and antisymmetry

Kolmogorov-Smirnov test demonstrated that signed difference between right and left hemiskulls did not differ significantly ($D = 0.088$, $p = 0.844$). Thus, we focused on the study of entire skull form FA and DA. We also visually

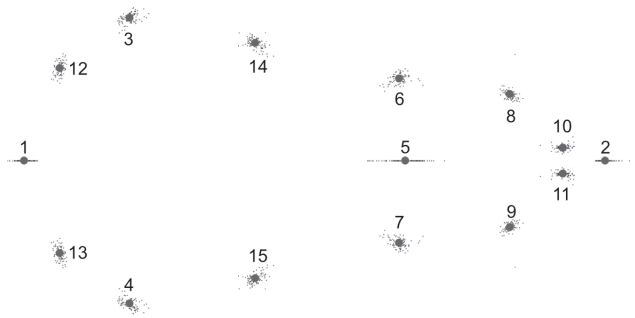

Figure 2. Scatter plot of points of left-right differences for each land mark after superimposition by the Procrustes algorithm. There was no evidence for clustering of these points that would have suggested antisymmetry.

Table 1. Loadings for Principal Components 1 and 2, which explained a 65.3% of the total observed variance (PC1 + PC2 = 39.1% + 26.1%). Differences were located mainly on neurocranium length (coordinates x 3, 4, 12 and 13) and orbital length and width (landmarks x,y 14 and 15) (in bold).

Coordinate	PC1	PC2
x1	0	0
y1	0.078497	-0.47503
x2	0	0
y2	-0.15667	0.225681
x3	**-0.38106**	0.150365
y3	0.186871	0.271757
x4	**0.381055**	-0.15037
y4	0.186871	0.271757
x5	0	0
y5	-0.2382	-0.51175
x6	-0.12242	0.082166
y6	-0.10229	-0.27036
x7	0.122419	-0.08217
y7	-0.10229	-0.27036
x8	-0.11485	0.037143
y8	-0.00824	0.137144
x9	0.114847	-0.03714
y9	-0.00824	0.137144
x10	-0.02638	-0.01853
y10	-0.14299	0.114636
x11	0.026379	0.018531
y11	-0.14299	0.114636
x12	**-0.21282**	0.049994
y12	-0.06794	0.03923
x13	0.212816	-0.04999
y13	-0.06794	0.03923
x14	-0.28404	0.094742
y14	0.292775	0.088144
x15	0.284044	-0.09474
y15	0.292775	0.088144

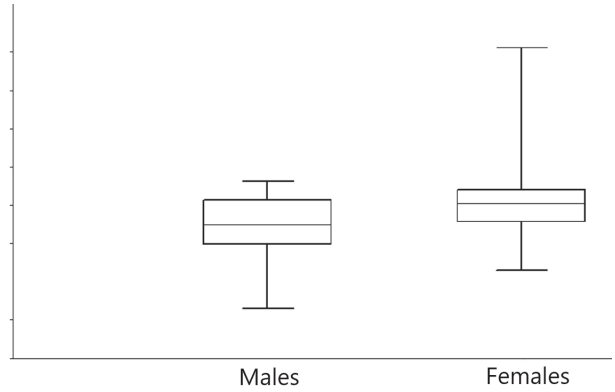

Figure 3. Box plot for skull sizes of *C. perspicillata* grouped by sex (21 males and 24 females), expressed as centroid size (*Y*-axis). For each sample, the 25-75 percent quartiles are drawn using a box. The median is shown with a horizontal line inside the box. The minimal and maximal values are shown with short horizontal lines ("whiskers"). Skull sizes appeared statistically different for both sexes (Levene's value 0.677, $F_{1,88}$ = 7.959, p = 0.0059), being those of females clearly bigger.

examined scatter plot of points of left-right differences for each landmark after superimposition by the Procrustes algorithm. There was no evidence for clustering of these points (as the equivalent to bimodal distributions of left-right differences) that would have suggested AS (Fig. 2).

Differences in size and shape asymmetry

Skull sizes appeared statistically different for sexes (Levene's value 0.677, $F_{1,88}$ = 7.959, p = 0.0059), being those of females clearly bigger (Fig. 3), but there were no significant differences between females' and males' shape asymmetry (Mahalanobis distances = 0.839, p = 0.262), thus in subsequent analyses sexes were not analysed separately. Morphometric CVA space reflected a gamut of continuous variation and overlap for both sexes (Fig. 4).

Procrustes ANOVA showed that FA, DA, and individual

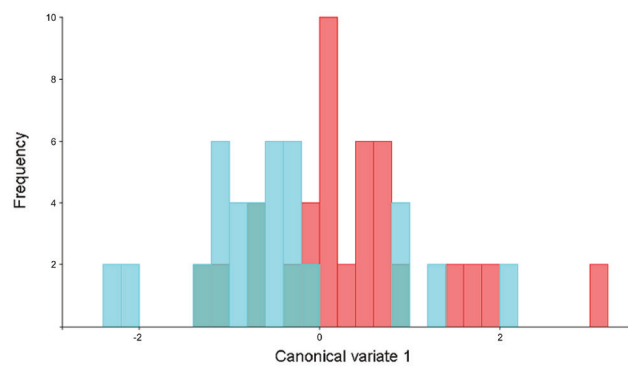

Figure 4. Canonical Variate Analysis results for the axis of CV1 for males (21) and females (24) of *C. perspicillata*.

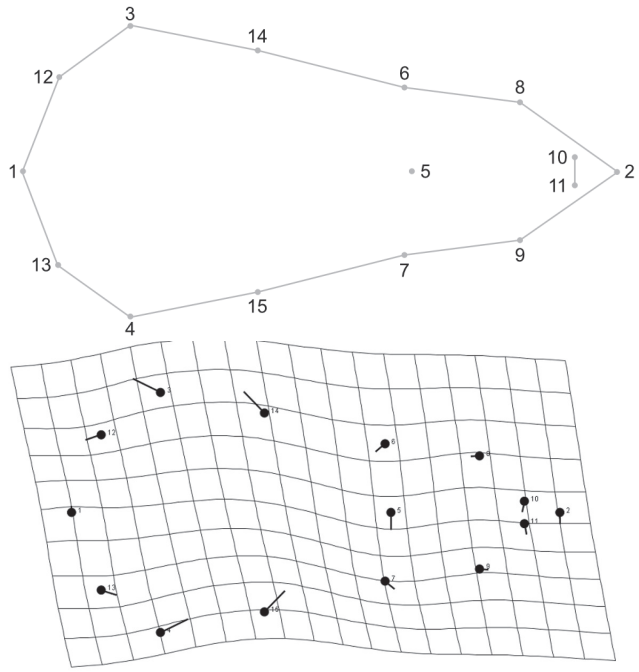

Figure 5. Deformation grid of shape differences detected by canonical variates for skulls of *C. perspicillata* (n = 45). Landmarks are represented by black filled circles. This grid produces a geometric description of shape to detect deformations relative to a general consensus to explain the shape change.

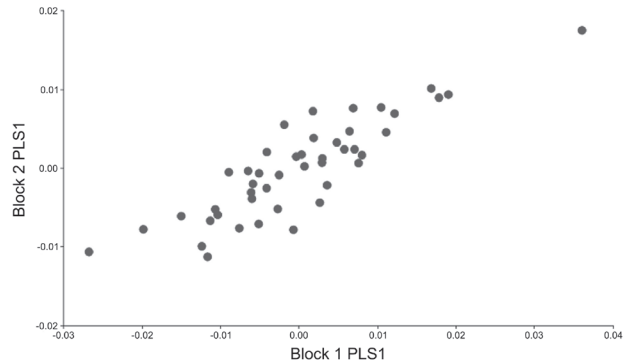

Figure 6. Scatter plot of the Partial Least Squares of two blocks (neurocranium and viscerocranium). PLS1 presented 66.1% of the total covariance, while PL2 presented 31.9% (10 000 permutation test rounds).

variation were found to exceed the error component, e.g., the contribution of measurement error to overall shape variation was small. FA and DA appeared statistically significant, but most of variation was concentrated in DA (89.5%), contrasting with shape FA, which contributed only to 2.1% to total shape. Skull asymmetry varied primarily along two first PCs which explained a 65.3% of the total observed variance (PC1 + PC2 = 39.1% + 26.1%). Shape changes detected by PC1 are illustrated on deformation grid (Fig. 5). Differences were located mainly on neurocranium length (coordinates *x*3, 4, 12 and 13) and orbital length and width (landmarks *x,y*14 and 15) (Table 1). These results prompted us to test whether the neurocranial area had a relatively independent shape change in viscerocranial variances.

The landmarks involving neurocranium (1, 3, 4, 12, 13, 14 and 15) were selected as a block; all of the other landmarks composed a second block involving viscerocranium, which was our hypothesized partition (Fig. 7). PLS1 presented 66.1% of the total covariance and PLS2 presented 31.9%, indicating that PLS1 represented the main covariance of two blocks. For PLS1, the pairwise correlation between blocks was 0.874 (p<0.001), as noted in the plots distributed around the diagonal line of the PLS1 scores coordinate in Fig. 6. The *RV* coefficient was 0.472, indicating that the overall strength of association between blocks was weak, although significant (p<0.001). Based on the PLS analysis results, a modularity analysis was performed to evaluate whether both parts were separate modules. The *RV* coefficient of the a priori hypothesis partition was 0.472, which was similar to that of the PLS analysis. Moreover, the random partition result showed that there was no partition with an *RV* less than or equal to the a priori hypothesis and thus, null hypothesis partition was accepted; the neurocranial and viscerocranial parts of the skull had different covariance. Therefore, the PLS analysis suggests that both parts of the *C. perspicillata* skull are separate modules, having no between-module integration.

Associations of size and shape variation

Correlations between the amount of shape asymmetry and CS were significant (3.2% of shape p = 0.022).

DISCUSSION

The use of geometric morphometrics in this study gave rise to a specific exploration in skull asymmetry of *C. perspicillata* skull. Our results showed highly significant FA and DA in skull shape similar for both sexes, with a size -but not shape- sexual dimorphism.

FA has been used as an indicator of developmental stability in populations and it would imply a low capacity to respond to developmental accidents that occur under environmental and/or genetic conditions (Auffray et al. 1999). The contribution of shape FA to the total shape variation was significant for both sexes, but clearly lower than DA. This would be explained by the high level of canalisation of skull shape (Urošević et al. 2015), which would prevent large fluctuations so skull asymmetry, ex-

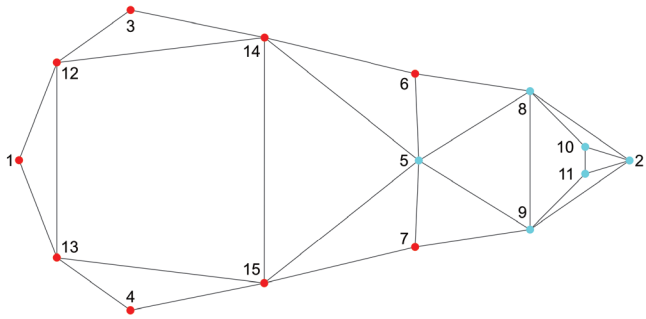

Figure 7. Modularity test results. The hypothesized partition: neurocranial part involving landmarks 1, 3 and 12-15, and the remaining landmarks as the visceral part; different colour presents different modules. Modules are units exhibiting a high degree of integration from many or strong interactions but relative independence from other such units.

pressed mainly as DA, must be interpreted as a reflection of adaptative traits.

Both PCA and CVA for asymmetric component showed that the braincase presented the larger variance. Echolocation has a great anatomical effect on the bat cranium (Brinkløv et al. 2011; Arbour et al. 2019). If we consider that this structural asymmetry may allow an asymmetric sound field and thus reduce left-right ambiguity in the echolocation (Au et al. 2006), the braincase, characterized by a significative DA, would reflect an asymmetrical support plate of the sensory apparatus (for instance ears) of the bats. To explain size sexual asymmetrical dimorphism, we argue that this can be due to that sexes have slight different in their preys, because different conformation of echolocation traits imply different ultrasound frequencies, and thus different prey sizes (Jakobsen et al. 2013). When allometry was tested we found that shape asymmetry and CS were correlated, meaning that an increase in size was accompanied by a more asymmetric shape. This presence of significant correlation of size and shape asymmetry suggests a developmental connection between them, meaning that size and shape are under similar developmental constraints, so the relative size of the skull has an effect on echolocation function in *C. perspicillata*.

The modularity test demonstrated that two skull modules -neurocranium and viscerocranium- would be units exhibiting a low degree of integration, e.g., with a relative high independence between them. In other words, neurocranium and viscerocranium would be distinct modules reflecting phenotypic and genetic variation.

Acknowledgements

We would like to thank to M.P. Rivas Pava for her generous support in handling the osteological material of the outstanding collection in *Universidad del Cauca*, in Popayán (Colombia). Moreover, we thank two anonymous reviewers whose helpful suggestions significantly improved the paper. We thank the *Campus Iberus*, Spain, for partial financial support for the field trips to museums.

Availability of data and material

The supplementary data for this article can be sent upon request to first author.

References

Arbour JH, Curtis AA, Santana SE (2019) Signatures of echolocation and dietary ecology in the adaptive evolution of skull shape in bats. Nat Commun 10:2036. https://doi.org/10.1038/s41467-019-09951-y

Au WWL, Kastelein RA, Benoit-Bird KJ, Cranford TW, McKenna MF (2006) Acoustic radiation from the head of echolocating harbor porpoises (*Phocoena phocoena*). J Exp Biol 209(14):2726-2733.

Auffray JC, Debat V, Alibert P (1999) Shape asymmetry and developmental stability. In Chaplain MAJ, Singh GD, McLachlan JC, eds. On Growth and Form: Spatio-temporal Pattern Formation in Biology. Wiley, Chichester, pp 309-324.

Bolzan DP, Pessôa LM, Peracchi AL, Strauss RE (2015) Allometric patterns and evolution in neotropical nectar-feeding bats (Chiroptera, Phyllostomidae). Acta Chiropt 17(1):59-73.

Bookstein FL (1991) Morphometric tools for landmark data: geometry and biology. Cambridge University Press, Cambridge, 435 pp.

Brinkløv S, Jakobsen L, Ratcliffe JM, Kalko EKV, Surlykke A (2011) Echolocation call intensity and directionality in flying short-tailed fruit bats, *Carollia perspicillata* (Phyllostomidae). J Acoust Soc Am 129(1):427-435.

Gardner AL (2007) Mammals of South America. Volume 1. Marsupials, xenarthrans, shrews, and bats. The University of Chicago Press, Chicago. p. 690.

Graham JH, Freeman DC, Emlen JM (1993) Antisymmetry, directional asymmetry, and dynamic morphogenesis. Genetica, 89(1-3):121-137.

Hammer Ø, Harper DAT, Ryan PD (2001) PAST v. 2.17c. Palaeontol Electron 4(1):1-229.

Jakobsen L, Brinkløv S, Surlykke A (2013) Intensity and directionality of bat echolocation signals. Front Physiol

4:89. doi: 10.3389/fphys.2013.00089.
Klingenberg CP (2011) MorphoJ: An integrated software package for geometric morphometrics. Mol Ecol Res 11(2):353-357.
Klingenberg CP, Barluenga M, Meyer A (2002) Shape analysis of symmetric structures: Quantifying variation among individuals and asymmetry. Evolution 56(10):1909-1920.
Klingenberg CP, McIntyre GS (1998) Geometric morphometrics of developmental instability: analyzing patterns of fluctuating asymmetry with procrustes methods. Evolution 52(5):1363-1375.
López-Aguirre C, Pérez-Torres J (2015) Asimetría cráneo-mandibular de *Artibeus lituratus* (chiroptera, phyllostomidae) en Colombia. Univ Sci 20(1):141-152.
López-Aguirre C, Pérez-Torres J, Wilson LAB (2015) Cranial and mandibular shape variation in the genus *Carollia* (Mammalia: Chiroptera) from Colombia: biogeographic patterns and morphological modularity. PeerJ 3:e1197.
McLellan LJ (1984) A morphometric analysis of *Carollia* (Chiroptera, Phyllostomidae). Am Mus Novit 2791:1-35.
Mendes M (2008) Asymmetry measures and allometric growth parameter estimates for investigate effect of early feed restriction on deviation from bilateral symmetry in broiler chickens. Arch Tierzucht 6:611-619.
Nuffel AV, Tuyttens FAM, Dongen SV, Talloen W, Poucke EV, Sonck B, Lens L (2007) Fluctuating asymmetry in broiler chickens: a decision protocol for trait selection in seven measuring methods. Poult Sci 86:2555-2568.
Rohlf FJ (2010) tpsDig, digitize landmarks and outlines. Version 2.16. Stony Brook: Department of Ecology and Evolution, State University of New York at Stony Brook.
Ruelas D (2017) Diferenciación morfológica de *Carollia brevicauda* y *C. perspicillata* (Chiroptera: Phyllostomidae) de Perú y Ecuador. Rev Peru Biol 24(4):363-382.
Ruelas D, López E (2018) Análisis morfogeométrico de las especies peruanas de *Carollia* (Chiroptera: Phyllostomidae). Mastozool Neotrop 25(2):419-438.
Tuyttens FAM, Maertens L, Van Poucke E, Van Nuffel A, Debeuckelaere S, Creve J, Lens L (2005) Measuring fluctuating asymmetry in fattening rabbits: a valid indicator of performance and housing quality? J Anim Sci 83(11):2645-2652.
Urošević A, Ljubisavljević K, Ivanović A (2015) Fluctuating asymmetry and individual variation in the skull shape of the common wall lizard (*Podarcis muralis* Laurenti, 1768) estimated by geometric morphometrics. Herpetol J 25(3):177-186.
Willig MR, Owen RD, Colbert RL (1986) Assessment of morphometric variation in natural populations: the inadequacy of the univariate approach. Syst Zool 35(2):195-303.

Acta Biologica Szegediensis

Volume 64(1):43-61, 2020
Acta Biologica Szegediensis
http://abs.bibl.u-szeged.hu/index.php/abs

DOI:10.14232/abs.2020.1.43-61

ARTICLE

The prevalence, preventive measures and economic impact of pandemic COVID-19 in India: the initial phase

Arindam Ganguly[1]*, Ujjal Konar[1], Animesh Kundu[1], Subhadeep Ghosh[1], Ishita Chatterjee[1], Susmita Nad[1], Sandeep Chatterjee[1], Sristishil Nandi[1], Sourav Singha[1], Sukhen Kali[2]

[1]Department of Microbiology, Bankura Sammilani College, Bankura, West Bengal, India
[2]Department of Commerce, Bankura Sammilani College, Bankura, West Bengal, India

ABSTRACT The novel coronavirus (SARS-CoV-2) is posing a serious threat to the mankind with its massive infection rate and potentially fatality. A total of 212 countries have been infected within the 112 days of first report causing 2 314 621 confirmed cases and 157 847 deaths worldwide. India, the country which is already battling with poverty, malnutrition and high population density is also at the second stage of coronavirus transmission. The situation is worsening and the attention has focused on the prevalence and preventive measures to be taken to protect 1.35 billion people of the largest democratic country of the world. In this review, a study has been designed to evaluate the prevalence, transmission, clinical symptoms, and preventive measures to control the community transmission of this fatal disease. The initial impact of coronavirus disease (COVID-19) outbreak on Indian economy has also been dealt with. This study reviews and summarizes the main points of the epidemic in India until the end of April 2020.
Acta Biol Szeged 64(1):43-61 (2020)

KEY WORDS
economy
pandemic
prevalence
SARS-CoV-2

ARTICLE INFORMATION
Submitted
22 May 2020.
Accepted
27 July 2020.
***Corresponding author**
E-mail: arindam_ganguly@yahoo.com

Introduction

Severe Acute Respiratory Syndrome coronavirus 2 (SARS-CoV-2), a contagious positive-sense single stranded RNA virus is the causative agent of ongoing global pandemic COVID-19 (Gorbalenya et al. 2020). Middle East Respiratory Syndrome (MERS) and Severe Acute Respiratory Syndrome (SARS) were well-known outbreaks of coronavirus that have been previously characterized as a major public health concern (Yin and Wunderink 2018). Prevalence and outbreak of novel coronavirus (2019-nCoV) from Wuhan, China has become pandemic, possessing an implausible threat to the mankind.

The situation of world trembled came in focus on New Year's Eve of 2019. On 31st December 2019, a cluster of 27 pneumonia cases of mysterious aetiology was first reported by Wuhan Municipal Health Commission in Wuhan City, Hubei province, China (Rapid Risk Assessment, ECDC). More arresting fact is that almost all of these people were directly or indirectly involved with the Wuhan's Huanan seafood wholesale market (a wholesale market of fish and live animals) which might point to a zoonotic origin (Wu et al. 2020). Clinical features common to several infectious diseases such as fever, dyspnoea, and bilateral lung infiltrations, pneumonia and its obscure aetiology call up the unintended consequences of previous exposure of SARS outbreak of 2002-2003 (Chen et al. 2020). Therefore, a surveillance definition and detection systems have been developed through World Health Organization (WHO). Laboratory investigations and bioinformatics analyses revealed novel coronavirus (2019-nCoV) as the causative agent of ongoing flu like illnesses on 9th January 2020 (Wu et al. 2020). Next day, the genome sequence of the novel coronavirus was made publicly available and uploaded in the GenBank database (accession number- MN908947) by the Shanghai Public Health Clinical Center & School of Public Health (Holmes 2020). WHO announced "COVID-19" and "severe acute respiratory syndrome coronavirus 2 (SARS-CoV-2)" as the name of this new disease and its causative agent respectively on 11th February 2020 (Wu et al. 2020).

Apart from the scientific investigation, SARS-CoV-2 starts to assert its terribleness. In a span of few days, a leading number of people got infected and most of them were fighting for their lives in hospitals. As of 20th January 2020, a total of 217 COVID-19 affected cases were reported from China (Wang et al. 2020). First confirmed case outside the China was reported from Thailand followed by Japan, South Korea and eventually spread to the other countries (Nishiura et al. 2020). As of 20th April, 2314621 confirmed cases of COVID-19 were reported worldwide, affecting more than 210 counties and territories (WHO, COVID-19 situation report- 91).

First case of death from COVID-19 was reported on 11th January 2020. On 15th January 2020, a second death has taken place. Both the deceased patients were more than 60-years old male who were suffering from other health issues as well (Hui et al. 2020). The World Health Organization declared the novel coronavirus outbreak as pandemic (WHO Director-General's opening remarks at the media briefing on COVID-19). Europe and United States gradually turned into the epicentre of the pandemic, infecting more than 1.4 million people worldwide. After the 112 days of first report, with over, 157 847 worldwide deaths, COVID-19 have wreaked large-scale damage throughout the world (WHO, COVID-19 situation report- 91).

India is the second most populated country in the world with the population density of 382/km^2 (niti.gov.in). It is also the seventh largest country in the world, covering an area of about 3 287 263 km^2 (https://www.india.gov.in). With a finest architectural heritage, spectacular landscapes and myriad attractions, the country is the most popular tourist destination in the world. It shares about more than 3 400 km border with China, the epicentre of COVID-19. Therefore, it bears a great possibility of human transmission of the disease and may possess a major rise in the case of fatality. At present, 18 601 confirmed COVID-19 cases were reported in India and the situation is worsening alarmingly (Ministry of Health and Family Welfare). The attention has focused on the prevalence and preventive measures to be taken to protect 1.35 billion people of the largest democratic country of the world. The present study evaluates the initial scenario of pandemic SARS-CoV-2 infection in India.

Transmission

COVID-19 is highly contagious disease, entitled pandemic (WHO Director-General's opening remarks at the media briefing on COVID-19) by WHO as the cases of the infection continued to swell with over 1.4 million confirmed cases reported globally so far. As per the early cases reported from Wuhan, it is assumed that the disease was spread from a zoonotic source (Report of the WHO-China Joint Mission on Coronavirus Disease 2019) followed by a massive human to human transmission and become a global health concern.

Person to person transmission mainly exhibits via direct contact with infected personals or by respiratory droplet produced during coughing and sneezing from an infected individual. However, SARS-CoV-2 may not be airborne (Khamsi 2020). Close contact with infected person, contact with contaminated surfaces, fomites or items are the most susceptible way of transmission of COVID-19. Viruses are inhaled into the body through mouth, nose or possibly by eyes. Infected people are thought to be most contagious when they are symptomatic. However, transmission is also possible from asymptomatic persons (Rothe et al. 2020).

India at present is in the second stage of coronavirus transmission and most of the positive cases have been reported in people with a travel history from affected countries. A lot of cases were observed where family members of the infected person also tested positive with COVID-19. However, community transmission has not been noticed so far.

Some report stated that peoples arriving from virus infected countries or suspected of coronavirus infection were escaping from quarantine centres or providing wrong information in India owing to isolation and social fears that can lead to the unnecessary spread of the deadly disease further (11 coronavirus suspects flee from a hospital in Maharashtra).

Prevalence of COVID-19 in India

First case of SARS-CoV-2 infection in India was reported on January 30th, 2020 (India's first coronavirus case confirmed in Kerala). In a span of four days, two other positive cases were also reported in Kerala (Second case of coronavirus confirmed in Kerala, Kerala now confirms third case of coronavirus, patient had returned from China's Wuhan), prompting the local government to declare a state disaster on February 3 (Kerala government declares coronavirus as state disaster). Surprisingly, all three patients were students who had returned on vacation from Wuhan to Kerala. They have recovered and stable now (Kerala defeats coronavirus; India's three COVID-19 patients successfully recover). Consequently, more than 3400 persons who came in contact with these patients have been quarantined in Kerala to contain the coronavirus outbreak. After 3rd February, India passes through a calm phase of about a month in regard to the global coronavirus outbreak as no new case was reported. The next positive report was obtained in a 45-year-old person in Delhi on 2nd March who had a travel history from Italy (Coronavirus hits Delhi: Two new cases detected in national capital and Telangana). On the same day, a 24-year-old engineer in Hyderabad who had travel history from Dubai was tested positive (Nichenametla 2020). The Govt. of Telangana identified 36 people who had been in contact with the Hyderabad engineer had developed symptoms of coronavirus infection. The next report of infection emerged from Jaipur where an Italian couple have tested positive and were immediately hospitalized. In addition, the entire tourist group including the

Table 1. Prevalence of COVID-19 pandemic in India by states and union territories (as of 20th April 2020)

States & Union Territory of India	Total confirmed cases	Deaths	Cured/Discharge /Migrated	Fatality rate (%)	Recovery rate (%)
Andhra Pradesh	722	20	92	2.77	12.74
Arunachal Pradesh	1	-	-	0	0
Assam	35	1	19	2.85	54.28
Bihar	113	2	42	1.76	37.17
Chhattisgarh	36	-	25	0	69.44
Goa	7	-	7	0	100
Gujarat	1939	71	131	3.66	6.76
Haryana	254	3	127	1.18	50
Himachal Pradesh	39	1	16	2.56	41.02
Jharkhand	46	2	-	4.34	0
Karnataka	408	16	112	3.92	27.45
Kerala	408	3	291	0.73	71.32
Madhya Pradesh	1485	74	127	4.98	8.55
Maharashtra	4666	232	572	4.97	12.26
Manipur	2	-	2	0	100
Meghalaya	11	1	-	9.09	0
Mizoram	1	-	-	0	0
Nagaland	-	-	-	0	0
Odisha	74	1	24	1.35	32.43
Punjab	245	16	38	6.53	15.51
Rajasthan	1578	25	205	1.58	13
Sikkim	-	-	-	0	0
Tamil Nadu	1520	17	457	1.11	30.06
Telangana	873	23	190	2.63	21.76
Tripura	2	-	1	0	50
Uttar Pradesh	1184	18	140	1.52	11.82
Uttarakhand	46	-	18	0	39.13
West Bengal	392	12	73	3.06	18.62
Andaman and Nicobar	16	-	11	0	68.75
Chandigarh	26	-	13	0	81.25
Dadra, Nagar Haveli, Daman and Diu	-	-	-	0	0
Delhi	2081	47	431	2.25	20.71
Jammu and Kashmir	314	4	38	1.27	12.10
Ladakh	18	-	14	0	77.78
Lakshadweep	-	-	-	0	0
Puducherry	7	-	3	0	42.86
TOTAL	**18601**	**590**	**3252**	**3.17**	**17.48**

driver has been shifted to an ITBP facility at Chhawla for testing. Of them, fourteen tourists and the driver were tested positive on 4th March and quarantined (Italian tourist in Jaipur tests positive). Meanwhile, on the same day a man from New Delhi with a travel history from Italy, was also tested positive, taking the total number of positive cases in India to 29 (tracing the Italian connection to India's fresh coronavirus count). On 8th March, five new cases were reported from a family in Kerala (five more people from Kerala test positive for coronavirus). Five new cases of COVID-19 were reported on 9th March, and another six Tuesday, bringing the total count to 50 by 10th March (Rawat 2020). India's first fatality from the virus was reported on 12th March in Delhi (India's first COVID-19 death confirmed in Karnataka). On 13th March 2020, a second death has taken place (Perappadan 2020). Both the deceased patients were more than 60-years aged and also suffering from other health issues. Fresh cases have continued to emerge every day, since peoples returned from abroad and subsequently spread to almost

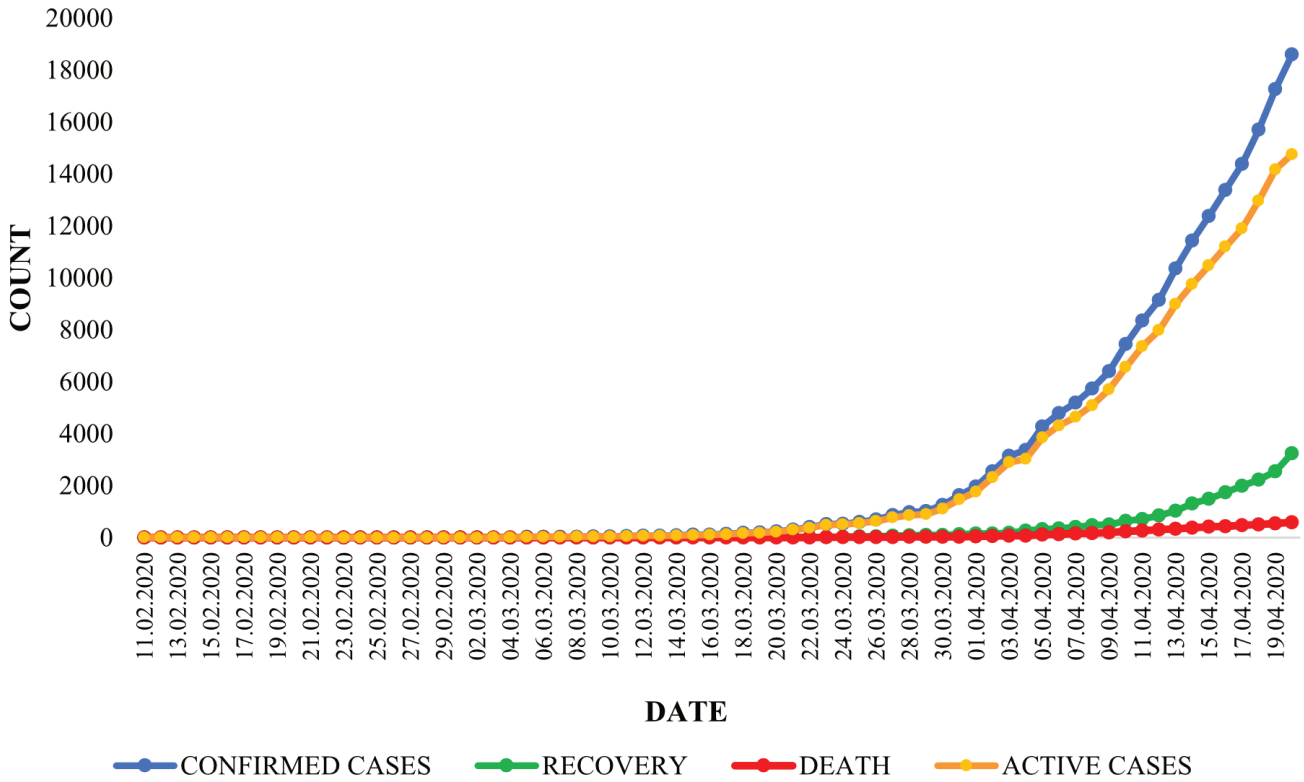

Figure 1. Day wise increase of COVID-19 cases in India (As of 20th April, 2020).

all other states and Union Territories throughout India.

Cases of local transmission increases alarmingly from an international religious event in which over 3400 people from India and abroad had gathered at the Nizamuddin area of New Delhi. Many of them have returned to their locality through public transport (Haider 2020). The matter came in focus when 10 Indonesians who attended the event in Delhi test positive in Telangana on 20 March (nearly 100 Delhi Mosque-linked coronavirus cases, 2100 evacuated). That lead the central government as well as state government to carried out an intensive contact tracing and sampling process in the states where the attendees of this event had travelled to. Some of the deaths in states like Karnataka, Jammu and Kashmir also have links to this event (Suffian 2020).

The initial prevalence of COVID-19 in India is represented in Table 1. The total number of active COVID-19 cases in India rose beyond 5000 on 7th April, less than a week after the crossing of 1000 marks. Within next two weeks, number of confirmed cases surge up to 18 601 (Fig. 1) (Ministry of Health and Family Welfare). As of, 20th April, a total of 18 601 persons have tested positive across India out of which 590 peoples have succumbed to the disease and 3252 peoples got recovery (Table 2). The epidemiological curve of COVID-19 in states and union territories of India is represented in Fig. 2. Most of the confirmed cases in India were noticed from Maharashtra followed by Delhi, Gujrat and other 29 states and union territories (Fig. 3). It was noticed that, 42% of the total corona infected patient in India belongs to the age between 21-40 years old but account for 7% of the fatalities so far. Report also stated that the rate of infection and fatality were higher in males compared to females (Dey 2020). Though most of the deceased patients in India were above 60 years old (63%) and had other health issues and co-morbidities (Dey 2020). Highest number of death was reported from Maharashtra; while the highest fatality rate was seen in Meghalaya. Remarkable number of recoveries was also noticed from Kerala, Chandigarh, Chhattrishgarh. However, the total fatality rate and recovery rate in India was 3.17% and 17.48%, respectively.

The government has identified 170 districts in 27 states as the existing hotspots across the country including major metropolitan cities like Delhi, Mumbai, Chennai, Bengaluru, Hyderabad and Kolkata, where the cases were largely concentrated (Govt. identifies 170 Covid-19 hotspots: here's the full list). Among the hotspot's areas, 10 districts including South Delhi, New Delhi, Mumbai City, Thane, Pune, Indore, Ahmedabad, Jaipur, Hyderabad and Chennai are worst affected and account for at least 45%

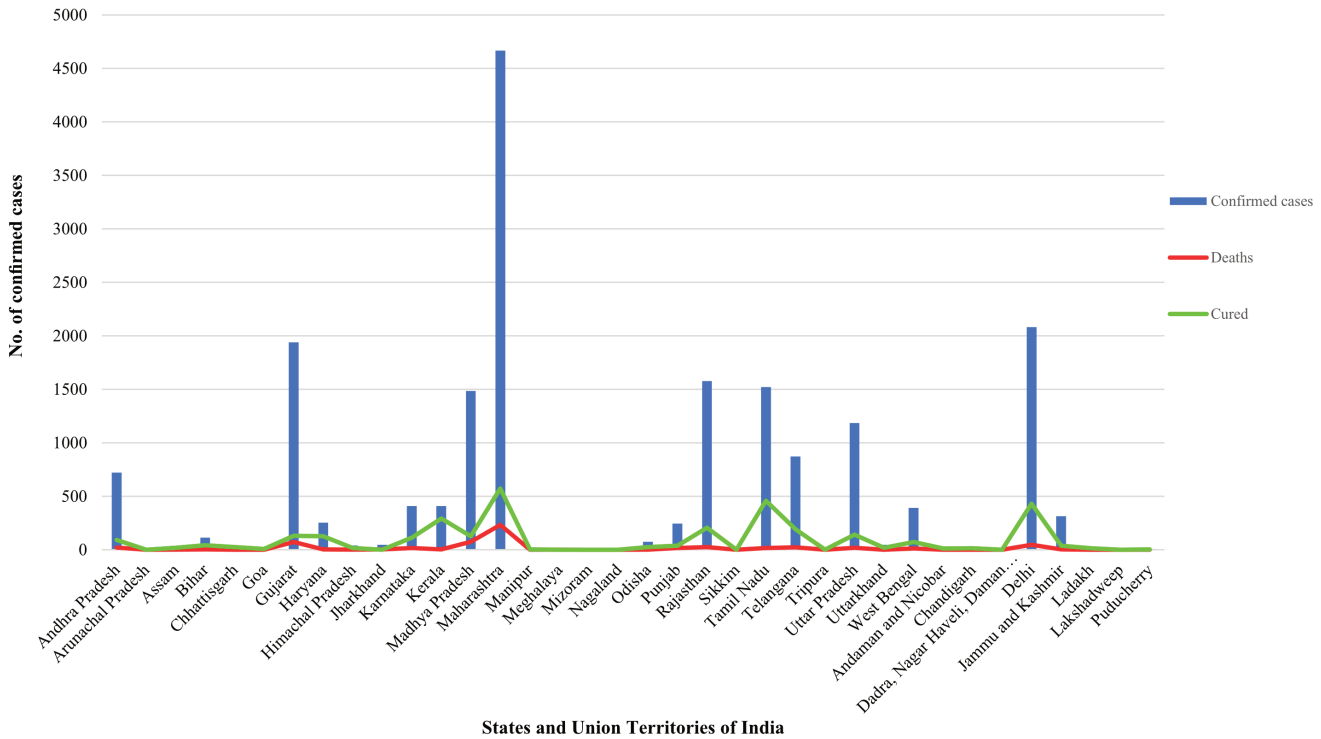

Figure 2. Epidemiologic curve of COVID-19 laboratory cases in different states and union territories of India (As of 20th April, 2020).

of the total COVID-19 cases in India (Govt. identifies 170 Covid-19 hotspots). All these hotspots areas are classified as red zones and sealed totally as well as an embargo has imposed on the movement of citizens. However, complete lockdown and quarantine programmes have vastly helped to contain the spread in India till now. Though, with the sharp spike in the number of Novel Coronavirus cases and reports of local transmission emerging across the country in last few days, at present India is on the brink of community transmission.

Clinical manifestations

Symptoms are the subjective evidence of any bodily disorder or inner turmoil or disease that is apparent to the patient. Infected patients start to show symptoms within a period of 2-14 days after the exposure to the corona virus (Backer et al. 2020). Clinical signs and symptoms of COVID-19 infected patients are non-specific and varied according to the degree of immunity of the patients as well as the virulence of the SARS-CoV-2 virus (Table 3). It is also possible to be infected with the virus without showing any symptoms of illness. Such asymptomatic cases are noticed in a leading percentage (80%) in India (Thacker 2020). Most common symptoms seemed in COVID-19 infection are fever (≥38 °C), asphyxia, tiredness and dry cough that are almost like common cold or flu (Huang et al. 2020). Some patients may have mild symptoms like nasal congestion, runny

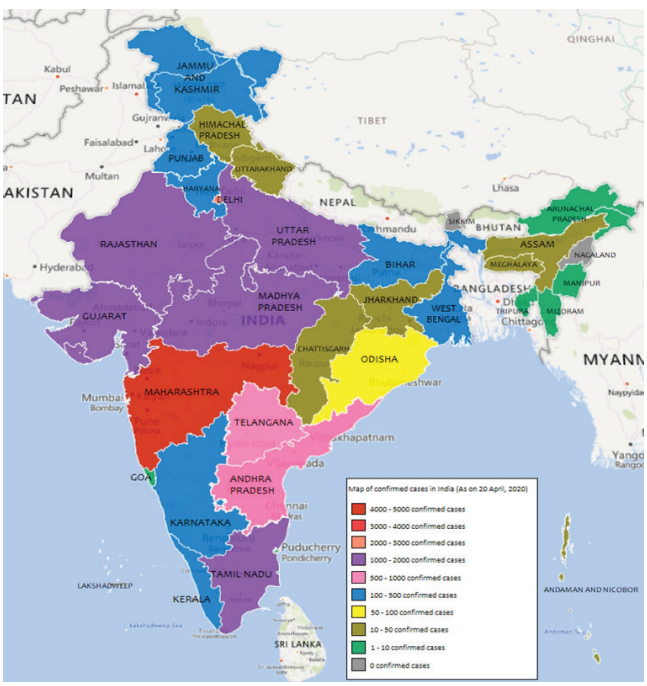

Figure 3. Map of COVID-19 pandemic prevalence in India.

Table 2. Date wise COVID-19 case count in India (As of 20th April, 2020).

	Confirmed cases		Recovery		Death		
Date	**New**	**Total**	**New**	**Total**	**New**	**Total**	**Active cases**
30.01.2020	1	1	-	-	-	-	1
31.01.2020	-	1	-	-	-	-	1
01.02.2020	-	1	-	-	-	-	1
02.02.2020	1	2	-	-	-	-	2
03.02.2020	1	3	-	-	-	-	3
04.02.2020	-	3	-	-	-	-	3
05.02.2020	-	3	-	-	-	-	3
06.02.2020	-	3	-	-	-	-	3
07.02.2020	-	3	-	-	-	-	3
08.02.2020	-	3	-	-	-	-	3
09.02.2020	-	3	-	-	-	-	3
10.02.2020	-	3	-	-	-	-	3
11.02.2020	-	3	-	-	-	-	3
12.02.2020	-	3	-	-	-	-	3
13.02.2020	-	3	-	-	-	-	3
14.02.2020	-	3	-	-	-	-	3
15.02.2020	-	3	-	-	-	-	3
16.02.2020	-	3	-	-	-	-	3
17.02.2020	-	3	-	-	-	-	3
18.02.2020	-	3	-	-	-	-	3
19.02.2020	-	3	-	-	-	-	3
20.02.2020	-	3	-	-	-	-	3
21.02.2020	-	3	-	-	-	-	3
22.02.2020	-	3	-	-	-	-	3
23.02.2020	-	3	1	1	-	-	2
24.02.2020	-	3	-	1	-	-	2
25.02.2020	-	3	-	1	-	-	2
26.02.2020	-	3	-	1	-	-	2
27.02.2020	-	3	-	1	-	-	2
28.02.2020	-	3	1	2	-	-	1
29.02.2020	-	3	-	2	-	-	1
01.03.2020	-	3	-	2	-	-	1
02.03.2020	-	3	-	2	-	-	1
03.03.2020	2	5	-	2	-	-	3
04.03.2020	1	6	-	2	-	-	4
05.03.2020	23	29	1	3	-	-	26
06.03.2020	1	30	-	3	-	-	27
07.03.2020	1	31	-	3	-	-	28
08.03.2020	3	34	-	3	-	-	31
09.03.2020	9	43	-	3	-	-	40
10.03.2020	1	44	-	3	-	-	41
11.03.2020	16	60	-	3	-	-	57
12.03.2020	13	73	-	3	1	1	69
13.03.2020	1	74	2	5	1	2	67
14.03.2020	8	82	1	6	-	2	74
15.03.2020	25	107	4	10	-	2	95
16.03.2020	7	114	-	10	-	2	102
17.03.2020	23	137	3	13	1	3	121

Table 2. Continued.

	Confirmed cases		Recovery		Death		
Date	**New**	**Total**	**New**	**Total**	**New**	**Total**	**Active cases**
18.03.2020	45	182	-	13	-	3	166
19.03.2020	14	196	-	13	1	4	179
20.03.2020	44	240	1	14	-	4	222
21.03.2020	75	315	-	14	1	5	296
22.03.2020	88	403	9	23	2	7	373
23.03.2020	116	519	-	23	3	10	486
24.03.2020	19	538	1	24	-	10	504
25.03.2020	69	607	17	41	3	13	553
26.03.2020	87	694	4	45	5	18	631
27.03.2020	176	870	31	76	1	19	775
28.03.2020	106	976	11	87	5	24	865
29.03.2020	48	1024	9	96	6	30	898
30.03.2020	227	1251	6	102	6	36	1113
31.03.2020	386	1637	31	133	1	37	1467
01.04.2020	327	1965	17	151	13	50	1764
02.04.2020	581	2546	11	162	12	62	2322
03.04.2020	608	3154	22	184	6	68	2902
04.04.2020	220	3374	83	267	9	77	3030
05.04.2020	907	4281	51	318	34	111	3851
06.04.2020	508	4789	35	353	13	124	4312
07.04.2020	405	5194	49	402	25	149	4643
08.04.2020	540	5734	71	473	17	166	5095
09.04.2020	677	6411	30	503	33	199	5709
10.04.2020	1036	7447	140	643	40	239	6565
11.04.2020	918	8356	73	716	34	273	7367
12.04.2020	796	9152	141	857	35	308	7987
13.04.2020	1211	10363	179	1036	31	339	8988
14.04.2020	1076	11439	270	1306	38	377	9756
15.04.2020	941	12380	183	1489	37	414	10477
16.04.2020	1007	13387	259	1748	23	437	11201
17.04.2020	991	14378	244	1992	43	480	11906
18.04.2020	1334	15712	239	2231	27	507	12974
19.04.2020	1553	17265	316	2547	36	543	14175
20.04.2020	1336	18601	705	3252	47	590	14759

nose, aches and pain, sore throat and diarrhea. Elderly (aged over 60 years) and immune-suppressed peoples (such as hypertension, diabetes, cardiovascular disease, chronic respiratory disease and cancer) are more likely to develop serious illness, ranging from severe pneumonia to multi-organ dysfunction and seek medical attention. Chest radiography revealed the evidence of pneumonia with bilateral ground-glass opacities and consolidation (Huang et al. 2020).

Preventive measures

India is an emerging and developing country (Silver 2020). However, despite its expanding economy, poverty in India is widespread. About 64 million people in India live in slum in an inscrutable unhygienic condition (India census says 1 in 6 lives in unsanitary slums) and approximately 21.9% people of India's total population are thriving under poverty (Habitat for Humanity in India). Therefore, if the community transmission starts in India, it may become the next epicentre of the SARS-CoV-2. However, India has a proud history to lead the world in eradicating fatal diseases like small pox and polio (India has tremendous

Table 3. Clinical signs and symptoms of COVID-19.

Number of days	Symptoms
1st -3rd	Fever, mild sore throat
4th	Extreme sore throat, increased body temperature, loss of appetite, headache, diarrhea
5th	Tiredness, muscle pain, dry cough
6th	Fever (100˚ F), dry cough, asphyxia, vomiting or diarrhea
7th	High fever (>100˚ F), severe cough, entire body pain, vomiting and diarrhea
8th-9th	Increase of all of the above symptoms, extreme high fever, increased asphyxia

capacity in eradicating coronavirus pandemic: WHO).

Revising its capacity to fight against pandemic, several measures have been taken both in national and state level in India. India started to screen passengers arriving from China, Hong Kong, Thailand and Singapore from the early week of February at 21 identified international airports by the Airport Health Organisation (Coronavirus: India starts screening passengers from Singapore). On 14th February 2020, Directorate General of Civil Aviation (DGCA) asked airports and airlines to screen passengers also coming from Japan and South Korea (Coronavirus: DGCA extends airport screening to passengers arriving from Japan, South Korea). Later on 4th March, compulsory screening was announced for all the international travellers, including aircraft crew members upon arrival from all the countries to contain outbreak or spreading of coronavirus in India (Coronavirus: All international arrivals to India to share travel history at airports). According to health officials, more than 1.5 million passengers had been screened at airports, limiting the entry of coronavirus. Besides it, thermal screening of passengers and crew members were conducted in twelve major ports (Kandala, Mumbai, JNPT, Marmugao, New Mangalore, Cochin, Chennai, Ennore, VO Chidambarnar, Visakhapatnam, Paradip and Kolkata) since February for disembarking seafarers and cruise passengers as a preventive measure to prevent the spread of Covid-19 infection (Coronavirus: Govt directs 12 major ports to put in place screening, quarantine system). Screening measures had also been implemented at 65 minor seaports and land borders (High level Group of Ministers reviews current status, and actions for prevention and management of COVID-19).

In light of the ongoing pandemic, on 11th March Government of India suspended all visas to India except diplomatic, official, United Nations/International organisations, employment and project visas from 13th March to 15th April 2020 (Coronavirus a pandemic: India shuts doors for outsider, under self-imposed quarantine). However, visas already issued for nationals of Italy, Iran, South Korea, and Japan were cancelled previously on 3rd March 2020 (Coronavirus outbreak: Govt. cancels Visas for Italy, Iran, Japan and South Korea, issues new travel advisory). Visa facilities had been suspended earlier from

Table 4. List of evacuated citizens from coronavirus affected countries (As of 20th April 2020

Date	Evacuated citizens		From	Quarantined at
	Indian	Foreigner		
1st February, 2020	324	-	Wuhan city, China	ITBP Chhawla camp and Army facility at Manesar
2nd February, 2020	323	7	Wuhan city, China	ITBP Chhawla Camp and Army facility at Manesar
27th February, 2020	76	36	Wuhan city, China	ITBP Chhawla Camp and Army facility at Manesar
27th February, 2020	119	5	Diamond Princess docked in Yokohama, Japan	Army facility in Manesar
10th March, 2020	58	-	Iran	Medical facility in Ghaziabad
11th March, 2020	74	9	Italy	Army facility in Manesar
13th March, 2020	44	-	Qom city, Iran	Indian Navy quarantine facility at Ghatkopar, Mumbai
15th March, 2020	218	-	Italy	ITBP Chhawla Camp
15th March, 2020	236	-	Iran	Indian Army Wellness Centre, Jaisalmer, Rajasthan
16th March, 2020	53	-	Tehran and Shiraz, Iran	Indian Army Wellness Centre, Jaisalmer, Rajasthan
22th March 2020	263	-	Rome, Italy	ITBP Chhawla Camp
25th March 2020	277	-	Tehran, Iran	Indian Army Wellness Facility, Jodhpur, Rajasthan
29th March 2020	275	-	Iran	Indian Army Wellness Facility, Jodhpur, Rajasthan
30th March 2020	35	-	Kabul, Afghanistan	ITBP Chhawla Camp

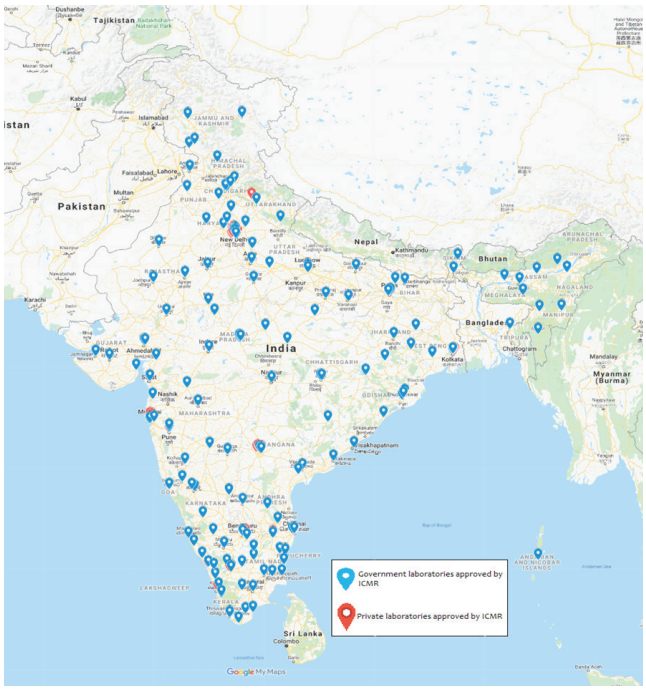

Figure 4. Map of diagnostic centre of COVID-19 disease in India approved by ICMR.

the mainland China, countries where the virus is on a rampage (Singh 2020).

However, in the wake of the COVID-19 outbreak, Government of India has undertaken evacuation operations from several countries to bring back Indian citizens as well as some nationals of other countries in order to ensure their safety and security and subsequently quarantined them to contain community spread (Table 4).

On 19th March, the DGCA had banned all international commercial flights landing in India for a week from 22 March (Kulkarni 2020) that was further extended till 14th April (Government extends ban on international flights till April 14). The domestic passenger flight operations were also suspended from midnight of March 24 (Coronavirus outbreak: Govt suspends all domestic flights from midnight of March 24). On 22nd March, the Union government suspended all passenger train services in the country followed by all inter-state passenger services including interstate transport buses and metro services in a bid to stop the spread of coronavirus (Coronavirus impact: Railways cancels all passenger trains till March 31).

After a surge of Covid-19 cases in India and a possible threat of community transmission, set up of new quarantine facility, isolation ward, specialized hospital for treatment of COVID-19 patients started in full swing throughout the country. Nine quarantine facilities, each of 200-300 personnel capacity had been established by Indian Air Force at nodal Indian Air Force (IAF) bases (IAF creates nine quarantine facilities at its nodal bases across country as coronavirus cases multiply). Besides it, quarantine facilities had been established at Jaisalmer and Jodhpur (army), Manesar (army), Kolkata (army), Chennai (army), Kochi (navy), Dundigal near Hyderabad (IAF), Bengaluru (IAF), Kanpur (IAF) and Jorhant (IAF). Defence forces were also prepared for any eventuality and ready to ramp up the capacity of the quarantine facilities (Gurung 2020). 285 beds had been designated by Ordnance Factory Board (OFB) for isolation wards (OFB designates 285 beds for coronavirus cases). A chain of 32 paramilitary forces hospitals with 1 900 beds earmarked for isolation and treatment of COVID-19 patients across the country (https://www.tribuneindia.com/news/nation/32-hospitals-for-paramilitary-forces-with-1-900-beds-to-treatcovid-19-patients-mha-61388. Accessed 26 March 2020). Government also granted emergency financial powers to army corps and divisional commanders for acquisition of medical equipment to set up quarantine facilities. West Bengal government converted the entire Calcutta Medical College Hospital, which has 2 200 beds, into an isolation and treatment centre for persons suspected to be infected with the novel coronavirus. All OPDs, Casualty ward in this hospital was closed temporarily, and no patients except COVID-19 could be admitted (West Bengal converts state-run hospital into COVID-19 isolation, treatment facility). Similar kind of approach was also taken by Bowring and Lady Curzon Medical College and Research Institute in Bengaluru (List of hospitals designated for treatment of COVID-19 patients in south India). Hospital with 1000 bed was constructed in Odisha (Mohanty 2020). Assam government started work to set up four temporary hospitals with 300 beds each across the state for treatment of COVID-19 patients. The government also established an isolation facility for 700 persons at the Sarusajai Sports Complex, Assam (Assam govt to set up 4 temporary hospitals for COVID-19). On 26th March Government of India also directed the private hospitals to begin treatment and admission of Covid-19 patients (Sharma 2020). Rajasthan government reserved 84 private hospitals in Jaipur district (Iqbal and Karmakar 2020). West Bengal government has also transformed 59 hospitals to treat COVID-19 patients covering all the districts of the state (https://m.economictimes.com/news/politics-andnation/all-22-districts-in-bengal-to-have-nodal-covid-19-hospital-mamatabanerjee/articleshow/74896587.cms. Accessed 30 March 2020). The Indian Railways were converted Non-AC sleeper coaches into isolation wards to meet the increasing demand for beds (Athrady 2020).

As of 21st April, a total number of 304 laboratories

(Governmental = 217; Private = 87) had been authorized by the Indian Council of Medical Research (ICMR) to process testing for COVID-19 (Indian council of medical research) (Fig. 4). Among them, National Institute of Virology (NIV), Pune functions as the nodal lab and resource centre for the Viral Research and Diagnostic Laboratories (VRDL) network and also performs quality control and quality assurance activities as well as provide technical training across India. National Pharmaceutical Pricing Authority and Drug Controller General of India instructed to ensure the availability of APIs (Active Pharmaceutical Ingredient) and drugs in the country amid the pandemic. The organisation had also been asked to monitor black-marketing or illegal hoarding. On 3rd March 2020, the Director General of Foreign Trade (DFGT) had issued notice to restrict the export of 26 APIs and formulation (Suneja 2020).

Central government assured that the frontline fighter of coronavirus outbreak including sweepers, ward-boys, nurses, paramedics, technicians, doctors and specialists would be covered by a special insurance scheme of 50 lakh (Noronha 2020). Insurance of Rs. 25 lakh and 10 lakh has been announced respectively by Gujrat (Coronavirus: Rs 25 lakh compensation for Guj frontline staff) and West Bengal (Combating COVID-19: West Bengal increases insurance coverage from Rs 5 lakh to Rs 10 lakh) state government for all those medical and supporting staffs. Some hotels and shared-living facilities across the mega-cities of India were earmarked as potential venues for accommodating healthcare workers. Central government directed the district magistrates, zonal deputy commissioners of municipal corporations and the deputy commissioner of police to take "strict penal action" against landlords for any harassment of doctors and paramedical staff to vacate their rented premises (Govt gives power to zonal DCs to take strict action against landlords evicting dics, paramedics). Government also arranged transport facility for medical staffs amid the lockdown.

Several government agencies along with private sector stepped up for mass production of ventilators, sanitizer, high grade protective material such as N-99 masks, gloves and personal protective equipment (PPE). The Ordnance Factory Board (OFB) increased the production rate of sanitizer, masks and body suits (Siddiqui 2020). Defence Research and Development Organisation (DRDO) designed ventilators and ramped up its production rate up to 10000 units per month (DRDO is stepping in to build ventilators and manufacture masks). State-run Bharat Electronics Limited (BEL) has been ordered to manufacture 30,000 ventilators amid shortage in wake of outbreak (Automobile manufacturers asked to make ventilators: Health Ministry). An order to manufacture 10,000 ventilators within a month had been given to Agva Healthcare, Noida (Coronavirus: Maruti, Noida firm got nod to supply 10 000 ventilators). Several automobile companies were also asked to focus on ventilator manufacturing (Automobile manufacturers asked to make ventilators: Health Ministry). Considering the shortage of ventilators and the rising number of cases in India, a group of doctors and engineers had been developed and tested 3D-printed splitters that can provide ventilator support to four patients using just one life support system (Badve 2020). A small IoT pendant called Kawach (shield) has been designed by a B-Tech student to promote social distancing among people (Ansari 2020).

Telecom agencies had set up a 30-seconds voice message to convey Do's and Don'ts as a default caller tunes to raise awareness on the coronavirus outbreak (Now, a caller tune for COVID-19). Public awareness campaigns had also saturated in every television channel. Telecom firms has taken initiative to post bulk SMS (Short Message Service) and Push notification on the simple 'Do's and Don'ts' to all the clients. Ministry of Health and Family Welfare, Government of India had been issued an indicative list of Do's and Don'ts for wide dissemination. A toll-free 24×7 helpline number, email ID for each state as well as countrywide have been activated by Union Health Ministry to address all queries concerning the disease (Health Ministry launches new toll-free number, email ID for queries on COVID-19). An App has been designed and promoted by the Central Government which will warn its user about the nearby presence of any corona-infected person.

As the coronavirus cases creeping forward, the government on 16th March declared a countrywide suspension of schools, colleges, universities, gyms, cinema halls, swimming pools and also asked to avoid mass gatherings as a precautionary measure. On the same day, Government has advised people to avoid non-essential travel and requested private companies to allow their employees to work from home (Schools Closed, Travel To Be Avoided, Says Centre On Coronavirus: 10 Points). All board examinations had been postponed.

Most of the COVID-19 infected individual of India had recent travel history in foreign countries. Therefore, in order to prevent local transmission, India's Prime Minister Mr. Narendra Modi appealed all citizens to observe 'Janata Curfew' (people's curfew) on 22nd March from 7 am to 9 pm. Later on 24th March, nationwide lockdown had been imposed for 21 days from 25th March to 14th April which was further extended till 3rd May under the provisions of the Disaster Management Act, 2005. The Prime Minister has also announced that the Centre had created a 'COVID-19 Economic Response Task Force' under the Union Finance Minister to deal with the economic repercussion of the current situation

(PM Narendra Modi forms economic response task force, calls for 'Janata Curfew'). Police were advised to follow the policy of explaining; persuading and requesting public to stay indoors. However, strict measurements had also been advised to maintain social distancing countrywide.

Aimed at avoiding panic among consumers, government decided to give permission to shops including ration shops (under Public Distribution System), dealing with food, groceries, fruits and vegetables, dairy and milk booths, meat and fish, animal fodder and pharmacy to remained available during lockdown. Home delivery of all essential commodities including food, pharmaceuticals, medical equipment through E-commerce also remained functional (Shops selling essentials, medicines will remain open throughout 21-day lockdown: Govt). The central government as well as state governments have issued free ration, required cash and other emergency facilities to the unorganised labour sector and all needy (Govt to provide 5 kg grains, 1 kg pulses for free over next 3 months: Nirmala Sitharaman). Jharkhand government decided to provide two months ration in advance (COVID-19: Jharkhand to give 2 months' ration in advance). Telangana government announced to provide extra 6 kg of rice to 87.59 crore (1 crore = 10 million) white ration card holders (Telangana Lockdown: 12 kg free rice per person, Rs 1 500 per family to be supplied for each white ration card). One month of free ration was also announced by Bihar Government for all ration card holders of the state (Bihar CM Nitish Kumar announces free ration for cardholders during coronavirus lockdown). West Bengal government has announced to provide rice from ration shops to a large sector of people free of cost for the next six months till September (Free foodgrains to all till September: CM). Paramilitary forces and Marine Commandos (MARCOS) of Indian Navy were also engaged to spread awareness and distribute rations among the tribal community living in inaccessible region of India (Combating COVID-19: Navy's MARCOS commandos reach out to fisherman at Wular Lake). Apart from ration assistance, 8.70 crore farmers across India to get Rs. 2000 as one-time relief through direct cash transfer before April first week (FM Nirmala Sitharaman announces Rs 1.7 lakh crore relief package for poor). They have also stated that the expenditure on the diagnosis and treatment of COVID-19 in Government premises will be carried out by the Government itself. Hence, it is assumed that the trajectory of the pandemic COVID-19 can be somewhat controlled in India.

Diagnosis

At a time when India's cumulative coronavirus infections have breached the 10000-mark, demand of testing kits and infrastructure has become the need of the hour. In India, laboratory tests were generally recommended and performed after appearance of severe breathing problem, sore throat like clinical manifestations. For diagnostic purpose, WHO recommended collection of samples from expectorated sputum, broncho-alveolar lavage or endotracheal aspirate from suspected individual (Hassan et al. 2020). These clinical samples were screened at the laboratory with RT-PCR. Use of specific primers and probes in the ORF1ab and N gene regions of SARS-CoV-2 were recommended by Chinese center for Disease Control and Prevention (China CDC) (Jung et al. 2020). Patient was confirmed as positive when both targets came positive. In case of discordance, or if the result was judged a weak positive, another clinical sample was requested and analyzed. Chest radiography, chest CT was done in selected patients as per the discretion of attending doctors when clinically instructed. Apart from this, viral isolation also performed from the specimen's airway epithelial cells and VeroE6 and Huh7 cell lines (Kothai and Arul 2020). However, isolation of viral genome from clinical samples is quite difficult and stringent biosafety level 3 (BSL 3) is required. In recent time a series of reliable and sensitive diagnostic tools were developed and deployed for rapid diagnosis of COVID 19. A molecular diagnostic company, Mylab, first Indian company to develop ICMR approved a Covid-19 test kit which has the ability to screen and detect the infection within 2.5 hours that is less than half of the hours taken by current protocols (Bose 2020). Mylab has the capacity to produce one lakh test kits per week and also ready to scale up the production to meet the increasing demands in India at an affordable price (Thacker 2020_b). ICMR had also recommended the use of rapid antibody test kit in hotspots, area with many cases across the country. Antibody test indicated the patient is infected or not by determining the presence of antibodies for coronavirus and it takes only 15-30 min (Shekhar 2020).

Though 217 government laboratories and as many as 87 private laboratories were made functional for testing till date (Fig.4), the numbers of tests being conducted daily are still insufficient. The ICMR has also allowed Truenat technology and Cartridge Based Nucleic Acid Amplification Test (CBNAAT) for the rapid and cheap detection of Covid-19 positive cases. As of 21st April, a total of 462621 tests had been conducted throughout India, just a minuscule portion given its population size. Therefore, Government should focus to increase the testing capacity to get a better grip on the situation.

Treatment

Since it's a new strain, there are no approved therapies till date. However, treatment is crucial to save the infected persons, especially high-risk patients – the elderly, those with debilitated immune-system and chronic illnesses, such as diabetes, respiratory disease and cardiovascular diseases. The preliminary treatment to manage severe acute respiratory infection (SARI) includes supportive oxygen care and mechanical ventilation (Hassan et al. 2020). Several clinical trials are recruiting globally as well as in India to assess the effect of antiviral medicines on infected personals. Remdesivir, a drug similar to a nucleotide, adenosine and intended to fight viral replication was tested in clinical trials through a compassionate use program in SARS-CoV-2 infected patients of the United States (NIH clinical trial of remedesivir to treat COVID-19 begins). Similar kind of clinical trials was also implemented in China (Joseph 2020). Treatment with intravenous remdesivir has no solid data till now to indicate its efficacy. Another report showed that the use of Favilavir (Favipiravir), an antiviral drug has secured approval as an investigational therapy from the National Medical Products Administration of China to treat Covid-19 infected patients (Favilavir approved as experimental coronavirus drug). Furthermore, a pilot investigator-initiated clinical trial (IIT) with APN01, a recombinant human angiotensin-converting enzyme 2 (rhACE2), is ongoing in the People's Republic of China to treat patients with SARS-CoV-2 infection (Apeiron begins pilot clinical trial with APN01 to treat coronavirus infection in China). India also expressed interest to participate in WHO solidarity trial for developing vaccines for COVID 19 (Thacker 2020$_c$). The treatment that has so far been attempted in India, using a combination of HIV, swine flu and malaria medicines. Doctors of Sawai Man Singh (SMS) Hospital in Jaipur treated an Italian lady with a dose of lopinavir 200 mg / ritonavir 50 mg twice a day in a combination with oseltamivir (drug used to treat swine flu), and chloroquine (used to treat malaria). Following this treatment, a remarkable improvement occurred and the woman got recovery from the COVID-19 (Indian doctors successfully cure Italian coronavirus patients). Use of this combination of anti-HIV drug (lopinavir and ritonavir) had also recommended by Union Health Ministry on a case-to-case basis especially for high-risk groups patients having hypoxia, hypotension, and organ dysfunction (Coronavirus: Health Ministry recommends anti-HIV drug combination lopinavir-ritonavir on case to case basis). ICMR recommended the limited use of hydroxy-chloroquine as a preventive medication for high-risk population such as healthcare workers involved in the treatment of suspected or confirmed cases of COVID-19 and peoples contact of positive cases (ICMR recommends hydroxychloroquine for high-risk population). US Centre of Disease Control and Prevention suggested the use of a combination of hydroxychloroquine and an antibiotic azithromycin (Information for Clinicians on Therapeutic Options for COVID-19 Patients). French doctors were also expanding use of hydroxychloroquine (Duqueroy 2020).

Economic effect

The effect of corona pandemic on global economy is a burning issue to discuss. In this section of the paper, we would like to address this issue on the perspective of Indian economy. In terms of notional Gross Domestic Product (GDP), India is the 5th largest country in the world and stood 3rd in terms of purchasing power Parity (PPP) in 2019 (World Economic Outlook Database, IMF, October- 2019). More or less 7% annual GDP growth has been recorded from 2014 to 2019 and Nominal GDP was 3.202 trillion US dollar in 2019 (IMF Database, Jan 28, 2020). However, growth of Indian economy shows a decline trend in the F-Y 2019–20. The situation seems to be further deteriorate due to the corona crisis in the last quarter in 2019-20 and estimated loss would be Rs. 9 lakh crore in the F-Y2019-20 which is equivalent to 3% of national GDP. The adverse effect of nationwide lockdown could be actually realised in 2020-21. Credit rating agencies like Fitch and Moody predict mere 3% to 3.5% growth rate in the 1st quarter of 2020-21 (Noronha and Sharma 2020). FICCI survey showed 53% of Indian businesses have indicated a marked impact of COVID-19 on business operations (Roychoudhury 2020). Economists also warn that the situation turns into worse further on the fact that how long the crisis lasts and what measures are taken by the government of the affected countries. Corona virus crisis will impact the Indian economy to a great extent. Productions as well as consumption of consumer durables, textiles, and automobiles are going to be effected badly. Apart from these sectors, tourism, aviation, hospitality, logistics sector would face a serious crisis even struggle for their existence in this situation. This crisis surely affects the small and marginal farmers due to problem of marketing their agro-products or force selling at low price to the local intermediaries and also to the daily workers for losing their jobs in both unorganised industrial sectors and agriculture.

Suggested economic measures/remedies

The present situation is very alarming for Indian economy and there was no indication for this sudden attack on In-

dian as well as on global economy. The situation could be tackled to a large extent if both short-term and long-term measures are taken by the central and state governments and central bank of India (R.B.I.). Central Government has already announced a stimulus package of Rs. 1.70 lakh crore for the weaker and needy section of the society to combat the crisis. Reserve Bank of India also has announced various measures like 3-month moratorium on term loans and EMIs outstanding as on 1st March, 2020, cut the REPO rate by 75 basis point (rate of interest at which RBI lends money to the commercial Banks) and Reverse REPO rate (rate of interest at which RBI lends money from the commercial Banks) by 90 basis point in order to generate more liquid money to the market, increase the limit of sanctioning loan without guarantee to the self- help groups. But these measures are temporary to fight the crisis and boost the economy immediately. The situation seems to be difficult in the next financial year where the main challenge of the government would be to bring back the growth of economy into the right track (maintain at least 6-7% annual growth) along with restore the upward demand- production-consumption cycle. India needs coordinated long-term fiscal actions and monetary stimulus to overcome this crisis. Fiscal and monetary stimulus package including subsidy, provision of loan at low interest rate, waive or moratorium of loan for at least 1 year to the farmers, marginal and small-scale industries would help to increase investment and production. CII also urged that RBI to consider relaxing the non-performing asset recognition norms from 90 days to 180 days till 30th September 2020. Slash down of rate of GST and direct tax (both for corporate and non-corporate assessee) is another weapon that government could exercise to provide more liquid money to the manufacturers and consumers. Government may also act as a partial guarantor of loan provided by the bankers to the small and medium businessmen and industrialists.

Conclusion

A perspective of COVID-19 in India including the transmission, prevalence, preventive measures and economic impact has been depicted in the study. As of now community transmission is not evident but gradually India is approaching towards 3rd phage of infection. The Govt. of India whole solely combating the situation by initial imposing of 21 days countrywide lockdown (seize of movement) to maintain social distancing as an immediate measure to curb the spread of infection which actually pays off in last few days. India's numbers are still small and coercible compared to many other developed countries and that's largely due to the early actions taken by both Government and social sectors. However, it's still a very early stage, though, and Government will have to do extensive testing and contact tracing. Primarily, the urgent need is to locate and seal all the hot spots of COVID-19 in the country and do mass testing of every citizens of that locality. The random testing of persons residing in slum areas, red-light areas must be the next priority. All the institutes, gymnasiums, cinema halls, swimming pools must be kept closed until the situation comes under control. Hospitals, police stations, banks, post office and marketplaces must be decontaminated at regular intervals. Decontamination is also essential to strengthen the health care infrastructure of the country. As the number of cases increases, it would be important to appropriately prepare health systems and use the existing resources strategically. The rapid test kits have to be made more available to every part of the country with top priority. In conformity with WHO, India has to go rapid test for every suspect and their contacts. The medicines, supportive care and ventilation facilities must be made available even to the underdeveloped rural areas. Every suspected person must be quarantined and tested. People must also be well aware about the current situation and extend their hands to the Govt. by restricting their unnecessary movements and gatherings. We are at verge of crisis where a huge number of people can get affected at once. With India's numbers of population, even small percentages shall generate millions of cases. Henceforth, mass awareness not only by the Government sectors but also by spiritual leaders would be effective. Besides it, NGOs and civil society, and those icons of the society, will have to do everything to minimize stigmatization of victims. As well as the whole country must stand united to cope with this extraordinary pandemic as the disease does not distinguish between rich or poor, between white or black skin. On the other hand, the length and depth of corona pandemic indicate the sign of global recession. India needs coordinated long-term fiscal actions and monetary stimulus to overcome this crisis. We only hope that the Indian economy will be mildly affected by the present crisis and there will be minimum adverse impact on it. Government must extend the period of lockdown but also allow essential sectors, farmers and traders by maintaining a delicate balance between medical emergency and economy.

References

Ansari D (2020) Indian engineering student develops a Rs500 device to ensure social distancing, Republic. Available: https://www.republicworld.com/technology-news/

gadgets/indian-engineering-student-develops-a-device-to-ensure-social-distance.html. Accessed 26 March 2020.

Apeiron begins pilot clinical trial with APN01 to treat coronavirus infection in China (2020) Medical Buyer. Available: https://www.medicalbuyer.co.in/apeiron-begins-pilot-clinical-trial-with-apn01-to-treat-coronavirus-infection-in-china/. Accessed 27 February 2020.

Assam govt to set up 4 temporary hospitals for COVID-19 (2020) Business Standard. Available: https://www.business-standard.com/article/pti-stories/assam-govt-to-set-up-4-temporary-hospitals-for-covid-19-120032600510_1.html. Accessed 26 March 2020.

Athrady A (2020) COVID-19: Indian Railways to convert 20,000 coaches as isolation wards, Deccan Herald. Available: https://www.deccanherald.com/national/covid-19-indian-railways-to-convert-20000-coaches-as-isolation-wards-819732.html. Accessed 31 March 2020.

Automobile manufacturers asked to make ventilators: Health Ministry (2020) The Economic Times. Available: https://m.economictimes.com/industry/auto/auto-news/automobile-manufacturers-asked-to-make-ventilators-health-ministry/articleshow/74890488.cms. Accessed 30 March 2020.

Backer JA, Klinkenberg D, Wallinga J (2020) Incubation period of 2019 novel coronavirus (2019-nCoV) infections among travellers from Wuhan, China, 20-28 January 2020. Euro Surveill 25(5):2000062.

Badve A (2020) Coronavirus India: Nagpur's Dr Anand Sancheti develops ventilator with splitters, Sakal Times. Available: https://www.sakaltimes.com/coronavirus-maharashtra/coronavirus-india-nagpur%E2%80%99s-dr-anand-sancheti-develops-ventilator-splitters. Accessed 5 April 2020.

Bihar CM Nitish Kumar announces free ration for cardholders during coronavirus lockdown (2020) The Print. Available: https://theprint.in/india/bihar-cm-nitish-kumar-announces-free-ration-for-cardholders-during-coronavirus-lockdown/386633/. Accessed 23 March 2020.

Bose M (2020) Pune based company develop coronavirus test kit. Deccan Herald. Available: https://www.deccanherald.com/national/west/pune-based-company-develop-coronavirus-test-kit-819019.html. Accessed 29 March 2020.

Chen N, Zhou M, Dong X, Qu J, Gong F, Han Y (2020) Epidemiological and clinical characteristics of 99 cases of 2019 novel coronavirus pneumonia in Wuhan, China: a descriptive study. Lancet 395(10223):507-513.

Combating COVID-19: Navy's MARCOS commandos reach out to fisherman at Wular Lake (2020) The Times of India. Available: https://timesofindia.indiatimes.com/india/combating-covid-19-navys-marcos-commandos-reaches-out-to-fishermen-at-wular-lake/articleshow/74882373.cms. Accessed 30 March 2020.

Combating COVID-19: West Bengal increases insurance coverage from Rs 5 lakh to Rs 10 lakh (2020) Business Standard. Available: https://www.business-standard.com/article/news-ani/combating-covid-19-west-bengal-increases-insurance-coverage-from-rs-5-lakh-to-rs-10-lakh-120033001697_1.html. Accessed 30 March 2020.

Coronavirus a pandemic: India shuts doors for outsider, under self imposed quarantine (2020) The Economic Times. Available: https://m.economictimes.com/news/politics-and-nation/coronavirus-a-pandemic-india-shuts-doors-for-outsiders-under-self-imposed-quarantine/articleshow/74582547.cms. Accessed 12 March 2020.

Coronavirus disease 2019 (COVID-19) Situation report-91 (2020) World Health Organization, Available: https://www.who.int/docs/default-source/coronaviruse/situation-reports/20200420-sitrep-91-covid-19.pdf?sfvrsn=fcf0670b_4. Accessed 20 April 2020.

Coronavirus hits Delhi: Two new cases detected in national capital and Telangana (2020) The Economic Times. Available: https://m.economictimes.com/news/politics-and-nation/coronavirus-reaches-national-capital-two-new-cases-detected-in-delhi-and-telangana/articleshow/74438803.cms. Accessed 04 March 2020.

Coronavirus impact: Railways cancels all passenger trains till March 31 (2020) Business Today. Available: https://www.businesstoday.in/current/economy-politics/breaking-all-railway-operations-to-be-suspended-till-march-25-due-to-coronavirus/story/398884.html. Accessed 22 March 2020.

Coronavirus outbreak: Govt cancels Visas for Italy, Iran, Japan and South Korea, issues new travel advisory (2020) India Today. Available: https://www.indiatoday.in/india/story/coronavirus-outbreak-govt-cancels-visas-for-italy-iran-japan-and-south-korea-issues-new-travel-advisory-1651955-2020-03-03. Accessed 03 March 2020.

Coronavirus outbreak: Govt suspends all domestic flights from midnight of March 24 (2020) The Economic Times. Available: https://m.economictimes.com/industry/transportation/airlines-/-aviation/coronavirus-outbreak-govt-suspends-all-domestic-flights-from-midnight-of-march-24/videoshow/74775917.cms. Accessed 23 March 2020.

Coronavirus suspects flee from a hospital in Maharashtra (2020) The Economics Times. Available: https://m.economictimes.com/news/politics-and-nation/11-coronavirus-suspects-flee-from-a-hospital-in-maharashtra/videoshow/74644936.cms. Accessed 16 March 2020.

Coronavirus: All international arrivals to India to share travel history at airports (2020) The Economic Times. Available: https://economictimes.indiatimes.com/news/politics-and-nation/all-international-arrivals-to-give-travel-history-at-airports/articleshow/74467810.cms

2020. Accessed 04 March 2020.
Coronavirus: DGCA extends airport screening to passengers arriving from Japan, South Korea (2020) India Today. Available: https://www.indiatoday.in/india/story/coronavirus-dgca-extends-airport-screening-to-passengers-arriving-from-japan-south-korea-1646572-2020-02-14. Accessed 04 April 2020.
Coronavirus: Govt directs 12 major ports to put in place screening, quarantine system (2020) India Today. Available: https://www.indiatoday.in/india/story/coronavirus-govt-directs-12-major-ports-to-put-in-place-screening-quarantine-system-1644321-2020-02-07 2020. Accessed 04 April 2020.
Coronavirus: Health Ministry recommends anti-HIV drug combination Lopinavir-Ritonavir on case to case basis (2020) India Today. Available: https://www.indiatoday.in/india/story/coronavirus-health-ministry-recommends-anti-hiv-drug-combination-lopinavir-ritonavir-case-to-case-basis-1656488-2020-03-17. Accessed 17 March 2020.
Coronavirus: India starts screening passengers from Singapore (2020) The Straits Times. Available: https://www.straitstimes.com/asia/south-asia/coronavirus-india-starts-screening-passengers-from-singapore. Accessed 04 April 2020.
Coronavirus: Maruti, Noida firm got nod to supply 10,000 ventilators (2020) Business Today. Available: https://www.businesstoday.in/current/corporate/coronavirus-maruti-noida-firm-get-up-govt-nod-to-supply-10000-ventilators/story/400080.html. Accessed 3 April 2020.
Coronavirus: Rs 25 lakh compensation for Guj frontline staff (2020) Business Standard. Available: https://www.business-standard.com/article/pti-stories/coronavirus-rs-25-lakh-compensation-for-guj-frontline-staff-120040500653_1.html. Accessed 5 April 2020.
COVID-19: Def min grants emergency financial powers to Army commanders to set up medical facilities (2020) Business Standard. Available: https://www.business-standard.com/article/pti-stories/covid-19-def-min-grants-emergency-financial-powers-to-army-commanders-to-set-up-medical-facilities-120032701830_1.html. Accessed 27 March 2020.
COVID-19: Jharkhand to give 2 months' ration in advance (2020) India Today. Available: https://www.indiatoday.in/india/story/covid-19-jharkhand-to-give-2-months-ration-in-advance-1659891-2020-03-26. Accessed 26 March 2020.
Dey S (2020) 63% of COVID-19 deaths in India among 60-plus. The Times of India. Available: https://timesofindia.indiatimes.com/india/63-of-covid-19-deaths-in-indian-among-60-plus/articleshow/75018702.cms. Accessed 07 April 2020.
DRDO is stepping in to build ventilators and manufacture masks (2020) Business Insider. Available: https://www.businessinsider.in/science/health/news/drdo-is-stepping-in-to-build-ventilators-and-manufacture-masks/articleshow/74905607.cms. Accessed 31 March 2020.
Duqueroy V (2020) COVID-19: More hydroxychloroquine data from France, more questions. Medscape. Available: https://www.medscape.com/viewarticle/927758. Accessed 30 March 2020.
Favilavir approved as experimental coronavirus drug (2020) Clinical Trials Arena. Available: https://www.clinicaltrialsarena.com/news/china-favilavir-testing-approval/. Accessed 21 February 2020.
Five more people from Kerala test positive for coronavirus (2020) The Economic Times. Available: https://m.economictimes.com/news/politics-and-nation/five-more-people-from-kerala-test-positive-for-coronavirus/articleshow/74534888.cms. Accessed 08 March 2020.
FM Nirmala Sitharaman announces Rs 1.7 lakh crore relief package for poor (2020) The Economic Time. Available: https://m.economictimes.com/news/economy/policy/fm-nirmala-sitharaman-announces-rs-1-7-lakh-crore-relief-package-for-poor/articleshow/74825054.cms. Accessed 27 March 2020.
Free foodgrains to all till September: CM (2020) The Statesman. Available: https://www.thestatesman.com/bengal/free-foodgrains-till-september-cm-1502868399.html. Accessed 21 March 2020.
Gorbalenya AE, Baker SC, Baric RS, Groot RJ-D, Drosten C, Gulyaeva AA, Haagmans BL, Lauber C, Leontovich AM, Neuman BW, Penzar D, Perlman S, Poon LLM, Samborskiy DV, Sidorov IA, Sola I, Ziebuhr J (2020) The species *Severe acute respiratory syndrome-related coronavirus*: classifying 2019-nCoV and naming it SARS-CoV-2. Nat Microbiol 5(5):536-540.
Government extends ban on international flights till April 14 (2020) The Economic Times. Available: https://m.economictimes.com/industry/transportation/airlines-/-aviation/government-extends-ban-on-international-flights-till-april-14/articleshow/74832326.cms. Accessed 26 March 2020.
Govt gives power to zonal DCs to take strict action against landlords evicting dics, paramedics (2020) The Hindu. Available: https://www.thehindu.com/news/national/covid-19-govt-gives-power-to-zonal-dcs-to-take-strict-action-against-landlords-evicting-docs-paramedics/article31159342.ece. Accessed 25 March 2020.
Govt identifies 170 Covid-19 hotspots: Here's the full list (2020) The Economic Times. Available: https://m.economictimes.com/news/politics-and-nation/govts-plan-to-contain-local-outbreak-is-yielding-results-lav-agarwal/articleshow/75159535.cms. Accessed 21 April 2020.
Govt to provide 5 kg grains, 1 kg pulses for free over next 3

months: Nirmala Sitharaman (2020) India Today. Available: https://www.indiatoday.in/india/story/nirmala-sitharaman-coronavirus-govt-to-provide-5-kg-grains-1-kg-pulses-for-free-3-months-1659949-2020-03-26. Accessed 26 March 2020.

Gurung SK, Army's desert quarantine largest in India, may get bigger (2020) The Economic Times. Available: https://m.economictimes.com/news/politics-and-nation/armys-desert-quarantine-largest-in-india-may-get-bigger/articleshow/74740878.cms. Accessed 21 March 2020.

Habitat for Humanity in India (2020) Available: https://www.habitat.org/where-we-build/india. Accessed 31 March 2020.

Haider T (2020) Timeline of how Nizamuddin Markaz defied lockdown with 3400 people at Tablighi Jamaat event. India Today. Available: https://www.indiatoday.in/india/story/timeline-of-nizamuddin-markaz-event-of-tablighi-jamaat-in-delhi-1661726-2020-03-31. Accessed 31 March 2020.

Hassan SA, Sheikh FN, Jamal S, Ezeh JK, Akhtar A (2020) Coronavirus (COVID-19): A review of clinical features, diagnosis, and Treatment. Cureus 12(3):e7355.

Health Ministry launches new toll-free number, email ID for queries on COVID-19 (2020) The Economic Times. Available: https://m.economictimes.com/news/politics-and-nation/health-ministry-launches-new-toll-free-number-email-id-for-queries-on-covid-19/articleshow/74661190.cms. Accessed 16 March 2020.

High level Group of Ministers reviews current status, and actions for prevention and management of COVID-19 (2020) Ministry of Health and Family Welfare, PIB Delhi. Available: https://pib.gov.in/PressReleseDetail.aspx?PRID=1604909. Accessed 02 March 2020.

Holmes E (2020) Initial genome release of novel coronavirus 2020. Available: http://virological.org/t/initial-genome-release-of-novel-coronavirus/319. Accessed 22 January 2020.

Huang C, Wang Y, Li X, Ren L, Zhao J, Hu Y, Zhang L, Fan G, Xu J, Gu X, Cheng Z, Yu T, Xia J, Wei Y, Wu W, Xie X, Yin W, Li H, Liu M, Xiao Y, Gao H, Guo L, Xie J, Wang G, Jiang R, Gao Z, Jin Q, Wang J, Cao B (2020) Clinical feature of patients infected with 2019 novel coronavirus in Wuhan, China. Lancet 395(10223):497-506.

Hui DS, Azhar EL, Madani TA, Ntoumi F, Kock R, Dar O, Lppolito G, Mchugh TD, Memish ZA, Drosten C, Zumla A, Petersen E (2020) The continuing 2019-nCoV epidemic threat of novel coronaviruses to global health – The latest 2019 novel coronavirus outbreak in Wuhan, China. Int J Infect Dis 91:264-266.

IAF creates nine quarantine facilities at its nodal bases across country as coronavirus cases multiply (2020) The Economic Times. Available: https://m.economictimes.com/news/defence/coronavirus-iaf-creates-nine-quarantine-facilities-at-its-nodal-bases-across-country/articleshow/74830456.cms. Accessed 26 March 2020.

ICMR (2020) Coronavirus disease 2019 (COVID-19) Testing Lab. Available: https://icmr.nic.in/. Accessed 21 April 2020.

ICMR recommends hydroxychloroquine for high-risk population (2020) The Economic Times. Available: https://m.economictimes.com/industry/healthcare/biotech/pharmaceuticals/indias-covid-task-force-recommends-hydroxychloroquine-for-high-risk-patients-with-strict-riders/articleshow/74774540.cms. Accessed 23 March 2020.

India census says 1 in 6 lives in unsanitary slums (2013) CBC. Available: https://www.cbc.ca/news/world/india-census-says-1-in-6-lives-in-unsanitary-slums-1.1403897. Accessed 03 April 2020.

India has tremendous capacity in eradicating coronavirus pandemic: WHO (2020) The Economic Times. Available: https://economictimes.indiatimes.com/news/politics-and-nation/india-has-tremendous-capacity-in-eradicating-coronavirus-pandemic-who/articleshow/74788341.cms. Accessed 03 April 2020.

India's first coronavirus case confirmed in Kerala (2020) The Economic Times. Available: https://economictimes.indiatimes.com/news/politics-and-nation/indias-first-coronavirus-case-confirmed-in-kerala/videoshow/73769702.cms. Accessed 30 January 2020.

India's first COVID-19 death confirmed in Karnataka (2020) The Hindu. Available: https://www.thehindu.com/news/national/coronavirus-live-updates-march-12-2020/article31046507.ece. Accessed 12 March 2020.

Indian doctors successfully cure Italian coronavirus patients (2020) Inside Over. Available: https://www.insideover.com/society/indian-doctors-successfully-cure-italian-coronavirus-patients.html. Accessed 17 March 2020.

Information for Clinicians on Therapeutic Options for COVID-19 Patients (2020) CDC. Available: https://www.cdc.gov/coronavirus/2019-ncov/hcp/therapeutic-options.html. Accessed 30 March 2020.

Iqbal M, Karmakar R (2020) Private hospitals in Jaipur reserved for COVID-19 treatment; MoUs signed in Assam. The Hindu. Available: https://www.thehindu.com/news/national/other-states/47-private-hospitals-in-jaipur-reserved-for-covid-19-treatment-mou-inked-in-assam/article31214568.ece. Accessed 31 March 2020.

Italian tourist in Jaipur tests positive (2020) The Hindu. Available: https://www.thehindu.com/news/national/other-states/italian-tourist-in-jaipur-tests-positive-for-covid-19/article30967526.ece. Accessed 03 March 2020.

Joseph A (2020) As the coronavirus spreads, a drug that once raised the world's hopes is given a second shot. Stat. Available: https://www.statnews.com/2020/03/16/

remdesivir-surges-ahead-against-coronavirus/. Accessed 16 March 2020.

Jung YJ, Park GS, Moon JH, Ku K, Beak SH, Kim S, Park EC, Park D, Lee JH, Byeon CW, Lee JJ, Maeng JS, Kim SJ, Kim S, Kim BT, Lee MJ, Kim HG (2020) Comparative analysis of primer-probe sets for the laboratory confirmation of SARS-CoV-2. bioRxiv. DOI:10.1101/2020.02.25.964775.

Kerala defeats coronavirus; India's three COVID-19 patients successfully recover (2020) The Weather Channel. Available: https://weather.com/en-IN/india/news/news/2020-02-14-kerala-defeats-coronavirus-indias-three-covid-19-patients-successfully. Accessed 14 February 2020.

Kerala government declares coronavirus as state disaster (2020) The Economic Times. Available: https://economictimes.indiatimes.com/news/politics-and-nation/kerala-government-declares-coronavirus-as-state-disaster/videoshow/73913272.cms. Accessed 03 February 2020.

Kerala now confirms third case of coronavirus, patient had returned from China's Wuhan (2020) India Today. Available: https://www.indiatoday.in/india/story/kerala-now-confirms-third-case-of-coronavirus-1642789-2020-02-03. Accessed 03 February 2020.

Khamsi R (2020) They say coronavirus isn't airborne - but it's definitely borne by air. Wired. Available: https://www.wired.com/story/they-say-coronavirus-isnt-airborne-but-its-definitely-borne-by-air/. Accessed 14 March 2020.

Kothai R, Arul B (2020) 2019 Novel Coronavirus: A mysterious threat from Wuhan, China- A current review. Int J Res Pharm Sci 11:7-15.

Kulkarni S (2020) India steps up fight against COVID-19, bans all international flights. Deccan Herald News. Available: https://www.deccanherald.com/national/national-politics/india-steps-up-fight-against-covid-19-bans-all-international-flights-815577.html. Accessed 20 March 2020.

List of hospitals designated for treatment of COVID-19 patients in south India (2020) The News Minute. Available: https://www.thenewsminute.com/article/list-hospitals-designated-treatment-covid-19-patients-south-india-121014. Accessed 24 March 2020.

Ministry of Health and Family Welfare, Government of India (2020) Available: https://mohfw.gov.in/. Accessed 20 April 2020.

Mohanty M (2020) Odisha announces Covid-19-dedicated hospitals with 1,000 beds. The Economic Times. Available: https://m.economictimes.com/industry/healthcare/biotech/healthcare/odisha-announces-countrys-first-covid-19-dedicated-hospitals-with-1000-beds/articleshow/74832053.cms. Accessed 27 March 2020.

Nearly 100 Delhi Mosque-linked coronavirus cases, 2,100 evacuated: 10 facts (2020) NDTV. Available: https://www.ndtv.com/india-news/coronavirus-india-delhi-markaz-nizamuddin-mosque-sealed-after-7-covid-19-deaths-850-moved-out-for-qu-2203336. Accessed 01 April 2020.

Nichenametla P (2020) Coronavirus threat looms over Bengaluru after Hyderabad techie tests positive for COVID-19. Deccan Herald. Available: https://www.deccanherald.com/national/south/coronavirus-threat-looms-over-bengaluru-after-hyderabad-techie-tests-positive-for-covid-19-809863.html. Accessed 02 March 2020.

NIH clinical trial of remdesivir to treat COVID-19 begins (2020) National Institute of Health. Available: https://www.nih.gov/news-events/news-releases/nih-clinical-trial-remdesivir-treat-covid-19-begins. Accessed 25 February 2020.

Nishiura H, Jung SM, Linton NM, Kinoshita R, Yang Y, Hayashi K, Kobayashi T, Yuan B, Akhmetzhanov AR (2020) The extent of transmission of novel coronavirus in Wuhan, China, 2020. J Clin Med 9(2):330.

Noronha G (2020) New India Assurance releases guidelines for Rs 50 lakh insurance coverage for health care providers. The Economic Times. Available: https://m.economictimes.com/industry/banking/finance/insure/new-india-assurance-releases-guidelines-for-rs-50-lakh-insurance-coverage-for-health-care-providers/articleshow/74896597.cms. Accessed 30 March 2020.

Noronha G, Sharma YS (2020) Coronavirus outbreak will set back India's growth recovery. The Economic Times. Available: https://m.economictimes.com/news/economy/policy/outbreak-will-set-back-indias-growth-recovery/articleshow/74663633.cms. Accessed 17 March 2020.

Now, a caller tune for COVID-19 (2020) The Hindu. Available: https://www.thehindubusinessline.com/info-tech/telcos-spread-awareness-on-covid-19-through-default-caller-tunes/article31014506.ece. Accessed 8 March 2020.

OFB designates 285 beds for coronavirus cases (2020) The Economic Times. Available: https://economictimes.indiatimes.com/news/defence/obf-designates-285-beds-for-coronavirus-cases/articleshow/74809298.cms. Accessed 25 March 2020.

Perappadan BS (2020) Delhi reports India's second COVID-19 death. The Hindu. Available: https://www.thehindu.com/news/national/coronavirus-delhi-reports-indias-second-covid-19-death/article31063274.ece. Accessed 13 March 2020.

PM Narendra Modi forms economic response task force calls for 'Janata Curfew' (2020) The Economic Times. Available: https://economictimes.indiatimes.com/news/politics-and-nation/pm-narendra-modi-forms-economic-response-task-force-calls-for-janata-curfew/articleshow/74715013.cms. Accessed 21 March 2020.

Rapid Risk Assessment: Cluster of pneumonia cases caused by a novel coronavirus, Wuhan, China (2020) European Centre for Disease Prevention and Control. Available:

https://www.ecdc.europa.eu/sites/default/files/documents/Risk-assessment-pneumonia-Wuhan-China-26-Jan-2020_0.pdf. Accessed 17 January 2020.

Rawat M (2020) Coronavirus in India: Tracking country's first 50 COVID-19 cases; what number tell. India Today. Available: https://www.indiatoday.in/india/story/coronavirus-in-india-tracking-country-s-first-50-covid-19-cases-what-numbers-tell-1654468-2020-03-12. Accessed 12 March 2020.

Report of the WHO-China Joint Mission on Coronavirus Disease 2019 (COVID-19) (2020) Available: https://www.who.int/docs/default-source/coronaviruse/who-china-joint-mission-on-covid-19-final-report.pdf. Accessed 24 February 2020.

Rothe C, Schunk M, Sothmann P, Bretzel G, Froeschl G, Wallrauch C, Zimmer T, Thiel V, Janke C, Guggemos W, Seilmaier M, Drosten C, Vollmar P, Zwirglmaier K, Zange S, Wölfel R, Hoelscher M (2020) Transmission of 2019-nCoV infection from an asymptomatic contact in Germany. N Engl J Med 382(10):970-971.

Roychoudhury A (2020) Economic Impact of Corona Virus, Business Standard. Available: https://www.business-standard.com/article/economy-policy/economic-impact-of-coronavirus-bad-in-jan-march-worse-in-april-june-120031800699_1.html. Accessed 22 March 2020.

Schools closed, travel to be avoided, say centre on coronavirus: 10 points (2020) NDTV. Available: https://www.ndtv.com/india-news/mumbai-s-siddhivinayak-temple-to-close-entry-for-devotees-from-today-amid-coronavirus-outbreak-2195660. Accessed 17 March 2020.

Second case of coronavirus confirmed in Kerala (2020) The Economic Times. Available: https://m.economictimes.com/news/politics-and-nation/2nd-case-of-coronavirus-confirmed-in-kerala/videoshow/73863126.cms. Accessed 03 February 2020.

Sharma N (2020) Private hospitals to treat Covid-19 patients from tomorrow. The Economic Times. Available: https://m.economictimes.com/news/politics-and-nation/pvt-hospitals-to-treat-covid19-from-tomorrow/articleshow/74800386.cms. Accessed 25 March 2020.

Shekhar S (2020) How rapid antibody tests are different from existing PCR tests for COVID-19, India Today. Available: https://www.indiatoday.in/india/story/how-rapid-antibody-tests-are-different-from-existing-pcr-tests-for-covid-19-explained-1663441-2020-04-05. Accessed 5 April 2020.

Shops selling essentials, medicines will remain open throughout 21-day lockdown: Govt (2020) The Economic Times. Available: https://m.economictimes.com/news/politics-and-nation/shops-selling-essentials-medicines-will-remain-open-throughout-21-day-lockdown-govt/articleshow/74811907.cms. Accessed 25 March 2020.

Siddiqui H (2020) Fight against Coronavirus: OFB and Defence PSUs to make ventilators and masks. Financial Express. Available: https://www.financialexpress.com/lifestyle/health/fight-against-coronavirus-ofb-and-defence-psus-to-make-ventilators-and-masks/1910914/. Accessed 27 March 2020.

Silver C (2020) The top economies in the world. Investopedia. Available: https://www.investopedia.com/insights/worlds-top-economies/. Accessed 03 April 2020.

Singh AT (2020) Government suspends air travel from China, declares all visas 'Invalid'; The Times of India. Available: https://weather.com/en-IN/india/news/news/2020-02-04-govt-suspends-air-travel-from-china. Accessed 04 February 2020.

Suffian M (2020) 3 Odisha persons who attended Tablighi Jamaat event in Delhi quarantined, India Today. Available: https://www.indiatoday.in/india/story/three-odisha-attended-tablighi-jamaat-event-delhi-quarantined-1661922-2020-03-31. Accessed 31 March 2020.

Suneja K (2020) Govt allows pharma formulations exports under export-linked scheme, The Economic Times. Available: https://economictimes.indiatimes.com/news/economy/foreign-trade/govt-allows-pharma-formulations-exports-under-export-linked-scheme/articleshow/74736847.cms. Accessed 20 March 2020.

Telangana Lockdown: 12 kg free rice per person, Rs 1,500 per family to be supplied for each white ration card (2020) Telangana Today. Available: https://telanganatoday.com/telangana-lockdown-12-kg-free-rice-per-person-rs-1500-per-family-to-be-supplied-for-each-white-ration-card. Accessed 22 March 2020.

Thacker T (2020) No symptoms in 80% of Covid cases raise concerns, The Economic Times. Available: https://m.economictimes.com/industry/healthcare/biotech/healthcare/no-symptoms-in-80-of-covid-cases-raise-concerns/articleshow/75260387.cms. Accessed 21 April 2020.

Thacker T (2020_b) Mylab partners with Serum Institute of India and AP Globale for testing kits. The Economic Times. Available: https://m.economictimes.com/industry/healthcare/biotech/healthcare/mylab-partners-with-adar-poonawalla-abhijit-pawar-to-scale-up-production-of-covid-19-test-kits/articleshow/74945929.cms. Accessed 03 April 2020.

Thacker T (2020_c) India to soon participate in WHO 'solidarity trial' for developing potential COVID-19 drugs; Government. The Economic Times. Available: https://m.economictimes.com/news/politics-and-nation/india-to-soon-participate-in-who-solidarity-trial-for-developing-potential-covid-19-drugs-govt/articleshow/74847941.cms. Accessed 28 March 2020.

Tracing the Italian connection to India's fresh coronavirus count (2020) The Economic Times. Available: https://m.economictimes.com/news/politics-and-nation/tracing-

the-italian-connection-to-indias-fresh-coronavirus-count/articleshow/74490038.cms. Accessed 5 March 2020.

Wang W, Tang J, Wei F (2020) Updated understanding of the outbreak of 2019 novel coronavirus (2019-nCoV) in Wuhan, China. J Med Virol 92(4):441-447.

West Bengal converts state-run hospital into COVID-19 isolation, treatment facility (2020) Deccan Herald. Available: https://www.deccanherald.com/national/east-and-northeast/west-bengal-converts-state-run-hospital-into-covid-19-isolation-treatment-facility-817439.html. Accessed 25 March 2020.

WHO Director-General's opening remarks at the media briefing on COVID-19 (2020) Available: https://www.who.int/dg/speeches/detail/who-director-general-s-opening-remarks-at-the-media-briefing-on-covid-19---11-march-2020. Accessed 11 March 2020.

World Economic Outlook Database, IMF, October, 2019 and January, 2020. Available: https://www.imf.org/external/pubs/ft/weo/2019/02/weodata/index.aspx. Accessed 5 April 2020.

Wu F, Zhao S, Yu B, Chen YM, Wang W, Song ZG, Hu Y, Tao ZW, Tian JH, Pei YY, Yuan ML, Zhang YL, Dai FH, Liu Y, Wang QM, Zheng JJ, Xu L, Holmes EC, Zhang YZ (2020) A new coronavirus associated with human respiratory disease in China. Nature 579:265-269.

Yin Y, Wunderink RG (2018) MERS, SARS and other coronaviruses as causes of pneumonia. Respirology 23:130-137.

Acta Biologica Szegediensis

Volume 64(1):63-71, 2020
Acta Biologica Szegediensis
http://abs.bibl.u-szeged.hu/index.php/abs
DOI:10.14232/abs.2020.1.63-71

ARTICLE

The Effect of Pesticide Application on QTLs Controlling Traits in Barley

Samira Bakhtiari, Hossein Sabouri*, Mehdi Mollashahi, Hossein Hosseini Moghaddam

Department of Plant Production, Collage of Agriculture Science and Natural Resource, Gonbad Kavous University, Gonbad Kavous, Golestan, Iran

ABSTRACT Among cereals, barley (Hordeum vulgare L.) ranks fourth in consumption worldwide. Among barley breeding goals, one can refer to gene mapping, studying their inheritance, and saturated genetic linkage maps. Problems with pesticide applications include reduced genetic diversity, reduced nitrogen fixation, and destruction of the habitat of especially endangered species. The effect of pesticide application on the emergence of QTLs expressing traits in experimental barley was investigated using 104 barley F2:4 families from Badia × Kavir cross. A total of 25 QTLs were mapped for all traits. In non-using pesticides, 12 QTLs were identified for peduncle length, stem diameter, flag leaf length, and awn length. It was found that qFL-4 has major effects on flag leaf length. For using the pesticide, 13 QTLs were detected that QTLs related to stem diameter, grain weight, flag leaf length explained a high percentage of phenotypic variation. The results of this study showed that pesticide application affects the expression of some genes in barley. Besides, major-effect trait-controller QTLs and their associated markers can be used in marker-assisted selection (MAS) programs.

Acta Biol Szeged 64(1):63-71 (2020)

KEY WORDS
barley
marker-assisted selection
pesticide
QTL

ARTICLE INFORMATION
Submitted
05 May 2020.
Accepted
14 July 2020.
***Corresponding author**
E-mail: hossein.sabouri@gonbad.ac.ir

Introduction

Barley (*Hordeum vulgare* L.,) is a diploid crop with 2n = 2x = 14 chromosomes (Germán et al. 2000). Among cereals, barley ranks fourth after wheat, rice, and corn. However, barley has the first planting in terms of the extent of expansion because it can be cultivated under different climatic conditions (Feug et al. 2006). Over $136{\times}10^6$ tons of barley are produced worldwide each year, mainly used for livestock nutrition, and for industrial application (Zong-Yun et al. 2006). Due to the economic importance of barley and the widespread cultivation of this cereal, its breeding is on the agenda of breeders. To accomplish barley breeding goals, gene mapping, a study of their inheritance, and saturated genetic linkage maps were necessary. One of the major challenges of barley breeding programs is determining the inheritance and locus of genes controlling these traits (Li et al. 2005; Hassan et al. 2010).

All cereals, including barley and wheat, are exposed to various pests and diseases. A pesticide is a substance or mixture of substances used to prevent, control or reduce pest damage. It can be a chemical compound (synthetic or natural), or a biological agent (biopesticide, e.g., a bacterium) eliminating various pests (e.g., insects, pathogenic microorganisms, weeds, nematodes) of the cultivated plant (Shibamoto and Bjeldanes 2009). Alongside the benefits of the pesticide application, there are problems such as reduced genetic diversity, reduced nitrogen fixation, and destruction of living habitats, especially endangered birds and species. In addition, humans receive pesticides through various means, including food consumption; exposure to food (especially fruits and vegetables) is five times more than other ways, such as air and drinking water (Shokrzadeh and Saravi 2011; Bonnechère et al. 2012). When flour and bread prepared, the amount of pesticides is slightly reduced by the procedure of grinding and baking. The highest residual concentration was observed in bran because most residues of pesticides accumulate in the grain exosporium (Kaushik et al. 2009).

Molecular markers made it possible to generate high-density genomic (genetic) linkage maps for many plants, including barley. These high-density genetic linkage maps based on molecular markers and QTLs (Quantitative Trait Loci) allow using Marker-Assisted Selection (MAS), and in this way selection is possible in the early generations of a breeding program which highly improves efficiency (Ayoub et al. 2003; Han et al. 1994).

In the study of a barley population derived from Steptoe × Morex cross, 3 QTLs were identified for grain yield using 15 Restriction Fragment Length Polymorphism (RFLP),

4 Random Amplification of Polymorphic DNA (RAPD), one microsatellite, and 77 Amplified Fragment Length Polymorphism (AFLP) markers. In the same study, it was found that for plant height, the number of spikelet's per spike and grain weight, there was one QTL on chromosome 3 (Kandemir et al. 2000). By conducting research on germination traits in 85 wheat double haploids lines and their parents, Landjeva et al. (2010) identified 20 QTLs, most of which were clustered on the 1DS chromosome. In a study, the QTLs of some major crop traits in barley, a double haploid barley generation derived from a cross between two six-row barley cultivars (Botania × Rolfi) were studied and RAPD markers were used to prepare the linkage map. Finally, 654 cM of the genome was covered in this study; 1-7 QTLs were determined for each of the attributes of plant height, spike yield, the weight of one thousand grains. It is worth noting that many of these QTLs overlap with previously identified QTLs (Manninen 2000).

The objectives of this study were to identify genetic loci controlling the traits related to yield and its components, to determine the contribution and mode of QTLs identified to the phenotypic variation in the attributes under pesticide application and non-application in the Badia × Kavir cross barley population.

Materials and Methods

Plant materials and phenotypic evaluation

In this study, 104 $F_{2:4}$ families from the Badia × Kavir cross as well as two parents were planted at the research farm of Gonbad Kavous University. The examined families were cultured using augmented design in two separate experiments (pesticide application and pesticide-free). In the pesticide-using experiment Deltamethrin, Dimethoate, Diazinon and Trichlorofon were applied for controlling pests. Barley families were planted in 0.3 m^2 (2 meters long rows). The distance between the plants was 25 cm in the rows. Peduncle length, stem diameter, flag leaf

Table 1. Chromosomal location and primer sequences of SSR markers used for linkage map.

Marker	Chromosome	Forward / Reverse sequence
HVM20	1	CTCCACGAATCTCTGCACAA / CACCGCCTCCTCTTTCAC
Bmag0782	1	ATGTACCATTACGCATCCA / GAAATGTAGAGATGGCACTTG
Bmac0032	1	CCATCAAAGTCCGGCTAG / GTCGGGCCTCATACTGAC
Bmag0718	1	ATCGTGACATCTCAAGAACA / CCTGATACTGCCTAGCATTAG
HVM36	2	TCCAGCCGAACAATTTCTTG / AGTACTCCCACACCACGTCC
GBM1462	2	CTGTGGCTAAAGAAGGCACC / AAGATTGCTGCAGGATAGGC
GBMS160	2	ATCCAGTGGCCTTTGTATGG / TCAGCTCCTCTCTCTTCATGTG
GBMS247	2	ACACCACATTCATCTTCCTTCA / CATTGCTCTGCTTCCTGTCA
HVM27	3	GGTCGGTTCCCGGTAGTG / TCCTGATCCAGAGCCACC
Bmag0603	3	ATACCATGATACATCACATCG / GGGGGTATGTACGACTAACTA
Bmag0225	3	AACACACCAAAAATATTACATCA / CGAGTAGTTCCCATGTGAC
Bmag0013	3	AAGGGGAATCAAAATGGGAG / TCGAATAGGTCTCCGAAGAAA
HVM67	4	GTCGGGCTCCATTGCTCT / CCGGTACCCAGTGACGAC
Cit7	4	GCAGCCAAGACCTTGAGAAAGC / GCCTGAACTAGCCCGAGAAATG
EBmac0906	4	CAAATCAATCAAGAGGCC / TTTGAAGTGAGACATTTCCA
HVM40	4	CGATTCCCCTTTTCCCAC / ATTCTCCGCCGTCCACTC
HVM30	5	AGTGGGGAATGAGAGAATGG / TGCTTGTGGGGCATCACAC
GMS001	5	CTGACCCTTTGCTTAACATGC / TCAGCGTGACAAACAATAAAGG
EBmac0684	5	TTCCGTTGAGCTTTCATACAC / ATTGAATCCCAACAGACACAA
Bmag0113	5	GGAATCTTCTGGAACGTC / TTAAGAAGATCATTGTATTGAAGA
HVM65	6	AGACATCCAAAAAATGAACCA / TGGTAACTTGTCCCCCAAAG
Bmac310	6	CTACCTCTGAGATATCATGCC / ATCTAGTGTGTGTTGCTTCCT
Bmac0040	6	AGCCCGATCAGATTTACG / TTCTCCCTTTGGTCCTTG
GBMS0083	6	ACACTATACACATATAT / GAATCCCAACAGACACA
HVM4	7	AGAGCAACTACCAGTCCAATGGCA / GTCGAAGGAGAAGCGGCCCTGGTA
GBMS0111	7	ATATTTATGAAACGGTGTTCG / GGGTTTATCCTCTGCAGG
Bmag0135	7	ACGAAAGAGTTACAACGGATA / GTTTACCACAGATCTACAGGTG

Table 2. Sequences of ISSR, IRAP and iPBS markers used for linkage map.

Marker	Sequence
iPBS	
2231	ACTTGGATGCTGATACCA
2074	GCTCTGATACCA
2076	GCTCCGATGCCA
2415	CATCGTAGGTGGGCGCCA
2221	ACCTAGCTCACGATGCCA
IRAP	
IRAP56	TGAGTTGCAGGTCCAGGCATCA
IRAP54	ACCCCTTGAGCTAACTTTTGGGGTAAG
IRAP50	CACTTCAAATTTTGGCAGCAGCGGATC
ISSR	
ISSR16	CTCTCTCTCTCTCTCTG
ISSR20	CTCTCTCTCTCTCTCT
ISSR22	CTCTCTCTCTCTCTCTT
ISSR29	TCTCTCTCTCTCTCTCA
ISSR30	GAGGAGAGAGAGAGAG

length, flag leaf width, flag leaf weight, number of grains, grain weight, awn length, spike weight, and grain weight were measured for 20 plants per families and parents in both experiments.

DNA and PCR extraction

Twenty young leaves from each family were randomly selected and genomic DNA extraction was carried out using the CTAB method (Saghi Maroof et al. 1994). Horizontal gel electrophoresis (8% agarose gel) was used to check quality of DNA. Simple Sequence Repeat (SSR), Inter Simple Sequence Repeat (ISSR), Inter Primer Binding Site (iPBS) and Inter Retrotransposon Amplified Polymorphism (IRAP) markers were used as for as providing of genetic linkage map (Table 1-2). Materials and PCR thermal program for different markers are listed in Tables 3-6.

Altogether, 28 SSR, 19 ISSR, 3 IRAP and 5 iPBS markers (93 alleles) were used to determine the genotype on the studied population. After the PCR reaction, amplified DNA was electrophoresed on 6% polyacrylamide gel. Fast silver nitrate method (An et al. 2009; Byum et al. 2009) was used for visualization of the gel.

Table 3. Materials used in polymerase chain reaction for ISSR, iPBS and IRAP markers.

Components	Concentration	Amount (µl)
Buffer PCR10X	1X	1
$MgCl_2$	50 mM	0.48
dNTP	10 µl	0.6
Taq DNA Polymerase Enzyme		0.12
Primer	60 ng	1.5
DNA diluted	0.75-0.5 ng	2.5
H_2O		3.8
Final volume		10

Table 4. Thermal program for amplification of ISSR, iPBS and IRAP markers.

Step	Temperature (°C)	Time	Number of cycles
Primary denaturing	95	5'	1
Denaturing	95	45"	
Annealing	-	45"	10
Synthesis	72	45"	
Denaturing	95	45"	
Annealing	-	45"	25
Synthesis	72	45"	
Final amplification	72	5'	1

Statistical analysis

Map Manager QTX17 software (Manley and Olson 1999) was used for genetic mapping and MapChart software (Voorrips 2002) for drawing of map. The point that had the highest LOD value was identified as the region most likely to have QTL. The critical limit for detecting QTLs was obtained by the permutation test (LOD = 2). The exact position of the QTL relative to both markers was determined in cM. QTLs were named according to the method of McCouch et al. (1997). First, the letter *q* and then the trait abbreviation was capitalized and separated using a dash from the chromosome number on which the QTL was identified. It is worth noting that the mean of each family was used for each trait in the QTL analysis. QTL was analyzed using QGene software (Nelson 1997).

Results

The phenotypic distributions of barley studied traits width in the $F_{2:4}$ populations grown in the using and no using pesticides environments are shown in Fig. 1. Means of traits among parents was significant for all traits in both of condition except shoot thickness. The genotypes in the $F_{2:4}$ population differed significantly ($P < 0.05$) for all traits (Table 7), indicating the presence of sufficient genetic variation. In all traits, $F_{2:4}$ progeny was observed that fell beyond the high or low mean of the two parents (Fig. 1-2). For all characters, the number of observed extreme individuals significantly ($P < 0.01$) exceeded the expected, suggesting transgressive segregation.

A genetic linkage map was generated using 28 SSR markers, 19 ISSR markers, 3 IRAP markers, and 5 iPBS

Table 5. Materials used in polymerase chain reaction for SSR markers.

Components	Concentration	Amount (µl)
Buffer PCR10X	1X	1
$MgCl_2$	50 mM	0.48
dNTP	10 mM	0.6
Taq DNA Polymerase Enzyme		0.12
Forward primer	60 ng	0.75
Reverse primer	60 ng	0.75
Diluted DNA	0.75-0.5 ng	2.5
H_2O		3.8
Final volume		10

Table 6. Thermal program for amplification of SSR markers.

Step	Temperature (°C)	Time	Number of cycles
Primary denaturing	94	5'	1
Denaturing	94	1	
Annealing	64	30"	18
Synthesis	72	1'	
Denaturing	72	1'	
Annealing	94	1'	30
Synthesis	55	1'	
Final amplification	72	5'	1

markers (93 alleles) as well as 104 F2 individuals. The markers used were divided into 7 linkage groups corresponding to 7 barley chromosomes. Based on the Kosambi's mapping function (Kosambi 1994), the map length was estimated to be 617.5 cM and the average marker interval was 5.41 cM (Fig. 3).

A total of 25 QTLs were mapped for traits. The minimum and maximum LODs were detected in the range of 2.038-4.537 for awn length and flag leaf length. The explained variance for traits in both conditions varied from 8.7 to 16.1 (Table 8).

In pesticide-free condition, 12 QTL were identified for peduncle length, stem diameter, flag leaf length, awn length and Peduncle length. qPL-3, in ISSR13-3-ISSR47-8 marker interval at position of 48 cM accounted for 9.2% of the total variation of peduncle length. Five QTLs controlled stem diameter (qSD-1, qSD-4a, arise-4b, qSD-6, qSD-7) at positions of 70, 0, 72.0, and 0 cM in ISSR47-1, ISSR31-6, ISSR20-1, ISSR38-6, ISSR48-1 flanked markers, that increased stem diameter with an additive effect from Badia. Three QTLs were identified at position 10, 68, 0 near Bmag0013, ISSR31-5, and ISSR31-6 markers for flag leaf length accounting for 11.5, 11.8, and 18.4% of the phenotypic variation, respectively (Fig. 4). For awn length, three QTLs (qRL-2a, qRL-3a, qRL-3b) on chromosomes 2 and 3 could account for about 29.3% of the total variation of this trait at positions 76, 2, and 68.

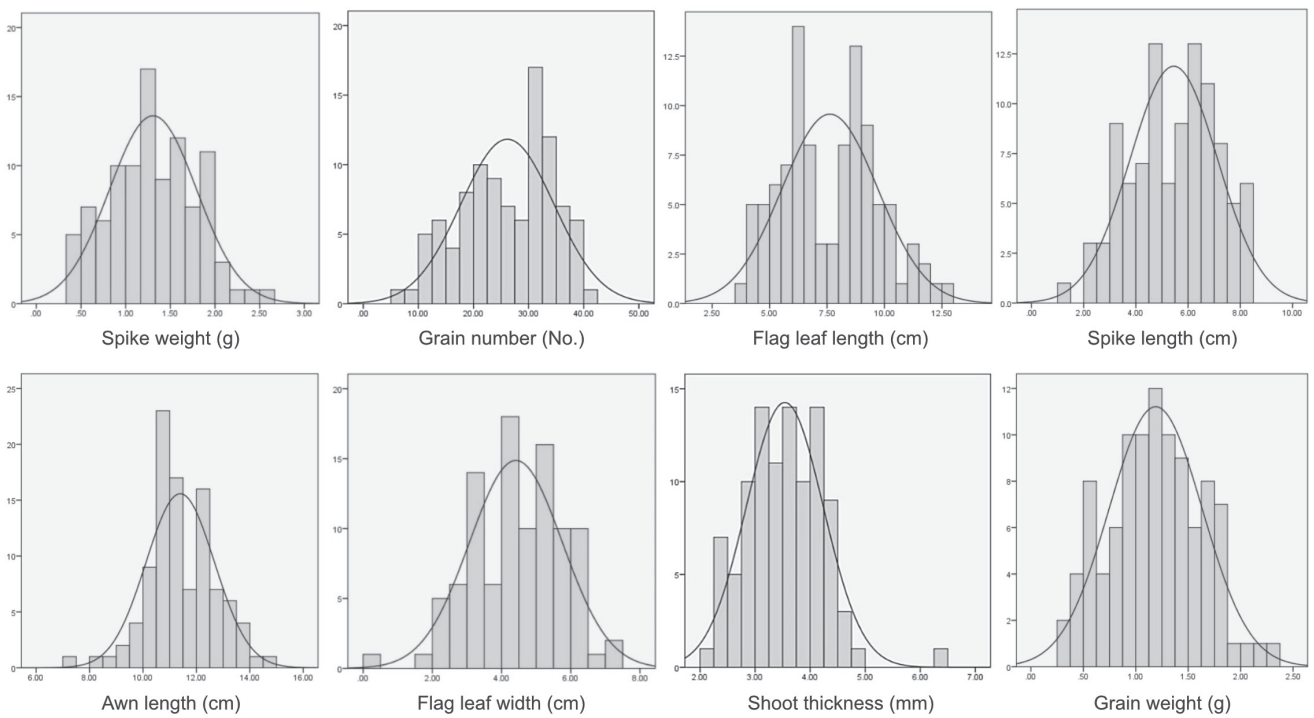

Figure 1. The histogram of studied traits in population where pesticides were not used.

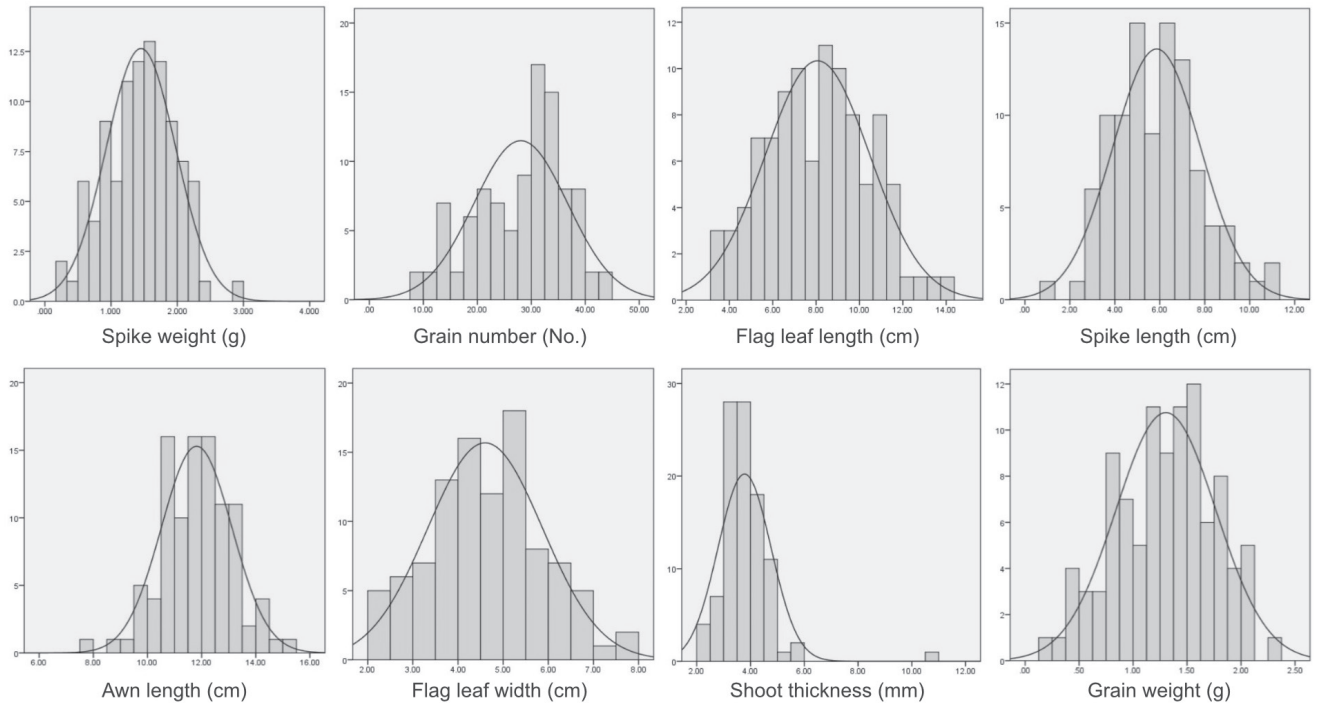

Figure 2. The histogram of studied traits in pesticide-treated population.

From these QTLs, qPL-3 was found to have major effects (R^2 = 11.8).

In pesticide-treated population, 13 QTLs were detected. For stem diameter, three QTLs (qSD-3, qSD-6a, qSD-6b) were detected on chromosomes 3, 6 (two QTLs) at positions 48, 2, and 18 cM in ISSR13-3 - ISSR47-8, ISSR38-6-Bmac310, and IRAP50-3-ISSR48-3 marker intervals. The stem diameter was found to have major effects, accounting for 10.9 and 16.5% of the phenotypic variation, respectively. For flag leaf length, 3 QTLs (qFL-3, qFL-7a, and qFL-7b) were identified on chromosomes 3, 7 (two QTLs) at positions 48, 102, and 106. For flag leaf width, qWI-6 at position 52 cM flanked by HVM65-Bmac0040 markers and was located with an LOD of 2.16. This QTL allele was transferred from Kavir with a negative additive effect.

For flag leaf weight, one QTL (qFWE-4) was identified at 2 cM from the beginning of the chromosome at

Table 7. Means comparison of parents for agronomically traits in no using pesticides and using pesticides.

Traits	Without pesticides			Treated with pesticides		
	Kavir	**Badia**	**T-test**	**Kavir**	**Badia**	**T-test**
Biomass (g)	126.378	149.077	**	95.632	116.321	**
Spike weight per plant (g)	34.421	51.746	**	27.632	46.325	**
Spike number per plant	34.000	45.000	**	26.000	33.000	**
Spike length (cm)	99.000	110.000	**	86.215	98.784	**
Grain yield per plant (g)	43.297	63.526	**	32.125	54.369	**
Peduncle length (cm)	3.000	6.420	**	2.690	5.632	**
Shoot thickness (mm)	4.100	4.480	ns	2.652	2.832	ns
Flag leaf length (cm)	11.300	9.900	**	8.321	7.954	**
Flag leaf weight (g)	0.140	0.020	**	0.122	0.018	**
Grain number	34.000	36.000	*	26.000	31.000	*
Grain weight (g)	1.340	1.820	**	1.126	1.325	*
Awn length (cm)	12.360	10.400	*	11.635	9.847	**

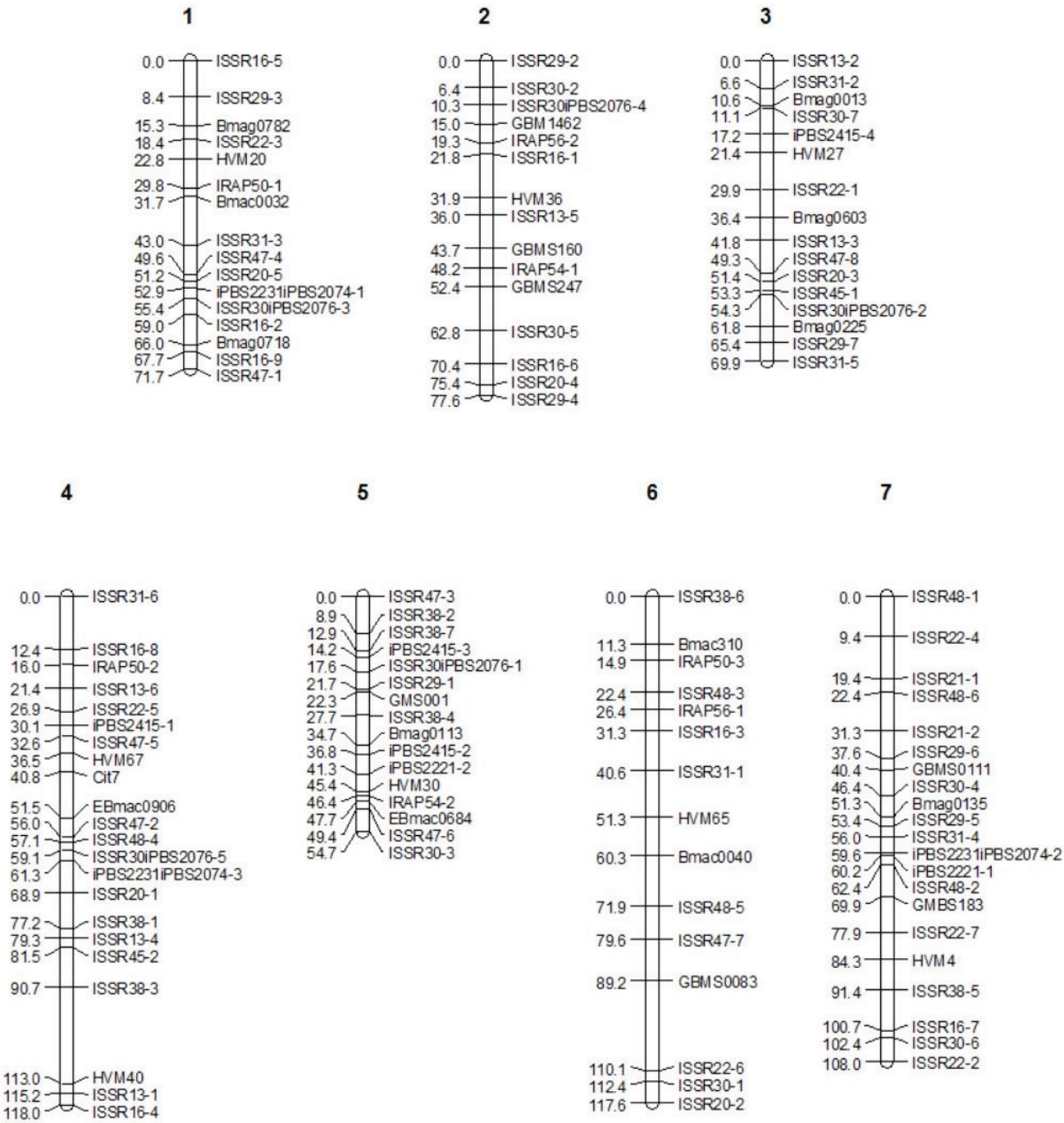

Figure 3. Linkage map caused Badia × Kavir cross based on 28, 9, 3 and 5 SSR, ISSR, IRAP and iPBS markers in F2:4 mapping population.

ISSR31-6-ISSR16-8 marker interval and LOD of 3.935 and phenotypic variance of 16.1 with a negative additive effect of Kavir. qSN-3 at 48 cM flanked by ISSR13-3-ISSR47-8 markers with an LOD of 2.213 accounted for 9.4% of the variation in grain number. For spike weight, one QTL was detected on chromosome 3 at 48 cM above the chromosome (Fig. 5). This QTL was within the ISSR13-3-ISSR47-8 marker interval and accounted for 13.2% of the variation with an LOD of 3.163. For grain weight, 3 QTLs (qSW-1a, qSW-1b, qSW-3) were identified that could account for 12.8, 12.8, and 15.7%, respectively, and had a positive additive effect for this trait at chromosomes 64,

Table 8. QTL detected for agronomical traits in F2:3 caused Badia × Kavir populations.

Trait	QTL	Chromosome	Position	Flanking marker	LOD	Additive	R^2	Allele direction
Without pesticides								
	qPLNUF-3	3	48	ISSR13-3- ISSR47-8	2.158	-0.813	9.2	Kavir
	qSTNUF-1	1	70	ISSR16-9-ISSR47-1	2.911	-0.713	12.2	Kavir
	qSTNUF-4a	4	0	ISSR31-6- ISSR16-8	2.289	0.581	9.7	Badia
	qSTNUF-4b	4	72	ISSR20-1-ISSR38-1	2.240	-0.583	9.5	Kavir
	qSTNUF-6	6	0	ISSR38-6-Bmac310	2.478	0.580	10.5	Badia
	qSTNUF-7	7	0	ISSR48-1-ISSR22-4	2.041	-0.437	8.7	Kavir
	qFLLNUF-3a	3	10	ISSR31-2- Bmag0013	2.745	-0.605	11.5	Badia
	qFLLNUF-3b	3	68	ISSR29-7-ISSR31-5	2.806	0.949	11.8	Kavir
	qFLLNUF-4	4	0	ISSR31-6- ISSR16-8	4.537	1.235	18.4	Kavir
	qALNUF-2	2	76	ISSR20-4 - ISSR29-4	2.038	-1.432	8.7	Badia
	qALNUF-3a	3	2	ISSR13-2 - ISSR31-2	2.072	-1.688	8.8	Badia
	qALNUF-3b	3	68	ISSR29-7 - ISSR31-5	2.802	-0.707	11.8	Badia
Treated with pesticides								
	qSTUF-3a	3	48	ISSR13-3 - ISSR47-8	2.57	-2.961	10.9	Badia
	qSTUF-6a	6	2	ISSR38-6 - Bmac310	4.025	-1.71	16.5	Badia
	qSTUF-6b	6	18	IRAP50-3 - ISSR48-3	2.303	-1.949	9.8	Badia
	qFLLUF-3	3	48	ISSR13-3 - ISSR47-8	2.2	-4.632	9.4	Kavir
	qFLLUF-7a	7	102	ISSR16-7- ISSR30-6	2.544	1.551	10.8	Badia
	qFLLUF-7b	7	106	ISSR30-6-ISSR22-2	2.413	2.525	10.2	Badia
	qFLWIUF-6	6	52	HVM65- Bmac0040	2.16	-0.672	9.2	Kavir
	qFLWEUF-4	4	2	ISSR31-6- ISSR16-8	3.935	0.194	16.1	Badia
	qGNUF-3	3	48	ISSR13-3-ISSR47-8	2.213	-11.546	9.4	Kavir
	qGWUF-1a	1	64	ISSR16-2- Bmag0718	3.06	0.272	12.8	Badia
	qGWUF-1b	1	66	Bmag0718-ISSR16-9	3.057	0.218	12.8	Badia
	qGWUF-3	3	48	ISSR13-3- ISSR47-8	3.809	-0.944	15.7	Kavir
	qSWUF-3	3	48	ISSR13-3- ISSR47-8	3.163	-0.945	13.2	Kavir

66, 48 cM in ISSR16-2-Bmag0718, Bmag0718-ISSR16-9, and ISSR13-3-ISSR47-8 marker intervals (Fig. 6).

To identify and map the dwarfism gene in 92 double haploid barley lines and its correlation with agronomical traits, Wang et al. (2010) identified two QTLs for spike emergence, two QTLs for spike length, one QTL for grain number, and one QTL for awn length on chromosome H3, which accounted for 70-81% of the relevant phenotypic variance of the trait. The results of Wang et al.'s (2010) work on chromosome #3 were consistent for awn length and grain number traits. In addition, Teulat et al. (2001a,b) identified two QTLs on chromosomes 3 and 4. The results of this study on chromosome #3 are consistent with the results of Teulat et al. (2001 a,b).

Discussion

The widespread use of various pesticides, including herbicides, insecticides, fungicides, and rodenticides, has long been a cause for concern for environmental pollution and endangering human health. Adverse effects of these compounds on living and non-living environment include accumulation and concentration of pesticides in the living body and entry into the food chain, and long-

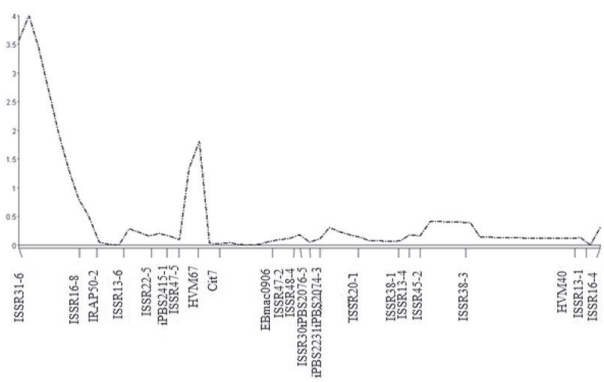

Figure 4. QTL mapping result for flag leaf length (on chromosome 3) in population where pesticides were not used.

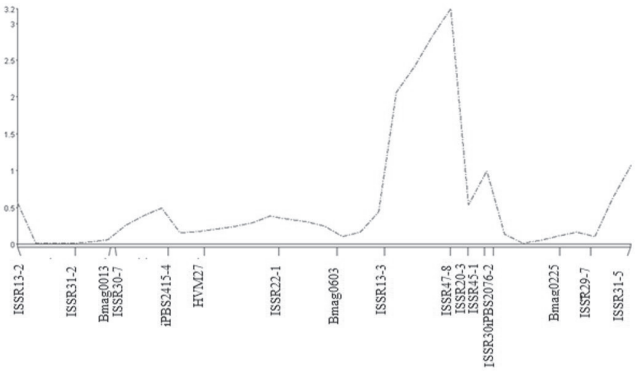

Figure 5. QTL mapping result for spike weight (on chromosome 3) in pesticide-treated population.

term contamination of water and soil resources with pesticides and their residues (Shaw et al. 1992; Newman 2008). The development of pesticide resistance in pest populations could increase with the elevated concentration of these compounds as well as with repeated applications (Hemingway and Ranson 2000; Brown and Pal 1971; Hemingway et al. 1992). The combination of different control methods, including environmental, biological, genetic, and chemical approaches, has been able to reduce environmental pollution and at the same time properly controls population of harmful pests.

This study sought to investigate the effect of pesticide application on the emergence and absence of QTLs in attribute controllers in barley. To do this, first a genetic map with molecular markers was developed. The obtained linkage map showed that the distribution of markers on linkage groups was not uniform and the highest number of markers belonged to linkage group #3 and the lowest number of markers to linkage group #5 (Fig. 3). Since the resulting map length was 617.5 cM and the interval between the two flanking markers was 5.41 cM, the resulting map was found to be suitable for gene mapping (Fig. 1).

The study identified 25 QTLs. Comparison of QTLs detected under both conditions, namely pesticide application and non-application showed that some chromosome regions play an effective role in controlling attributes under both conditions. For example, in ISSR13-3-ISSR47-8 and ISSR38-6-Bmac310 marker intervals, QTLs related to stem diameter, peduncle length, flag leaf length, and seed weight, were detected under both conditions; however, some regions played a role only in the absence of pesticide use, IRAP50-3-ISSR48-3, HVM65-Bmac0040. Therefore, it can be concluded that pesticide application is effective in the presence or absence of some genes in barley. The major-effect trait-controller QTLs concerned, and their associated markers can be used in MAS programs. The results showed that when plant populations are treated with pesticides, the expression of genes controlling traits is affected.

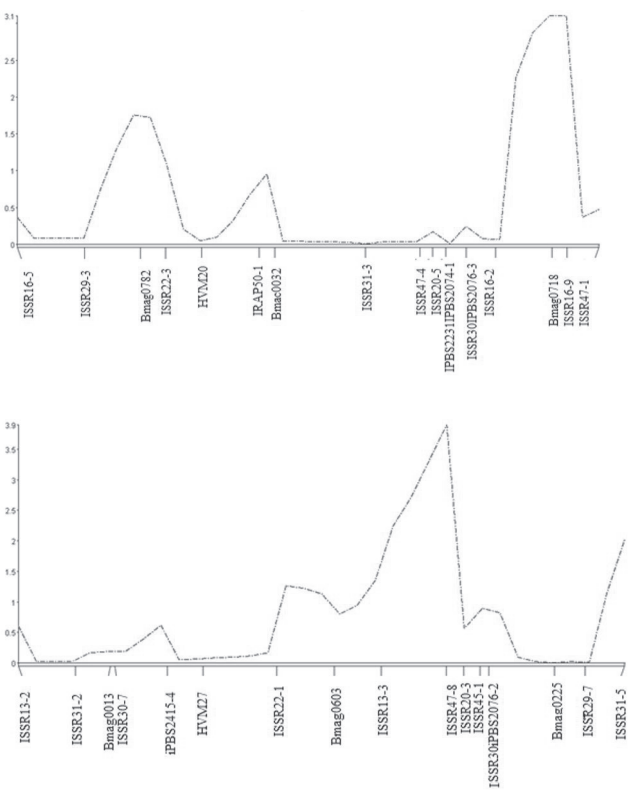

Figure 6. QTL mapping result for grain weight (on chromosome 1 and 3) in pesticide-treated population.

Acknowledgments

Samira Bakhtiari and the co-authors acknowledge the Research Deputy of Gonbad Kavous University for providing funding to complete this work.

References

An ZW, Xie LL, Cheng H, Zhou Y, Zhang Q, He XG (2009) A silver staining procedure for nucleic acids in polyacrylamide gels without fixation and pretreatment. Anal Biochem 391(1):77-79.

Ayoub M, Armstrong E, Bridger G, Fortin MG, Mather DE (2003) Marker-based selection in barley for a QTL region affecting alpha amylase activity of malt. Crop Sci 43:556-561.

Bonnechère A, Hanot V, Jolie R, Hendrickx M, Bragard C, Bedoret T (2012) Effect of household and industrial processing on levels of five pesticide residues and two deg-

radation products in spinach. Food Control 25:397-406.
Brown AWA, Pal R (1971) Insecticide resistance in arthropods. World Health Organization monograph series 2nd ed. 38:95-143.
Byum SO, Fang Q, Zhou H, Hickford JG (2009) An effective method for silver-staining DNA in large numbers of polyacrylamide gels. Anal Biochem 385(1):174-175.
Feug ZY, Liu XJ, Zhang YZ, Ling HQ (2006). Genetic diversity analysis of Tibetan wild barley using SSR markers. Acta Genet Sin 33:917-928.
Germán S, Arbelbide M, Abadie T, Romero R, Peculio A (2000) Characterization of photoperiod response of barley genotypes from diverse origin. In Logue S, ed., Barley Genetics VIII, Vol. III.-Contributed Papers. Glen Osmond, Adelaide University. p. 212-214
Han F, Ullrich SE (1994). Mapping of quantitative trait loci for malting quality traits in barley. Barley Genet Newsl 23:84-97.
Hassan M, Oldach K, Baumann U, Langridge P, Sutton T (2010) Genes mapping to boron tolerance QTL in barley identified by suppression subtractive hybridization. Plant Cell Physiol 33:118-198.
Hemingway J, Ranson H (2000) Insecticide resistance in insect vectors of human disease. Annu Rev Entomol 45:371-391.
Hemingway J, Small GJ, Monro A, Sawyer BV, Kasap H (1992) Insecticide resistance gene frequencies in *Anopheles sacharovi* populations of the Cukurova plain, Adana province, Turkey. Med Vet Entomol 6:342-348.
Kandemir N, Jones BL, Wesenberg DM, Ullrich SE, Kleinnofs A (2000) Marker-assisted analysis of three grain yield QTL in barley using near isogenic lines. Mol Breed 6:157-167.
Kaushik G, Satya S, Naik SN (2009) Food processing a tool to pesticide residue dissipation- A review. Food Res Int 42:26-40.
Kosambi DD (1994) The estimation of map distance from recombination values. Ann Eugen 12:172-175.
Landjeva S, Lohwasser U, Borner A (2010) Genetic mapping within the wheat D genome reveals QTL for germination, seed vigour and longevity, and early seedling growth. Euphytica 171:129-143.
Li JZ, Huang XQ, Heinrichs F, Ganal M, Roder MS (2005) Analysis of QTLs for yield, yield components, and malting quality in a BC3-DH population of spring barley. Theor Appl Genet 110:356-363.
Manly KF, Olson JM (1999) Overview of QTL mapping software and introduction to Map Manager QTL. Mamm Genome 10:327-334.
Manninen O (2000) Genetic mapping of traits important in barley breeding. Acad Dissert, Univ Helsinki, Helsingin yliopiston verkkojulkaisut, Helsinki.
McCouch SR, Cho YG, Yano M, Paul E, Blinstrub M (1997) Report on QTL nomenclature. Rice Genet Newsl 14:11-13.
Nelson JC (1997) QGENE: software for marker-based genomic analysis and breeding. Mol Breed 3(3):239-245.
Newman MC, Clements WH (2008) Ecotoxicology: A Comprehensive Treatment. CRC Press, USA. p. 880.
Saghi Maroof MA, Biyaoshev RM, Yang GP, Zhang Q, Allard RW (1994) Extra ordinarily polymorphic microsatellites DNA in barley species diversity, chromosomal location, and population dynamics. Proc Natl Acad Sci USA 91:4566-5570.
Shaw IC, Chadwick J (1992) Principles of Environmental Toxicology. Taylor & Francis, London, Bristol, PA. p. 216.
Shibamoto T, Bjeldanes LF (2009) Introduction to Food Toxicology. 2nd ed. Elsevier, p. 320.
Shokrzadeh M, Saravi SSS (2011) Pesticides in agricultural products: analysis, reduction, prevention. In Stoytcheva M, Ed., Pesticides-formulations, Effects, Fate. InTech, India, p. 225-242.
Teulat B, Merah O, Souyris I, This D (2001a) A new QTLs identified for plant water-status, water-soluble carbohydrate and osmotic adjustment in a barley population grown in a growth-chamber under two water regimes. Theor Appl Genet 103:16-170.
Teulat B, Merah O, Souyris I, This D (2001b) QTLs for agronomic traits from a Mediterranean barley progeny grown in several environments. Theor Appl Genet 103:774-787.
Voorrips RE (2002) Map chart: software for the graphical presentation of linkage maps and QTLs. J Hered 93(1):77-78.
Wang J, Yang J, McNeil DL, Zhou M (2010) Identification and molecular mapping of a dwarfing gene in barley (*Hordeum vulgare* L.) and its correlation with other agronomic traits. Euphytica 175:331-342.
Zong-Yun F, Xian-Jun L, Yi-Zhang Z, Hong-Qing L (2006) Genetic diversity analysis of Tibetan wild barley using SSR marker. Acta Genet Sin 33:917-923.

Acta Biologica Szegediensis

Volume 64(1):73-90, 2020
Acta Biologica Szegediensis
http://abs.bibl.u-szeged.hu/index.php/abs
DOI:10.14232/abs.2020.1.73-90

Abstracts of the Annual Conference of Doctoral School of Biology, University of Szeged – 2020.

Effect of landscape heterogeneity in conserving the arthropod fauna of forest-steppe in Great Hungarian Plain

Hardeep Kaur[1,2]

[1]Department of Ecology, Faculty of Science and Informatics, University of Szeged, Szeged, Hungary
[2]Doctoral School of Biology, Faculty of Science and Informatics, University of Szeged, Szeged, Hungary

Biodiversity loss is major threat to the survival of ecosystems and considered as major driver of ecosystem changes in Hungary as well. Main cause of decrease biodiversity is habitat fragmentation, habitat loss or habitat modification. Loss of biodiversity on a local spatial scale is much more alarming than global scale biodiversity decline, as it includes regional endemic flora and fauna. Understanding the effects of different landscape in the matrix, their quality and local attributes on the biota of habitat patches is often challenging The objective of this dissertation is to improve the understanding of distribution patterns of species and their preservation in highly modified landscapes of Great Hungarian Plain.

To achieve this goal firstly we studied the biota of natural forest fragments and hypothesized that the local and landscape level variable and their interactions have different effect on forest specialist and open-habitat plant, spider and carabid species. Secondly, we focus on biodiversity in these structurally complex habitat fragments while also considering the effects of fragment size and landscape quality on the species composition (beta-diversity) of arthropods and plants. Thirdly, we try to understand the importance of semi-natural linear landscape elements such as road-verges, in maintaining the connectivity between habitat fragments of highly modified landscapes and preserving the specialist fauna of arthropods in Great Hungarian Plain.

Our sampling was conducted in forest-steppe of Kiskunság region between Tisza and Danube interfluve. Sampling included, arthropods like spiders, true-bugs, ants, carabid beetles and plants and their identification to species level. We employ various statistical methods like, counting species richness and abundance, linear mix models, beta diversity indices, multivariate scaling and functional diversity according to our questions or hypothesis.

We found that increasing forest fragment size, forest habitat amount and forest edge length (local and landscape attributes) had in general positive effects on forest species, but negative on open-habitat species varying a bit among the studied taxa. Secondly, landscape quality and habitat type drive the diversity pattern of forest-steppe fragments and lastly, road-verges act as important secondary habitats for grassland species.

Supervisors: Róbert Gallé, Attila Torma
Email: hardypabla@gmail.com

Uncovering the mitotic interactome of protein phosphatase 4

Zoltán Kármán[1,2]

[1]HAS-BRC Momentum (*Lendület*) Laboratory of Cell Cycle Regulation, Institute of Biochemistry, Biological Research Centre, Szeged, Hungary
[2]Doctoral School of Biology, Faculty of Science and Informatics, University of Szeged, Szeged, Hungary

Protein phosphatase 4 (PP4) is an essential PP2A-like Ser/Thr phosphatase that control different cellular events, such as DNA repair, differentiation, apoptosis, cell cycle and various signaling processes. However, its role in the regulation of mitosis is poorly known. To better understand this, we aimed to uncover its mitotic interactome and define how PP4 bind its substrate proteins.

To achieve this, we generated transgenic flies overexpressing different functional domains of the regulatory R3 subunit (Falafel) of PP4, namely the EVH1 and the Smk-1 domains. We collected early syncytial embryos from these flies and performed an affinity purification followed by mass spectrometric analysis. With this approach, we were able to identify several possible novel mitotic interaction partners of PP4. We validated the real physical interaction partners with *in vitro* binding experiments, using GST-tagged EVH1 or Smk-1 as bait proteins and ^{35}S-methionine labelled *in vitro* produced prey proteins, respectively. After verifying the novel binding partners (potential substrates), we narrowed down the interacting surfaces in

Volume 64(1):73-90, 2020
Acta Biologica Szegediensis
http://abs.bibl.u-szeged.hu/index.php/abs

DOI:10.14232/abs.2020.1.73-90

order to define the substrate binding consensus motif of PP4. We found two motifs for the EVH1 domain, which could present in multiple copies within the partner proteins. With site specific mutagenesis we identified the exact residues and motifs, which are truly required for the interaction. From the Smk-1 binding partners, only one possesses such a motif, but after *in vitro* and *in vivo* experiments we could declare that the substrate binding of PP4 through the Smk-1 domain is achieved in a completely different, yet undescribed manner. We also found that a conserved leucine in Falafel's EVH1 domain is essential for substrate binding, since disrupting this amino acid would lead to the complete loss of the interaction.

Supervisor: Zoltán Lipinszki
E-mail: k.zoltan08@gmail.com

Non-canonical role of E2FB in auxin transport

Erika Őszi[1,2]

[1]Regulation of Plant Morphogenesis Group, Institute of Plant Biology, Biological Research Centre, Szeged, Hungary
[2]Doctoral School of Biology, Faculty of Science and Informatics, University of Szeged, Szeged, Hungary

Plant development, organ growth and their shape mainly depend on the regulation and orientation of cell division. Cell number is primarily determined by genetic program, but it also could be influenced by environmental conditions. Plant growth hormone auxin plays an essential role in determining the activity of proliferation, and thus has major impact on the final size and shape of a developing organ. The temporal and spatial activity of cell proliferation is controlled by complex regulatory mechanisms, but their nature is still not fully understood. It is strongly believed that the switch from proliferation to differentiation in plants is regulated by an evolutionarily conserved transcriptional regulatory mechanism called E2F-RB pathway.

In our study we focused on E2FB, one of the activator type E2Fs in *Arabidopsis*. Previously we have seen that ectopic E2FB could stimulate cell proliferation in the absence of growth hormone auxin. That indicates regulatory role for E2FB in auxin-driven cell proliferation. We propose a model where the RBR-free form of E2FB stimulates cell division, while their complex promotes cell cycle exit. How this switch could operate during plant development and whether it depends on auxin is not known yet.

As E2FB is a transcription factor it is expected to be localized in the nucleus. Indeed, we observed E2FB in the nucleus but surprisingly in association with the plasma membrane as well. We were curious whether recruitment of E2FB by the plasma membrane influenced its activity like it was reported on other membrane associated transcription factors (MTF) or E2FB has non-canonical role in the membrane. By analyzing the interacting partners of E2FB we have found membrane associated proteins involved in vesicular trafficking and auxin transport. The auxin efflux carrier protein PIN3 was one of these E2FB interactors. By using transient transfection system E2FB and PIN3 were found to be co-localized at the membrane. In addition, auxin transport enhanced by PIN3 was repressed when PIN3 was co-expressed with E2FB. That strongly suggests that E2FB has non-canonical function by regulating auxin transport in developing organs.

Supervisor: Zoltán Magyar
E-mail: oszi.erika@brc.hu

Assessment of intracellular singlet oxygen by GFP fluorescence in *Synechocystis* PCC6803

Gábor Patyi[1,2]

[1]Institute of Plant Biology, Biological Research Centre, Szeged, Hungary
[2]Doctoral School of Biology, Faculty of Science and Informatics, University of Szeged, Szeged, Hungary

Singlet oxygen ($^1O_2$) is a very important reactive oxygen species (ROS), it can damage a wide range of macromolecules, like lipids, carotenoids and proteins. Its formation takes place in the second photosynthetic reaction centre (PSII), during the photosynthetic reactions. In high light condition the generated triplet state chlorophyll can interact with the molecular oxygen leading to $^1O_2$ formation via energy transfer.

DOI:10.14232/abs.2020.1.73-90

This highly reactive ROS, besides its degradation effects can take part in signal transduction mechanisms and other intracellular reactions. This importance is the reason why we investigate the $^1O_2$ intracellular mechanisms. There are various $^1O_2$ detection methods, such as His mediated O_2 uptake, which allows calculating the rate of $^1O_2$ generation by the rate of O_2 consumption. However, still there is a lack in detection methods that could be used to detect the spatial distribution of $^1O_2$ generation inside intact cyanobacterial cells.

The Green Fluorescent Protein (GFP) is a very commonly used reporter protein in biological research nowadays. $^1O_2$ can damage this protein, hence quenching its fluorescence. We treated GFP producing *Synechocystis* PCC6803 cyanobacterial mutant cells with the $^1O_2$ sensitizer Rose bengal (Rb) and Methylene blue (Mb) dyes under high light conditions. We observed that the GFP fluorescence decreased suggesting that $^1O_2$ mediated degradation of GFP can be utilized for *in vivo* $^1O_2$ detection.

We investigated the specificity and sensitivity of the quenching reaction and established experimental parameters for a widely applicable *in vivo* $^1O_2$ assessment method protocol.

Supervisors: Imre Vass, Péter Kós
E-mail: gpatyi17@gmail.com

Synergistic radiosensitization of gold nanoparticles and the histone-deacetylase inhibitor SAHA on 2D and 3D cancer cells

Nóra Igaz[1,2]

[1]Department of Biochemistry and Molecular Biology, Faculty of Science and Informatics, University of Szeged, Szeged, Hungary
[2]Doctoral School of Biology, Faculty of Science and Informatics, University of Szeged, Szeged, Hungary

Anti-cancer agents applied in traditional chemotherapy have often just moderate success rate and exhibit low specificity during clinical cancer treatment. Chemotherapy is mostly accomplished in multimodal manner, i.e. in combination with other treatment modalities, like radiotherapy. Radiosensitizing agents are frequently utilized upon irradiation, since these compounds are capable to increase the efficiency and decrease the severe side effects of cancer therapy exerted by irradiation and help to attenuate the disadvantageous consequences of radiation treatments on healthy tissues.

Our aim was to investigate the radiosensitizing capability and the efficiency of gold nanoparticles (AuNPs) and of a histone-deacetylase inhibitor suberoylanilide hydroxamic acid (SAHA) in combination on 2D and 3D cell cultures of A549 lung adenocarcinoma, DU-145 and PC-3 prostate cancer and MCF-7 breast cancer cell lines.

According to our experiments, treatment of cancer cells with SAHA results in a high level of acetylated histones, which feature was not affected by the presence of AuNPs when combinational treatments were applied. Thus, we can conclude that AuNPs do not influence the histone-deacetylase-inhibiting activity of SAHA. The AuNP and SAHA combinational treatment synergistically decreased the viability of A549, DU-145, PC-3 and MCF-7 cells after 2 Gy irradiation. Moreover, the colony forming capabilities of cancer cells were significantly diminished upon irradiation with 2 Gy and 4 Gy doses. The amount of irradiation-provoked DNA double strand breaks was the highest in the AuNP and SAHA double treated cells, which we have visualized by γH2AX immunostaining. Significantly more γH2AX positive cells and γH2AX foci were counted after histone deacetylase inhibitor and nanoparticle combinational treatments compared to the untreated and to the AuNP- or SAHA-treated cells after 2 Gy irradiation. After studying the effect of AuNP, SAHA and their combination after irradiation on 2D cell cultures, we investigated the impact of individual and double treatments on 3D cell cultures as well. In 3D structure - as in *in vivo* tumors - the cells often manifest increased radio-, and drug-resistance due to integrin-mediated pathways. Following combinational treatments, the number of colonies formed by living cells in 3D spheroids was significantly reduced after irradiation with 2 and 4 Gy doses, moreover, significantly more γH2AX-positive cells were counted after 2 Gy irradiation in the AuNP+SAHA-treated samples than in the control or in cancer cells receiving individual treatments.

Our results suggest that inhibition of deacetylase activity by SAHA leads to a more relaxed chromatin structure, which increases the DNA damaging effect of ionizing radiation. Furthermore, irradiation can provoke the release of reactive electrons from AuNPs, causing substantial amount of DNA double strand breaks, which leads to enhanced cancer cell death.

Supervisor: Mónika Kiricsi
E-mail: noraigaz@gmail.com

Volume 64(1):73-90, 2020
Acta Biologica Szegediensis
http://abs.bibl.u-szeged.hu/index.php/abs

DOI:10.14232/abs.2020.1.73-90

Cellular and network mechanisms of physiological and pathophysiological brain states

Horváth-Furdan Szabina[1,2]

[1]Department of Physiology, Anatomy and Neuroscience, Faculty of Science and Informatics, University of Szeged, Szeged, Hungary
[2]Doctoral School of Biology, Faculty of Science and Informatics, University of Szeged, Szeged, Hungary

In the absence of sensory input, the mammalian brain exhibits a wide array of structured brain state dependent spontaneous activity as happens during relaxed wakefulness, sleep and epilepsy. In cortical areas brain state dependent neuronal activity is determined by both intrinsic and thalamocortical network interactions fine-tuned by neuromodulation.

Hyperpolarization-activated cyclic nucleotide-gated (HCN) channels and the Ih current are one of the major intrinsic drivers of thalamic oscillations, but their role in generating spike and wave discharges of absence epilepsy has remained elusive. We investigated whether reducing the expression of HCN channels in the ventrobasal thalamus (VB) using shRNA could suppress absence seizures (AS). Control and Stargazer mice were injected with either HCN-targeting or non-targeting shRNA before recording. Using patch clamp recordings, we examined the electrophysiological properties of VB neurons in slices. Our data demonstrate that our HCN-targeting shRNA does selectively affect Ih-dependent membrane properties of VB neurons without altering other neuronal properties. At the end of experiments, we did immunostaining. Our data indicate that HCN-targeting shRNA-infected mice VB neurons had a low HCN immunoreactivity compared to non-targeting shRNA-infected mice. Our finding provides that block of VB neuron HCN channels prevents AS.

In addition to intrinsic properties of thalamic neurons thalamocortical states areal so profoundly influenced by the lateral hypothalamus, a brain area involved in arousal and energy control but whether and how the LH can impact the activity of neuromodulatory circuits and the downstream consequences of this modulation have remained elusive. Using a combination of anterograde and retrograde viral tracing, optogenetics, in vitro and in vivo electrophysiology we investigated the effect of LH on one of the major neuromodulatory systems. The serotonergic system implicated in many (patho)physiological functions like the regulation of brain states, mood, reward and sensory processing. Our results show that LH GABAergic projections promote arousal from NREM but not REM sleep by selectively inhibiting DRN GABAergic neurons via GABAA receptors resulting in a prominent disinhibition of DRN output neurons. Our results identify a novel long-range inhibitory projection implicated in the control of serotonergic neuromodulation and arousal.

Supervisor: Magor László Lőrincz
E-mail: nadruf77@gmail.com

Characterization of plant growth-promoting activities of endophytic fungi isolated from *Sophora flavescens*.

Adiyadolgor Turbat[1,2]

[1]Department of Microbiology, Faculty of Science and Informatics, University of Szeged, Szeged, Hungary
[2]Doctoral School of Biology, Faculty of Science and Informatics, University of Szeged, Szeged, Hungary

Several studies of endophytic fungi indicated that they are excellent producers of compounds that can be exploited for agrochemical or medicinal purposes due to their biological activity. Endophytes are beneficial to the host plants in terms of production of plant growth regulating hormones, solubilisation of minerals and their antagonistic behaviour against plant pathogens and pests. The mineral solubilisation is the indirect way for the plant growth promotion and as the direct way of the promotion, it was demonstrated that endophytic fungi can produce phytohormones, such as gibberellins and indole acetic acid, which are able to improve plant growth and reduce the adverse impacts of abiotic stresses.

The indirect plant promoting activities of the isolates were examined including phosphate mobilization and siderophore productions. It could be concluded that the siderophore production is more common within the examined isolated fungal endophytes than the phosphate solubilisation. Almost all produced siderophores in a measurable amount except for SZMC 26657 strain, while only 5 showed phosphate mobilization activities. Regarding to the IAA plate assay, each isolate proved to

Volume 64(1):73-90, 2020
Acta Biologica Szegediensis
http://abs.bibl.u-szeged.hu/index.php/abs
DOI:10.14232/abs.2020.1.73-90

produce IAA, from which 7 strains showed production only in the presence of Trp and 2 only in the absence of Trp as well as 6 in both cultivation conditions. Therefore, 4 strains the SZMC 26659, 26661, 26651 and 26648 were positive for those three plant growth-promoting assays. The IAA production of the isolates in the ferment broth ranged from 0.02 to 1.2 μg/mL and from 0.1 to 16.0 μg/mL, in the absence and presence of Trp, respectively. Furthermore, chosen 6 isolates tested on their potential for plant growth-promoting activity on plant assay. As a consequence, the crude fungal IAA of the endophytes at concentrations of 0.1 and 1 μg/mL promoted the elongation of the lengths of all *Arabidopsis* roots significantly and the biomasses of plants were reduced due to the treatment of the fungal extracts, while the accumulation of photosynthetic pigments were increased only certain cases. Therefore, 15 isolates represented the genera of *Alternaria*, *Didymella*, *Fusarium* and *Xylogone*, which has not been previously reported as the fungal endophytes of *S. flavescens*.

Supervisor: András Szekeres
E-mail: Adiyadolgor_turbat@yahoo.com

NGS-based method for the investigation of homologous recombination repair and for the increase of genomic integration efficiency

Alexandra Gráf[1,2]

[1]Laboratory of Mutagenesis and Carcinogenesis Research, Institute of Genetics, Biological Research Centre, Szeged, Hungary
[2]Doctoral School of Biology, Faculty of Science and Informatics, University of Szeged, Szeged, Hungary

The integrity of the cell's genome is indispensable for its proper function. Reactive oxygen species, ionizing and UV radiation, or chemotherapeutic agents can cause double-strand DNA breaks (DSBs) that jeopardize genome stability, as they lead to chromosome rearrangements and possibly to cell death. Consequently, living cells' DNA is inherently unstable. An extensive network of pathways has evolved for the repair of DNA damage. During the repair of DSBs, two pathways play a major role: non-homologous end joining (NHEJ) and homologous recombination (HR). Both pathways function in eukaryotic cells, but their relative contribution to damage repair as well as the speed of the process and the outcome is variable. While for NHEJ a homologous template is not required, it is essential for HR. NHEJ potentially creates indels, so it can lead to mutations; in contrast, HR is an error-free pathway. For the fast and easy examination of different known and unknown genes that can influence HR or NHEJ events, the establishment of a precise, versatile method is needed.

Therefore, the aim of the project is to establish a system through which the events of double-strand break repair (DSBR) can be analyzed at the nucleotide level by next-generation sequencing. Our goal is to increase the number of HR-related repair events and to maximize the length of the DNA that can be integrated into the genome via HR. We plan to monitor the repair of artificial DSBs induced by the CrispR-Cas9 system, through silencing and/or overexpression of putative HR/NHEJ-related genes. Changes in the ratio of these processes will be measured, and possible new members will be identified. Then, the effect of DNA length on integration into the host cell's genome through HR will be examined. The aim is to maximize the length of the donor DNA as well as the ratio of its HR-based integration. Through this project, we will have a deeper insight into the DSBR process, which may lead to more efficient genome editing procedures.

Supervisor: Lajos Haracska
E-mail: graf.alexandra@brc.hu

Rapid decline of bacterial drug-resistance in an antibiotic-free environment through phenotypic reversion

Anett Dunai[1,2]

[1]Department of Biochemistry and Molecular Biology, Faculty of Science and Informatics, University of Szeged, Szeged, Hungary
[2]Doctoral School of Biology, Faculty of Science and Informatics, University of Szeged, Szeged, Hungary

Antibiotic resistance typically induces a fitness cost that shapes the fate of antibiotic-resistant bacterial populations. However, the cost of resistance can be mitigated by compensatory mutations elsewhere in the genome, and therefore the loss of

Volume 64(1):73-90, 2020
Acta Biologica Szegediensis
http://abs.bibl.u-szeged.hu/index.php/abs

DOI:10.14232/abs.2020.1.73-90

resistance may proceed too slowly to be of practical importance. We present our study on the efficacy and phenotypic impact of compensatory evolution in *Escherichia coli* strains carrying multiple resistance mutations. We have demonstrated that drug-resistance frequently declines within 480 generations during exposure to an antibiotic-free environment. The extent of resistance loss was found to be generally antibiotic-specific, driven by mutations that reduce both resistance level and fitness costs of antibiotic-resistance mutations. We conclude that phenotypic reversion to the antibiotic-sensitive state can be mediated by the acquisition of additional mutations, while maintaining the original resistance mutations. Detailed genetic analysis of the mar regulon also supports the phenotypic reversion hypothesis. MarR is a transcriptional regulatory protein that controls the activity of the mar regulon in *E. coli* through the repression of marA. The mar regulon participates in controlling several genes involved in antibiotic-resistance, including the AcrA/AcrB/TolC multidrug-efflux system. In response to antibiotic stresses (e.g. doxycycline or ciprofloxacin), marR is regularly mutated both in clinical and in laboratory settings, leading to increased expression of marA and other members of the mar regulon. This resistance mutation has an associated fitness cost, promoting the accumulation of further mutations. Our study indicates that this can be achieved by a compensatory mutation in the promoter region of the mar operon. This compensatory mutation increases bacterial fitness, susceptibility to multiple antibiotics alike, and restores wild-type-like membrane permeability, probably through changing the activity of the mar regulon.

Our study indicates that restricting antimicrobial usage could be a useful policy, but for certain antibiotics only.

Supervisor: Csaba Pál
E-mail: dunai.anett@gmail.com

Investigations into the fly population of a white button mushroom (*Agaricus bisporus*) growing house in Hungary

Büchner Rita[1,2]

[1]Department of Microbiology, Faculty of Science and Informatics, University of Szeged, Szeged, Hungary
[2]Doctoral School of Biology, Faculty of Science and Informatics, University of Szeged, Szeged, Hungary

In Hungary over 30 000 tons of white button mushroom (*Agaricus bisporus*) is produced each year. Besides being the most popular cultivated mushroom in our country, it dominates the European and American mushroom industry. Producers face everyday challenges when it comes to protecting their crops from different pathogens. The most harmful fungal diseases of white button mushroom are green mould, dry bubble, wet bubble and cobweb, while further important pathogens involve various bacteria and viruses. Pests, such as certain flies, nematodes and mites also contribute to crop losses, either directly by crop consumption or indirectly, by acting as vectors in transmitting different diseases. Flies are very motile and could change their position fast by flying or walking on the surface of the mushroom growing material. As they move, spores, bacteria and mites might be carried on their bodies, thereby spreading them within and between mushroom growing houses.

Information about the mushroom fly populations in our country is very limited. A Hungarian mushroom growing facility, producing more than 7000 tons of white button mushrooms yearly was investigated in terms of fly populations over a 3-year period. In 2017, 2018 and 2019 deceased flies were collected mushroom growing houses, examined by microscopy and identified at the species level by the PCR amplification and sequence analysis of a fragment of the COI (cytochrome oxidase I) gene. Our results revealed the presence of members of the Sciaridae family: *Lycoriella sativae*, *L. castanescens*, *Bradysia tilicola* and *B. vagans*. In the year 2019, *Megaselia halterata*, belonging to the Phoridae family was also detected.

To investigate the attractant and repellent properties of plant essential oils to mushroom flies, experiments were designed and conducted in the same years. Fly traps containing essential oils suspended in water or beer were kept in the mushroom growing houses for 5 days. Lemon, thyme and citronella proved to be repellents while beer, cinnamon, and in most cases essential oils suspended in beer had attractant properties.

Supervisor: László Kredics, Lóránt Hatvani
E-mail: buchner-rita@freemail.hu

Volume 64(1):73-90, 2020
Acta Biologica Szegediensis
http://abs.bibl.u-szeged.hu/index.php/abs

DOI:10.14232/abs.2020.1.73-90

Towards the biological control of devastating forest pathogens from the genus *Armillaria*

Chen Liqiong[1,2]

[1]Department of Microbiology, Faculty of Science and Informatics, University of Szeged, Szeged, Hungary
[2]Doctoral School of Biology, Faculty of Science and Informatics, University of Szeged, Szeged, Hungary

Armillaria species are among the economically most relevant soilborne tree pathogens causing devastating root diseases worldwide. Biocontrol agents are environment-friendly alternatives to chemicals in restraining the spread of *Armillaria* in forest soils. *Trichoderma* species may efficiently employ diverse antagonistic mechanisms against fungal plant pathogens. The aim of this paper is to isolate indigenous *Trichoderma* strains from healthy and *Armillaria*-damaged forests, characterize them, screen their biocontrol properties, and test selected strains under field conditions.

Armillaria and *Trichoderma* isolates were collected from soil samples of damaged Hungarian oak and healthy Austrian spruce forests and identified to the species level. In vitro antagonism experiments were performed to determine the potential of the *Trichoderma* isolates to control *Armillaria* species. Selected biocontrol candidates were screened for extracellular enzyme production and plant growth-promoting traits. A field experiment was carried out by applying two selected *Trichoderma* strains on two-year-old European Turkey oak seedlings planted in a forest area heavily overtaken by the rhizomorphs of numerous *Armillaria* colonies.

Although *A. cepistipes* and *A. ostoyae* were found in the Austrian spruce forests, *A. mellea* and *A. gallica* clones dominated the Hungarian oak stand. A total of 64 *Trichoderma* isolates belonging to 14 species were recovered. Several *Trichoderma* strains exhibited in vitro antagonistic abilities towards *Armillaria* species and produced siderophores and indole-3-acetic acid. Oak seedlings treated with *T. virens* and *T. atrobrunneum* displayed better survival under harsh soil conditions than the untreated controls. Conclusions: Selected native *Trichoderma* strains, associated with *Armillaria* rhizomorphs, which may also have plant growth promoting properties, are potential antagonists of *Armillaria* spp., and such abilities can be exploited in the biological control of *Armillaria* root rot.

Supervisor: László Kredics
E-mail: liqiongchen2016@163.com

Linear scale up of aflatoxin separation by centrifugal partition chromatography

Gábor Endre[1,2]

[1]University of Szeged, Faculty of Science and Informatics, Department of Microbiology, Szeged, Hungary
[2]Doctoral School of Biology, Faculty of Science and Informatics, University of Szeged, Szeged, Hungary

Mycotoxins are the secondary metabolites produced by certain filamentous fungi. Within these toxic compounds, aflatoxins are playing an outstanding role due to their high-level toxicity, which causes remarkable problems in food industry and agriculture. Plenty of methods are available for monitoring or measuring these compounds from various matrices, which requires relatively high amounts of pure aflatoxins.

Liquid-liquid chromatography, which is based on a distribution of components between two phases in a biphasic solvent system, could serve solutions in their purifications. One of the technical implementations of this technique is Centrifugal Partition Chromatography (CPC), which is the hydrostatic version of countercurrent chromatography.

Aspergillus parasiticus (SZMC 2473) was cultivated on a complete malt broth. The four main aflatoxins (AFB1, AFB2, AFG1 and AFG2) were extracted from the fermentation material. In order to have the compounds purified, a 75-minute-long method was developed and applied for the separation and purification of the aflatoxins on a 250 ml laboratory scale CPC column. The stationary phase was the lower phase of the toluene/acetic acid/water = 30/24/50 ternary system, while the elution was carried out with the organic phase. With this method, from 4,5 l fermentation material a total of 1350 mg aflatoxins could be purified with the lowest purity of 92% and with the recovery of 96%.

In order to maximize the amount of pure aflatoxins, the capacity of the 250 ml CPC column was tested and a linear scale up was achieved to a 1000 ml CPC column with the same ternary system. Several concentrations of the desired compounds were injected to both columns, to achieve the maximal capacity of the system. During the scale up, the flow rate and the injec-

Volume 64(1):73-90, 2020
Acta Biologica Szegediensis
http://abs.bibl.u-szeged.hu/index.php/abs

DOI:10.14232/abs.2020.1.73-90

tion volume was linearly increased (quadruplicated). The same stationary/mobile phase ratio was set on the one litre column as well as on the smaller one before. Because the 1 litre column is bigger, to achieve the same gravitational field the rotation speed of the column had to be slower. With the increased application the amount of purified aflatoxins are expected to be more than quadruplicated.

Supervisors: Mónika Varga, András Szekeres
E-mail: egabcy@gmail.com

Bacterial biocontrol of *Armillaria* root rot

Orsolya Kedves[1,2]

[1]Department of Microbiology, Faculty of Science and Informatics, University of Szeged, Szeged, Hungary
[2]Doctoral School of Biology, Faculty of Science and Informatics, University of Szeged, Szeged, Hungary

The genus *Armillaria* is among the most important fungal root rot pathogens. The genus includes at least 40 species, with five morphological species being present in Europe. Members of the genus show diverse lifestyles ranging from saprotrophs to devastating tree pathogens. They cause root rot disease in both gymno- and angiosperms in more than 500 host plant species across the world.

Plant-associated biocontrol agents (BCAs) have important roles in plant growth and health. Direct plant growth promotion by microorganisms is based on improved nutrient acquisition and hormonal stimulation. Diverse mechanisms are involved in the suppression of plant pathogens which is often indirectly connected with plant growth. Bacterial BCAs may be promising alternatives to chemical pesticides for controlling *Armillaria* root rot. This study aimed the selection and characterization of potential bacterial BCAs for the control of *Armillaria* root rot. The examined BCAs (2 *Bacillus*, 11 *Paenibacillus* and 29 *Pseudomonas* strains) derived from the rhizosphere of infected trees with high presence of the fungal pathogen. The isolates were screened for plant growth promoting properties. During the experiments we examined the siderophore production with the chrome azurol S agar plate method, the phosphate mobilization on Pikovskaya agar plate method, the extracellular enzyme activities and the indole-3-acetic acid (IAA) production with colorimetric methods. Bacterial isolates were screened for their antagonistic abilities against *Armillaria* isolates *in vitro* using dual-culture confrontation test. In addition, to understand the mechanism of antagonism, the samples were examined by scanning electron microscopy (SEM). The plant growth promotion abilities of the above-mentioned BCA strains on conifer seeds were also investigated.

Most of the examined bacteria could inhibit the growth and the rhizomorph formation of all investigated *Armillaria* strains, furthermore, they were able to mobilize phosphorous and to produce siderophore, IAA and extracellular enzymes.

Based on the results, *Paenibacillus* and *Pseudomonas* strains have beneficial properties which could be exploited during the biological control of *Armillaria* root rot.

Supervisors: László Kredics, György Sipos
E-mail: kedvesorsolya91@gmail.com

Mass spectrometric analysis of the human urinary O-glycoproteome

Ádám Pap[1,2]

[1]Laboratory of Proteomics Research, Biological Research Centre, Szeged. Hungary
[2]Doctoral School of Biology, Faculty of Science and Informatics, University of Szeged, Szeged, Hungary

Glycosylation is among the most complex protein post-translational modifications (PTM). Its biological roles are very diverse, ranging from the controlling of protein structure to immunomodulatory functions. Our group focuses on the analysis of mucin-type O-glycosylation which is the most commonly occurring O-glycosylation type on secreted and membrane-bound proteins. Its role has been implicated in receptor activation, leukocyte extravasation and different types of cancer metastasis. All this gathered knowledge on mucin-type O-glycosylation fueled our curiosity to investigate this type of PTM in human urine.

We analyzed three urine samples from healthy donors, three samples from donors that were diagnosed with superficial

DOI:10.14232/abs.2020.1.73-90

bladder cancer and three samples from donors suffering from advanced bladder cancer. After sample preparation and mass spectrometric measurement we analyzed the data carefully with two aims. Our main goal was to determine which proteins are O-glycosylated with what type of O-glycans in urine. However, to answer this question, first we had to develop a data interpretation method that uses multiple sources of mass spectrometric information.

With the data interpretation method developed we were able to identify multiple O-glycan structures that were linked to specific proteins for the first time. With this information in hand we can compare the O-glycosylation pattern of urinary proteins from healthy and diseased individuals to find some O-glycans that may serve as biomarker candidates for bladder cancer.

Supervisor: Zsuzsanna Darula
E-mail: pap.adam@brc.hu

Large- and small-scale environmental factors drive distributions of ant mound size across a latitudinal gradient

Orsolya Juhász[1,2]

[1]Department of Ecology, Faculty of Science and Informatics, University of Szeged, Szeged, Hungary
[2]Doctoral School of Biology, Faculty of Science and Informatics, University of Szeged, Szeged, Hungary

Red wood ants are keystone species of forest habitats in Europe, as being true ecosystem engineers. In their nest surroundings they affect many habitat characteristics, but also the occurrence and distribution of several plant and animal species. On the other hand, several environmental factors and habitat characteristics can affect the size of their nest mounds, an important trait being in relation to the colony size and its well-being. However, we still lack information about the distribution and environmental requirements of this species in Central Europe, mostly in the light of climate change.

In this study, we investigated the effect of large- (latitude and altitude) and small-scale environmental factors (e.g., characteristics of the forest) on the mean size of nest mounds of *Formica polyctena* in the lowland, transition and mountain areas of Central Europe (altogether 12 regions). We predicted that the change in the mound size is in accordance with the Bergmann's rule that states that the body size of endotherm animals changes along with latitude and/or altitude.

We found that the size of the mounds increased along the studied latitudinal gradient, being in accordance with Bergmann's rule. Altitude, on the other hand, did not have any effect on the size of the mounds. The irradiation was the most important environmental factor responsible for the changes in mound size, but temperature, and small-scale factors, like the diameter of the trees and their distance from the nest, were also involved.

Considering our results in the light of the global climate change, we can better understand the long-term effects and consequences of the changing environmental factors on this ecologically important ant group. This knowledge can help decision-makers and forest managers to plan forest management tactics in concordance with the assurance of the long-term survival of red wood ants.

Supervisor: István Elek Maák
E-mail: orsolya40@gmail.com

The effect of tight junction modulator peptide PN159 and sodium bicarbonate on human bronchial epithelial cells expressing wild-type and mutant CFTR channel

Ilona Gróf[1,2]

[1]Institute of Biophysics, Biological Research Centre, Szeged, Hungary
[2]Doctoral School of Biology, Faculty of Science and Informatics, University of Szeged, Szeged, Hungary

Cystic fibrosis (CF) is a genetic disorder, caused by the mutation of the gene for cystic fibrosis transmembrane conductance regulator (CFTR) protein. The loss of CFTR function leads to dramatically impaired ion (HCO_3^-, Cl^-) and fluid movement, which produces the respiratory abnormalities that characterize CF. While the role of chloride is widely investigated, less is known about bicarbonate. Empirical observations indicate the clinical usefulness of inhaled sodium bicarbonate as an adjuvant

Volume 64(1):73-90, 2020
Acta Biologica Szegediensis
http://abs.bibl.u-szeged.hu/index.php/abs

DOI:10.14232/abs.2020.1.73-90

therapy in CF due to its bacteriostatic and mucosolvent properties, but its direct effect has not been studied on respiratory epithelial cells. Our aim was to (i) establish and characterize co-culture models of human CF bronchial epithelial (CFBE) cell lines expressing wild-type (WT) or mutant (ΔF508) CFTR channel with human vascular endothelial cells, (ii) to investigate the response of the CFBE cell line pair to the cell penetrating and tight junction modulator peptide PN159; and (iii) to investigate the effects of sodium bicarbonate on these bronchial epithelial cells.

Treatment of the cells with PN159 peptide for 30 minutes caused the full opening of the barrier showed by the lower resistance-, higher permeability values and the changes in immunostaining of junctional proteins. However, this opening effect was reversible after 24-hour recovery. These data indicate that PN159 peptide efficiently and reversibly opened the junctions in CFBE cells similarly to our previous studies on models of the intestinal epithelium and the blood-brain barrier. There were no differences between the reaction of the CFBE cell line pair to the peptide.

The presence of vascular endothelial cells induced tighter barrier properties in bronchial epithelial cells: the resistance was higher and permeability values were lower. Sodium bicarbonate treatment slightly reduced the viability of WT-CFBE cells but not that of the mutant CFBE cells. Sodium bicarbonate (100 mM) significantly decreased the more alkaline intracellular pH of the mutant CFBE cells to the level of WT-CFTR CFBE cells, while the barrier properties of the models were only minimally changed by the treatment. Our observations indicate that sodium bicarbonate is beneficial to mutant CFBE cells suggesting that it may have a therapeutic effect on bronchial epithelium in CF.

Supervisors: Mária A. Deli, Alexandra Bocsik
E-mail: grof.ilona@brc.hu

The role of heat shock protein 27 in the regulation of neuroinflammation

Brigitta Dukay[1,2]

[1]Institute of Biochemistry, Biological Research Centre, Szeged, Hungary
[2]Doctoral School of Biology, Faculty of Science and Informatics, University of Szeged, Szeged, Hungary

Hsp27 is a member of the small heat-shock protein family and has an important role in the maintenance of normal cellular protein homeostasis, which is disturbed in case of inflammation. Neuroinflammation has been described as a common characteristic of most brain diseases, however, it is crucial for both neuronal tissue damage and healing following CNS injury. According to earlier results, Hsp27 can regulate the release of various inflammatory factors, proposing that it is involved in the regulation of this immune response, but its exact role is still poorly understood.

Therefore, we investigated the role of Hsp27 in acute neuroinflammatory processes in an Hsp27-overexpressing transgenic mouse model. We treated 7 day-old wild-type and Hsp27 transgenic mice with ethanol to induce neuroinflammation. Following ethanol treatment, the gene expression level of certain inflammation-related cytokines was significantly higher in Hsp27 transgenic mice compared to wild-type ones. The enhanced cytokine production was accompanied by apoptosis and morphological changes of microglia, followed by astrogliosis. The level of gliosis was also higher in certain brain regions of the transgenic animals compared to those of wild-type littermates, whereas Hsp27 overexpression slightly moderated the level of apoptosis. We also established primary astrocyte, microglia, and neuronal cell cultures from wild-type and Hsp27 transgenic animals, which were subjected to ethanol and cytokine treatment. After treatments, we quantified the concentrations of released Hsp27 and TNFα in the supernatants as well as the level of Hsp27 within the cells. We could not detect Hsp27 in the supernatants of any of the cell cultures, which suggests that intracellular Hsp27 was responsible for the immunoregulatory effects. Astrocytes showed the highest Hsp27 expression under inflammatory conditions, but in neurons it was also upregulated. Interestingly, microglia from transgenic animals released a significantly higher amount of TNFα compared to wild-type microglia in response to cytokine treatment, although it did not show Hsp27 expression. We assume that the remaining transgenic astrocytes in the primary microglia culture could be responsible for this, as these glial cells can activate each-other in several ways. Taken together, Hsp27 overexpression resulted in a more intense inflammation, but it also protected against apoptosis, proposing a balancing role for Hsp27 in neuroinflammation.

Supervisors: Miklós Sántha, Melinda E. Tóth
E-mail: dukay.brigi@gmail.com

Volume 64(1):73-90, 2020
Acta Biologica Szegediensis
http://abs.bibl.u-szeged.hu/index.php/abs

DOI:10.14232/abs.2020.1.73-90

The role of Ring1 and YY1 binding protein in the retinoic acid signalling pathway regulation during neural differentiation of mouse embryonic stem cells

Enikő Sutus[1,2]

[1]Laboratory of Embryonic and Induced Pluripotent Stem Cells, Institute of Genetics, Biological Research Centre, Szeged, Hungary
[2]Doctoral School of Biology, Faculty of Science and Informatics, University of Szeged, Szeged, Hungary

Ring1 and Yy1 Binding Protein (RYBP) is a core member of the non-canonical Polycomb Repressive Complexes 1 (ncPRC1s), which are essential epigenetic regulators of cell identity. We have previously reported that RYBP is important for central nervous system (CNS) development in mice and that *Rybp null* mutant (*Rybp*$^{-/-}$) mouse embryonic stem (ES) cells has an impaired differentiation ability in vitro as they form more progenitor and less terminally differentiated neural cells. Moreover, the increased neural progenitor pool formation was linked with the elevated level of the neural progenitor marker gene *Pax6* (Paired Box 6).

Since *Pax6* stands under the regulation of the retinoic acid (RA) signalling pathway, I have investigated whether *Rybp* can regulate the RA pathway with special focus on *Pax6* during the time curse of *in vitro* neural differentiation of mouse ES cells. The results showed that all the examined RA signaling pathway members were overexpressed in the *Rybp*$^{-/-}$ neural cultures and the rate of neural progenitor formation in the *Rybp null* mutants after RA induction was increased. By utilising luciferase reporter assays, we also demonstrated that RYBP was able to repress the *Pax6* gene through its *P1* promoter, and that the repression is attenuated when the other ncPRC1 member, Ring Finger Protein 1 (RING1) was present, suggesting that RYBP repress *Pax6* in a Polycomb dependent manner, via the ncPRC1. We also demonstrated that there were an increased rate of apoptosis and necrosis in the neural cultures when *Rybp* was absent. *Rybp* can function both as a pro and anti-apoptotic gene, depending on the given cell type and context. Our results suggest that *Rybp* exerts an anti-apoptotic function during neural differentiation and that in the lack of *Rybp* neural progenitors are prone to die, which is likely lead to the impaired terminal differentiation.

Taken together, in my PhD work I demonstrated that RYBP regulate the gene expression of *Pax6* via ncPRC1, and in the lack of *Rybp* the RA pathway increased, due to cells undergo apoptosis and necrosis, which can be one of the causatives of the impaired terminal differentiation towards neuronal lineages from progenitors.

Supervisor: Melinda Pirity
E-mail: sutus.eniko@gmail.com

Expansion of genetic resources of national maize breeding materials with innovative methods

Feríz Rádi[1,2]

[1]Institute of Plant Biology, Biological Research Centre, Szeged, Hungary
[2]Doctoral School of Biology, Faculty of Science and Informatics, University of Szeged, Szeged, Hungary

The importance of corn in the world economy is growing year by year: The growing population of the Earth requires more and more food produced on continuously decreasing agricultural lands. Extensive production is being replaced by intensive crop production that is dependent on highly productive hybrids. In order to maintain a competitive status for maize among crops there is a need for adaptive potential to intensive cultivation systems and to extreme environmental conditions generated by climate change. These requirements can be interpreted in terms of genetic background, insuring adaptation to weather and soil conditions. It is important to note that these changes are not spontaneous in nature and in agriculture, but their result from long and persistent work by breeders.

This dissertation deals with the further development of Hungarian maize lines using the modern, precision breeding techniques, developing future-oriented and competitive technologies. In addition to shortening the time, the goal is to generate genetic variance for special traits as efficiently as possible, regardless of genotype. Having haploid maize plants, our goal was to develop an *in-planta* method for oligonucleotide-directed mutagenesis (ODM) using a recessive, albino mutational marker. By introducing the oligonucleotides into the meristem, we were able to induce a point mutation at a targeted site of the phytoene desaturase gene (PDS) in the genome with strong phenotypic feedback. Our technology development program is currently a pioneer of Hungarian precision maize breeding, and our stated intentions and long-term objectives include the routine application of the methods developed here at the forefront of national maize breeding. Precision breeding methods can provide

Volume 64(1):73-90, 2020
Acta Biologica Szegediensis
http://abs.bibl.u-szeged.hu/index.php/abs

DOI:10.14232/abs.2020.1.73-90

a solution for breeding corn cultivars with yield stability, improved seed quality, efficient use of water and nutrition, or high adaptation capability. It is very important to emphasize that the technologies we use and develop are genotype independent and do not require the incorporation of a foreign gene. Eliminating these two factors is a key goal that has so far been the biggest barrier to molecular breeding of corn.

Supervisor: Dénes Dudits
E-mail: rferiz92@gmail.com

Creation of an overexpression strain collection and searching for putative virulence related genes *in Candida parapsilosis*

Sára Pál[1,2]

[1]Department of Microbiology, Faculty of Science and Informatics, University of Szeged, Szeged, Hungary
[2]Doctoral School of Biology, Faculty of Science and Informatics, University of Szeged, Szeged, Hungary

C. parapsilosis is a commensal of the human skin, however also recognized as an opportunistic fungal pathogen. It is particularly associated with low birth weight neonatal and nosocomial infections claiming for extensive survey of the virulence factors of *C. parapsilosis*.

We aimed to create and characterize an overexpression (OE) mutant strain collection involving ORFs that are thought to be involved in the pathogenesis of the fungus. We successfully generated 37 barcoded OE mutant strains by using Thermo Fisher Gateway™ cloning method.

Six mutants showed growth disabilities in the presence of cell wall or membrane perturbants, like SDS, Caffeine, Calcofluor White and Congo Red in comparison with the control. Besides that, altered level of phagocytosis was established in the case of six OE strains, respectively. One mutant strain was less effective in forming a biofilm compared to the control. Three mutants were found to be more virulent than the control strain, while one mutant hasn't got any effect to the mortality of the larvae in *G. mellonella* model. We selected two strains (one with lower and another one with higher killing efficiency in insect model) for mice infection experiments in order to determine the fungal burden in the brain, spleen, liver and kidneys. Both mutants showed higher fungal burden in the brain, and lower fungal burden in the spleen. Only one mutant showed increased and decreased CFU levels in the kidney and the liver. In conclusion out of the 37 mutants we had generated, 11 showed alteration in at least one assay. Two of these (OE_CPAR2_109520, OE_CPAR2_302400) showed difference in their virulence compared to the control strain. The ortholog of CPAR2_109520 in *C. albicans* is *TUP1*, a transcriptional corepressor involved in filamentous growth, while CPAR2_302400 is the ortholog of *MGT1* from *Saccharomyces cerevisiae* that encodes a methyltransferase involved in protection against DNA alkylation damage.

According to our results, several mutants from our OE collection showed a phenotype different from the control under conditions that are thought to impact the pathogenicity of this species.

This project was funded by GINOP-2.3.2-15-2016-00015, LP2018-15/2018, NKFIH K 123952, 20391-3/2018/FEKUSTRAT and Richter Gedeon Talentum Foundation.

Supervisor: Attila Gácser
Email: palsara0713@gmail.com

A specific acetylation mimicking point mutation of H3.3A ameliorates Huntingtin induced phenotypes in a fly model

Anikó Faragó[1,2]

[1]Department of Biochemistry and Molecular Biology, Faculty of Science and Informatics, University of Szeged, Szeged, Hungary
[2]Doctoral School of Biology, Faculty of Science and Informatics, University of Szeged, Szeged, Hungary

Huntington's disease (HD) is an inherited neurological disorder with fatal consequences. HD is caused by a dominant muta-

DOI:10.14232/abs.2020.1.73-90

tion – expansion of a CAG trinucleotide repeat – in the huntingtin gene resulting in an expanded polyglutamine domain in the Huntingtin (Htt) protein. Mutant Htt forms intracellular aggregates and abnormal interactions with other proteins, for example histone acetyltransferase (HAT) enzymes. While reduced activity of HATs enhances mutant Huntingtin toxicity, inhibition of histone deacetylases ameliorates HD phenotypes. As disturbed histone acetylation and consequent transcriptional dysregulation might be partially responsible for the manifestation of HD, we aimed to identify epigenetic marks that play a role in this process.

To investigate the effects of specific histone modifications on HD pathogenesis we generated point mutations of H3.3A histone transgenes mimicking different post-translational modifications (PTM) of lysine (K) residues, arginine (R) mimicking unmodified, glutamate (Q) mimicking acetylated, while methionine (M) mimicking methylated lysine (K9R, K9Q, K9M, K14R, K14Q, K27R, K27Q and K27M). We investigated the effects of these transgenes in a *Drosophila* model of HD by analyzing changes in Huntingtin induced phenotypes, such as lethality, early death, neurodegeneration, motor impairments and daily activity.

According to our results altering the acetylation status of K14 lysine has promising effects. K14Q ameliorated, whilst K14R exacerbated HD phenotypes. Using K14Q we observed improvement in all investigated phenotypes such as eclosion rate, lifespan, neuronal survival and climbing ability, moreover hyperactivity observed in HD flies was decreased. Our findings suggest H3K14 as potential therapeutic target in HD.

Supervisor: László Bodai
E-mail: f.ancsi93@freemail.hu

RAD18-dependent activation of FAN1 by PCNA to rescue DNA inter-strand crosslinks

Qiuzhen Li[1,2]

[1]HCEMM-BRC Mutagenesis and Carcinogenesis Research Group, Institute of Genetics, Biological Research Centre, Szeged, Hungary
[2]Doctoral School of Biology, Faculty of Science and Informatics, University of Szeged, Szeged, Hungary

The Rad18 DNA damage tolerance (DDT) pathway can resolve stalled replication forks during DNA replication. Upon DNA lesion, PCNA acts as central hub, which can be monoubiquitylated by Rad18/Rad6, and translesion synthesis (TLS) polymerases are recruited by the monoubiquitinated PCNA. The Fanconi anaemia (FA) pathway is one of the main processes responsible for the repair of DNA interstrand crosslinks (ICL) at the S/G2 cell cycle checkpoint. In the FA pathway, FANCD2/FANCI-associated nuclease 1 (FAN1) can be activated via its UBZ domain, and it can digest the ICL-neighbouring region due to its structure-specific endonuclease activity thus facilitating the bypass of the lesion. Surprisingly, depletion of FAN1 affects neither ICL-induced double-strand DNA break formation nor leads to the development of FA. Rather, germline FAN1 mutations cause caryomegalic interstitial nephritis. FAN1 also contains an uncharacterized PIP domain. DNA repair proteins are often recruited to specific sites of DNA damage through protein-protein interactions. Therefore, the research purpose of this study is to ask whether FAN1 interacts with ub-PCNA via its PIP domain or UBZ domain. We are also going to illustrate the role of Fan1 in the Rad18 DDT pathway. Since the recruitment of TLS polymerase eta (Pol η) is the key step to repair DNA damage, we are going to examine the crosstalk between FAN1 and Pol η.

Previously, we proved that FAN1 is indeed regulated by the Rad 18 DDT pathway *in vivo* and colocalizes with PCNA. In our current study, FAN1 was expressed in yeast with an engineered N-terminal GST tag and purified. I demonstrated *in vitro* that the nuclease activity of FAN1 can be enhanced by PCNA. The PIP-domain-mutated FAN1 shows deficient nuclease activity in the presence of PCNA, which indicates that PCNA can stimulate the nuclease activity of FAN1 via its PIP domain. I could also demonstrate that the digestion specificity of FAN1 could be altered in the presence of PCNA. PCNA is able to position FAN1 to cut a specific site on the 5' flap substrate. I synthesized a DNA molecule mimicking an ICL replication fork substrate, which FAN1 is able to digest in a nuclease assay, due to PCNA, and the gap is filled by Pol η specifically, not by other TLS polymerases (Pol ι and Pol κ). To sum up, our current results indicate that FAN1 does not only play a role in the FA pathway, but it also participates in the Rad6/Rad18 DDT pathway upon stalled replication. FAN1 might be a crosstalk protein, which regulates these two pathways in different cell cycles.

Supervisor: Lajos Haracska
Email: qiuzhenli2010@gmail.com

Volume 64(1):73-90, 2020
Acta Biologica Szegediensis
http://abs.bibl.u-szeged.hu/index.php/abs

DOI:10.14232/abs.2020.1.73-90

Analyzing the importance of ubiquitin-dependent selective autophagy in *Drosophila*

Adél Ürmösi[1,2]

[1]HAS-BRC Momentum (*Lendület*) *Drosophila* Autophagy Research Group, Institute of Genetics, Biological Research Centre, Szeged, Hungary
[2]Doctoral School of Biology, Faculty of Science and Informatics, University of Szeged, Szeged, Hungary

Autophagy is an evolutionarily conserved intracellular degradation process of cellular self-eating and the major pathway for degradation of cytoplasmic material by the lysosomal machinery. Selective autophagy receptors can recognize ubiquitinated aggregates and bind to Atg8/LC3 proteins to ensure the capture of cargo into autophagosomes. In *Drosophila*, only one autophagy receptor for ubiquitinated protein aggregates is known: p62/Ref(2)P. p62 possesses a C-terminal ubiquitin-binding domain (UBA), an N-terminal PB1 domain to mediate aggregate formation, and a LIR (LC3-interacting region) motif in an unstructured region, which is responsible for LC3/Atg8a binding on autophagic membranes.

To investigate the role of p62/Ref(2)P, we replaced two previously characterized key amino acids within the LIR motif: a tryptophan and an isoleucine to alanines by editing the endogenous gene using CRISPR. We generated *Drosophila* lines carrying a p62-LIR mutation, which disrupted the autophagic degradation of p62 and ubiquitinated cargo.

Flies homozygous for the mutation are viable and fertile, and accumulation of p62 and ubiquitinated protein aggregates was observed in various tissues in homozygous and heterozygous animals. We observed age-dependent accumulation of the p62/Ref(2)P, with an increased accumulation in older flies. The LIR mutants had a similar lifespan as WT flies under normal conditions and during complete starvation. To test their oxidative stress tolerance, we fed LIR mutant and control flies with agents that induce oxidative stress (e.g., paraquat). Interestingly, LIR mutant flies are less sensitive to paraquat treatment, and express higher levels of oxidative stress response genes like glutathione-S-transferase. LIR-mutant flies have fewer mitochondria containing reactive oxygen species, while basal mitochondrial degradation by mitophagy remains similar. However, if mitophagy is induced by an iron chelator, we observe a mitophagy defect in these flies. This leads us to think that there are other mitophagy receptors in flies independent of mitochondrial ubiquitination that function under basal conditions. Lastly, autophagy was earlier shown to be critical for neuronal function, supposedly via the continuous selective turnover of ubiquitinated cargo. Accordingly, *Atg* mutant animals show developmental delay, increased stress sensitivity, ataxia, neurodegeneration, and as a consequence, shortened lifespan. None of these phenotypes are due to the loss of selective ubiquitin-dependent autophagy based on analyses of our p62-LIR mutants.

Supervisor: Gábor Juhász
E-mail: urmosiadel@gmail.com

Analysis of genes encoding possible spore coat-like proteins in opportunistic human pathogenic fungi

Csilla Szebenyi[1,2,3]

[1]Department of Microbiology, Faculty of Science and Informatics, University of Szeged, Szeged, Hungary
[2]HAS-USZ Momentum (*Lendület*) Research Group Fungal Pathogenicity Mechanisms Research Group, Szeged, Hungary
[3]Doctoral School of Biology, Faculty of Science and Informatics, University of Szeged, Szeged, Hungary

Members of the order Mucorales can be agents of life-threatening, opportunistic human infections, known as mucormycosis. Because of the devastating outcome of this disease, which has been observed despite the current treatment options, it is urgent to identify the possible virulence factors. CotH proteins are widely present in Mucorales and previous studies showed the importance of one of these proteins in the pathogenicity of this fungal group.

A new type of spore coat-like protein family and represents five possible spore-coat proteins encoding genes (i.e. *cotH1-cotH5*) of the β-carotene producing filamentous fungus, *M. circinelloides* disrupted individually by a recently developed *in vitro* plasmid-free CRISPR-Cas9 method. Pathogenicity of the *cotH3*, *cotH4*, and *cotH5* gene disrupted and *cotH4* gene complemented mutants was tested in *D. melanogaster* and MS12-*ΔcotH3+pyrG* and MS12-*ΔcotH4+pyrG* mutant strains resulted in a lower mortality rate. The MS12- *ΔcotH3+pyrG* and MS12-*ΔcotH4+pyrG* mutant strains exhibited markedly reduced virulence in a murine model. The spore coat of *cotH4* gene disrupted mutant spores presented several deviations from what was observed with the wild-type

DOI:10.14232/abs.2020.1.73-90

strain: the thickness of the spore wall differs significantly from the control based on our TEM results. Staining with the anionic dye, calcofluor white (CFW) that binds to the chitin in the fungal cell wall, a change the intensity of the dye was observed.

This study was created to assess the importance of possible spore-coat proteins in the biological processes of *M. circinelloides*. Understanding CotH proteins as possible factors in fungal pathogenicity are crucial for developing new antifungal strategies.

Supervisors: Tamás Papp, Gábor Nagy
e-mail cím: szebecsilla@gmail.com

Development of high throughput mass spectrometric methods for the analysis of selected groups of primary and secondary metabolites

Dávid Rakk[1,2]

[1]Department of Microbiology, Faculty of Science and Informatics, University of Szeged, Szeged, Hungary
[2]Doctoral School of Biology, Faculty of Science and Informatics, University of Szeged, Szeged, Hungary

The microbial metabolites could be divided into two groups. The primary metabolites directly involved in normal growth, development and reproduction, while secondary metabolites play role in the other functions of the organisms. From the quantity of primary metabolites different biological processes could study for example the energy level. Meanwhile, the high throughput quantifications of certain secondary metabolites, such as mycotoxins, are crucial for food safety and human health. The high speed and accurate quantification of metabolites simultaneously can be only provided with the novel sophisticated mass spectrometric (MS) techniques such as instruments containing Orbitrap mass analyzers.

In my research work two multiplexing based LC-MS method were developed and validated to the measurements of various metabolites from different biological samples.

In the first method, the primary metabolites of the central biochemical pathway were investigated represented the members of the tricarboxylic acid cycle and related molecules. During this method development, new approaches were applied specialized to multiplex acquisition mode resulting the complete workflow for this type of analyses. It was certified that the method possesses proper sensitivity for quantification of the selected metabolites in various biological matrices. A secondary metabolite, the European Union regulated mycotoxins were also examined applying a multiplexing based LC-MS method. According to the lower limit of quantifications of the tested compounds, the method was sensitive enough for detection of mycotoxins at the levels of their maximum limits in the applied matrices except for HT2 toxin. Furthermore, the performance parameters were also over the limits of the acceptable criteria providing an applicable technique for the routine analysis.

Finally, it could be concluded that the application of multiplex acquisition mode has remarkable advantages and could serve rapid simultaneous quantification possibilities for the defined group of analytes.

Supervisor: András Szekeres
E-mail: rakkdavid@gmail.com

CRISPR/Cas9 and IS element-mediated engineering of prokaryotic genomes

Ranti Dev Shukla[1,2]

[1]Department of Biochemistry, Synthetic and Systems Biology Unit, Biological Research Centre, Szeged, Hungary
[2]Doctoral School of Biology, Faculty of Science and Informatics, University of Szeged, Szeged, Hungary

Phage engineering project: Using phage therapy to fight bacterial infections has a renaissance in the age of rapidly emerging antibiotic-resistant pathogens. However, we have limited knowledge about the cell biology and immunology fundamentals of phage therapy necessitating more investigations using *ex vivo* infection models. *E. coli* K1 is a nosocomial pathogen responsible for urinary tract infections, neonatal meningitis and sepsis. To aid studies concerning the treatment of *E. coli* K1 infections using phage K1F, we have applied the CRISPR/Cas system to engineer K1F phage tagged with GFP. Our collaborators at the University of Warwick used the green fluorescent phages with red fluorescent bacteria to study the phage-mediated eradication of *E. coli* from a urinary epithelial cell culture. Importantly, this research demonstrated that phages can enter urinary epithelial

Volume 64(1):73-90, 2020
Acta Biologica Szegediensis
http://abs.bibl.u-szeged.hu/index.php/abs

DOI:10.14232/abs.2020.1.73-90

cells by phagocytosis independently from bacteria, and K1F phages can kill *E. coli* inside the eukaryotic cells. This result was published in Scientific Reports. Currently, we are working on the deletion of an essential phage gene to make the phages replicable only in hosts that provide this protein in trans. This way, the engineered phages will not amplify in the patient, making the phage count controllable similarly to the dosage of any conventional pharmaceutical.

E. coli engineering project: E. coli is a popular host for the production of valuable metabolites by expression of complete metabolic pathways. Using episomal (plasmid) DNA is convenient but has drawbacks including increased metabolic burden, the requirement for selection in the form of antibiotics, instability and gene copy number variation. Chromosomal integration offers a stable and selection-free alternative to using DNA plasmids for expression of foreign proteins and metabolic pathways. Requirement of landing pads is usually a limiting factor for chromosomal integration. We introduce the use of IS (Insertion sequences) elements as landing pads which are segments of bacterial DNA, able to move within bacterial genome and allow the amplification of transgenes. We applied IS elements to integrate a 7.5 kb long 5 gene operon, responsible for violacein production, into the *E. coli* chromosome. We got success in IS*3* as well as IS*1*-mediated integration of violacein pathway. Further we succeeded in IS3-mediated copy number amplification of violacein pathway. IS*1* mediated amplification experiments are in progress.

Supervisor: Tamás Fehér
E-mail: rantibio@gmail.com

Multidisciplinary research of natural and anthropogenic mummies – Multidisciplinary research of the mummies curated in the Egyptian collection of the Hungarian Natural History Museum

Enikő Szvák[1,2]

[1]Department of Biological Anthropology, Faculty of Science and Informatics, University of Szeged, Szeged, Hungary
[2]Doctoral School of Biology, Faculty of Science and Informatics, University of Szeged, Szeged, Hungary

During history, people wanted to preserve their body mostly for religious reasons for the beyond of afterlife or the future. Nowadays the researchers investigate these bodies with modern technological methods to gain information on the diseases of the past, traumatic injuries, eating habits and general health status of the people lived ones. Our research goal was to conduct the most comprehensive series of studies as many as possible. As the primary consideration was to preserve the remains, especially in case of the fragmentary and incomplete specimens of bad preservation, the sampling numbers were minimal. The biological anthropological investigation methods helped estimate the sex and the age at death of the specimens. The paleopathological studies lighted that the individuals, once lived in Egypt, what kind of diseases suffered from.

The research team has experts from various fields, chemists, physicists, radiologists, molecular biologists and a-DNA specialists, therefore we were able to apply physical, chemical, medical diagnostic methods, imaging technologies (ICP-OES, GC-MS, FAAS, FTIR, X-ray, CT, SEM and Keyence 3D microscope) in the multidisciplinary study.

Mostly non-invasive techniques were used. The invasive technique was applied only in case of the radiocarbon dating; but it was necessary, as the age of some mummies were disputed.

In the new phase of the project, the aim is to identify the mummification process itself and determine the materials used during the mummification process. To ascertain the social status of the mummies and the region of the mummification process organic chemistry analyses were performed. There are specimens form the Gamhud site in Vienna, in Prague and in Warsaw as well. The mummified remains curated in the Kunsthistorisches Museum, Vienna were investigated in 2017 as part of a short study tour. As a reference material, a comparative analysis with an Egyptian mummy collection of the same age in Mannheim, Germany was performed as well.

Future plans include C14 and isotope analysis of the entire Egyptian collection of the Hungarian Natural History Museum and to compare our material to others stored in other foreign collections.

Supervisor: Ildikó Pap
E-mail: szvak.eniko@bio.u-szeged.hu

Volume 64(1):73-90, 2020
Acta Biologica Szegediensis
http://abs.bibl.u-szeged.hu/index.php/abs

DOI:10.14232/abs.2020.1.73-90

Drosophila alternative linker histone BigH1 enables rapid nuclear divisions during early development

Anikó Szabó[1,2,3]

[1]Institute of Biochemistry, Biological Research Centre, Szeged, Hungary
[2]Department of Biochemistry and Molecular Biology, Faculty of Science and Informatics, University of Szeged, Szeged, Hungary
[3]Doctoral School of Biology, Faculty of Science and Informatics, University of Szeged, Szeged, Hungary

Linker histone H1 proteins are essential for the formation of higher-order chromatin structure. Their role is to seal the nucleosome by binding to the entry and exit site of nucleosomal DNA, thus stabilizing the structure. Linker histones have many tissue- and developmental stage-specific variants. In many organisms, the initiation of embryogenesis requires an alternative linker histone, often called oocyte-specific or embryonic linker histone variant. In *Drosophila*, BigH1 has been described as the early embryo-specific alternative linker histone, however its role during embryogenesis remains elusive.

Our work is centred on investigating why BigH1 is required during early development. For this purpose, we generated mutant fly lines in which the coding sequence of BigH1 is exchanged completely or partially with the coding sequence of somatic H1, resulting in domain switches between the two linker histone types. Analysis of the fly lines revealed that somatic H1 can completely replace BigH1 during early embryogenesis at normal temperature, as mutant flies are viable and fertile without developmental defects. We have also discovered that the N-terminal region of BigH1 is required for normal expression of the protein, however the exchange of the N-terminal domain does not impact development. Further experiments revealed that the C-terminal and globular domains of BigH1 are essential for proper nuclear divisions at low temperature, as replacing these domains with that of H1 results in severe mitotic defects and embryonic lethality. We have found that the complete replacement of BigH1 with H1 leads to enlarged nuclei, indicating altered chromatin organisation. Our experiments on the stability of nucleosomes and on their association with linker histones demonstrate that BigH1 performs its specific function in early embryogenesis by being a more dynamic linker histone that facilitates fast nucleosome exchange in S-phase during the rapid nuclear divisions in the early embryo, while providing greater stability to nucleosomes compared to somatic H1.

Supervisors: Imre Boros, László Henn
E-mail: assuming_control@hotmail.com

Investigation of the effects of *Candida* on the progression of oral squamous cell carcinoma

Máté Vadovics[1,2]

[1]Department of Microbiology, Faculty of Science and Informatics, University of Szeged, Szeged, Hungary
[2]Doctoral School of Biology, Faculty of Science and Informatics, University of Szeged, Szeged, Hungary

A large number of commensal microbial species reside in the human body that have co-evolved with the human genome and adopted to the host immune system. Previously it has been shown that defects in regulatory processes or alterations in the composition of microbiome can lead to various diseases, including cancer. A previous study has shown that the number of *Candida* cells in this particular niche is significantly higher in patients with oral squamous cell carcinoma (OSCC) compared to healthy individuals. Our aim is to examine how the fungal cells affect the progression of OSCC.

In order to investigate the effects of heat-killed and live *Candida* cells on the metastatic activity of the cancerous cells we used a metastatic (HO-1-N-1) and a non-metastatic (HSC-2) OSCC cell line. Cell migration, matrix metalloproteinase (MMP), proliferation activity and 3D tumor spheroid formation of HSC-2 and HO-1-N-1 OSCC cells were investigated after fungal stimuli.

The migration capacity of HO-1-N-1 cells was significantly higher if we treated the tumor cells with heat-killed *Candida* compared to the untreated samples. Prominent MMP activity and larger spheroid formation were detected after 24h pre-incubation with heat-killed *C. albicans* and *C. parapsilosis*. Both cell lines showed increased proliferation activity upon treatments, which clearly indicates that the presence of heat-killed fungi can accelerate cancer cell proliferation. In contrast to these results, live *Candida* treatment resulted in reduced migration activity and increased MMP activity of OSCC cells. No proliferation activity change was obtained.

Our *in vivo* experiments showed the tumor was growing faster in SCID mice if we pre-incubated the OSCC cells with *Candida*

Volume 64(1):73-90, 2020
Acta Biologica Szegediensis
http://abs.bibl.u-szeged.hu/index.php/abs

DOI:10.14232/abs.2020.1.73-90

parapsilosis before the tumor cell injection to the tongue of the mice. Furthermore, we set up an *in vivo* experimental model for investigation of the effect of oral candidiasis on the OSCC in immunosuppressed wild type mice.

Supervisor: Attila Gácser
E-mail: vadovicsmate@gmail.com

A human BBB model in an organ-on-a-chip device and the effect of fluid flow

Ana Raquel Santa-Maria[1,2]

[1]Institute of Biophysics, Biological Research Centre, Szeged, Hungary
[2]Doctoral School of Biology, Faculty of Science and Informatics, University of Szeged, Szeged, Hungary

Blood brain barrier-on-a-chip model are cutting edge microengineered devices, but only a few combine the crucial parameters. Our laboratory developed an organ-on-a-chip device to study the blood brain barrier (BBB), which enables visual observation, transendothelial electrical resistance (TEER) and permeability measurements. The objective of our study was to optimize a human BBB cell culture model in the organ-on-a-chip and determine the effect of the fluid flow in the barrier properties of the BBB model.

The device was built up from a porous cell culture membrane sandwiched between two layers of PDMS and a top and bottom plastic slide coated with gold electrodes. A peristaltic pump was used to circulate the cell culture medium to mimic the blood flow. The stem cell derived $CD34^+$ human endothelial cells in co-culture with bovine pericytes were cultured in the device, as a human BBB model.

We optimized the co-culture of stem cell derived $CD34^+$ human endothelial cells with bovine pericytes in the device. The resistance was measured in real time, and the flow conditions elevated the TEER significantly, which was also confirmed by ZO-1 and β-catenin immunostainings. To investigate the differences after fluid flow condition a gene expression study was performed. This organ-on-a-chip device for study a human BBB model, provides users with a standardized and reliable platform to perform pathology and pharmacology experiments. Our device is a cutting-edge invention in the barrier-chip field.

This work was supported by the European Training Network H2020-MSCA-ITN-2015, grant number 675619, and NNE-129617-M-ERA.NET2 nanoPD grant.

Supervisor: Maria A. Deli
Email: anaraquel.santamaria@brc.hu